EFFECT OF IONS ON PARTICLE SIZE AND MORPHOLOGY IN CALCIUM CARBONATE ($CaCO_3$) CRYSTALLIZATION

A Thesis Submitted to
the Graduate School of
İzmir Institute of Technology
in Partial Fulfillment of the Requirements for the Degree of

MASTER OF SCIENCE

in Chemical Engineering

by
Ahmed OSMAN ADAM OSMAN

December 2021

IZMIR

ACKNOWLEDGMENTS

In the Name of Allah, the Most Compassionate, the Most Merciful. Peace and blessing be upon prophet Muhammad and on his family. To those who have departed this world but will always have a place in my heart. My heartfelt thanks go out to Prof.Dr. EKREM ÖZDEMİR, my esteemed supervisor, for his tremendous supervision, support, and guidance during the duration of my Master's degree in science. I'd want to offer my heartfelt gratitude to the members of my committee. My thanks go out to the Turkish Scholarship Program for providing me with the financial assistance I needed to pursue my studies at the Department of Chemical Engineering at the Izmir Institute of Technology. My gratitude also goes out to Yaşar Kemal Recepoğlu and Ali Hamid khalif. My gratitude also goes out to my family and friends, who have been encouraging and supportive throughout my education journey.

Ahmed OSMAN ADAM OSMAN.

ABSTRACT

EFFECT OF IONS ON PARTICLE SIZE AND MORPHOLOGY IN CALCIUM CARBONATE ($CaCO_3$) CRYSTALLIZATION

The particle sizes of calcium carbonate ($CaCO_3$) produced by the chemical crystallization method were reported to be almost always larger than 3 μm. An experimental setup was developed to crystalize $CaCO_3$ from sodium carbonate (Na_2CO_3) and calcium chloride ($CaCl_2$) solutions in a plug flow reactor (PFR) with a retention time of 9 seconds and added into a stabilizing solution of calcium hydroxide. The $CaCO_3$ particles were produced with a size larger than 13 μm in the PFR tubular reactor. Effect of cations such as hydroxide form of sodium (Na^+), potassium (K^+), calcium (Ca^{++}), and barium (Ba^{++}) as well as anions such as the sodium form sulfate ($SO_4^{=}$), nitrate (NO_3^-), carbonate ($CO_3^{=}$) and bisphosphate ($HPO_4^{=}$) were investigated. While cations produced calcite particles at sizes larger than 2 μm in the presence of Na^+ and K^+ ions, nano-calcite particles in the presence of Ca^{++} ions. A new crystalline form, Barytocalcite ($BaCa(CO_3)_2$), and whitherite ($BaCO_3$) particles were produced in solution containing Ba^{++} ions. The size and morphology of vaterite and calcite particles did not change as particles in the PFR tubular reactor in the presence of $SO_4^{=}$, NO_3^-, and $CO_3^{=}$ ions. Different crystal forms were synthesized in the presence of $HPO_4^{=}$ ion. These formations clearly indicated the dissolution and recrystallization of $CaCO_3$ particles. A novel technique was devised for the continuous production of nano-$CaCO_3$. It was demonstrated that nano-calcite particles of about 350 nm were produced by the chemical method not previously reported in the literature.

ÖZET

KALSİYUM KARBONAT ($CaCO_3$) KRİSTALİZASYONUNDA İYONLARIN TANECİK BOYUTU VE MORFOLOJİSİ ÜZERİNE ETKİSİ

Kimyasal kristalizasyon yöntemiyle üretilen kalsiyum karbonatın ($CaCO_3$) partikül boyutlarının neredeyse her zaman 3 μm'den daha büyük olduğu rapor edilmektedir. Bir borulu akış reaktöründe (PFR) 9 saniye alıkonma süresi ile sodyum karbonat (Na_2CO_3) ve kalsiyum klorür ($CaCl_2$) çözeltilerinden $CaCO_3$ kristalize etmek üzere bir deney düzeneği geliştirildi ve elde edilen $CaCO_3$ medyum stabilizör olarak kullanılan çözeltiye doğrudan aktarıldı. PFR boru reaktörde kalsitten oluşan 13 μm'den büyük boyutta $CaCO_3$ partikülleri üretildi. Hidroksit formu olan sodyum (Na^+), potasyum (K^+), kalsiyum (Ca^{++}), ve baryum (Ba^{++}) gibi katyonların ve sodyum formu olan sülfat ($SO_4^=$), nitrat (NO_3^-), karbonat ($CO_3^=$) ve bifosfat ($HPO_4^=$) gibi anyonların etkisi araştırıldı. Na^+ ve K^+ iyonlarının varlığında 2 μm'den büyük boyutlarda kalsit partikülleri üretilirken, Ca^{++} iyonları varlığında nano-kalsit tanecikleri üretilmiştir. Ba^{++} iyonları içeren çözeltide yeni bir kristal form olan Baritokalsit ($BaCa(CO_3)_2$) ve beyaz cevher ($BaCO_3$) partikülleri üretilmiştir. Vaterit ve kalsit partiküllerinin boyutu ve morfolojisi, $SO_4^=$, NO_3^-, ve $CO_3^=$ iyonlarının varlığında PFR borulu reaktörde sentezlenen taneciklere göre değişmediği görüldü. $HPO_4^=$ iyonu varlığında farklı Kristal formları sentezlendi. Bu oluşumlar, $CaCO_3$ taneciklerinin çözüldüğünü ve yeniden kristalleştiğini açıkça göstermiştir. Sürekli nano-$CaCO_3$ üretimi için yeni bir teknik geliştirildi. Literatürde daha önce bildirilmeyen kimyasal yöntemle yaklaşık 350 nm boyutlarda nano-kalsit taneciklerinin üretildiği gösterildi.

TABLE OF CONTENTS

LIST OF FIGURES

Figure **Page**

Figure **Page**

Figure **Page**

Figure **Page**

Figure **Page**

Figure **Page**

LIST OF TABLES

Table **Page**

CHAPTER 1

INTRODUCTION

Calcium carbonate ($CaCO_3$) is one of the most abundant minerals on the earth. Seven percent (7%) of the Earth's crust has been estimated to be $CaCO_3$[1]. $CaCO_3$ may be found in limestone, chalk, and marble in nature. In industry, $CaCO_3$ can be used as a filling material in polymeric composite materials, toothpaste, paper manufacturing, cement industry, and in drugs as in medicine. Precipitation of $CaCO_3$ in heating systems is undesirable since it leads to the formation of scales and reduce the heat transfer efficiency[2]. Knowing the mechanism of $CaCO_3$ crystallization or its inhibition may help to reduce the scale formation in heating pipes.

$CaCO_3$ is widely used as filling material in polymeric composite materials. For this purpose, the naturally mined $CaCO_3$ from the earth's crust is crushed, grinded, and sieved to reduce its particle size. This type of $CaCO_3$ is called as ground calcium carbonate (GCC). It was shown that the tensile yield strength of polymeric composite materials reduced significantly when filled with mm-sized or µm-sized particles. When nano-sized $CaCO_3$ particles were used in the polymeric composite materials[3], the change in the tensile yield strength was insignificant. Therefore, it is important to produce nano-sized $CaCO_3$ particles in order to improve the product quality of the composite materials. The fact that the particle size could only be reduced up to 1 µm in the GCC process and nano-sized $CaCO_3$ particles cannot be obtained by the crushing, grinding, and sieving of the natural $CaCO_3$ minerals.

Nano-sized $CaCO_3$ can be produced by the recrystallization processes, the product of which is called as precipitated calcium carbonate (PCC). There are mainly two types of PCC processes: One is the carbonization method, which consumes an aqueous solution of calcium hydroxide ($Ca(OH)_2$) and a gaseous carbon dioxide (CO_2)[4]. The other is the chemical method, which consumes aqueous solution of calcium chloride ($CaCl_2$) and aqueous solution of sodium carbonate (Na_2CO_3). Carbonation is a heterogeneous process for solıd-liquid-gas reactions. Chemical precipitation processes,

on the other hand, include the homogeneous phase mixing of aqueous solutions containing calcium ion (Ca^{++}) and carbonate ion ($CO_3^{=}$) in a controlled environment[3]. Although nano-sized $CaCO_3$ particles can be readily syntheszed by the carbonization method[5], particle with almost always larger than 3 μm sizes are obtained in the chemical method[6]. Therefore, it is important to understand the mechanism on the formation of $CaCO_3$ particles and develop a method to obtain nano-$CaCO_3$ particles by the chemical method.

Here, it was shown in our lab that the $CaCO_3$ particles are stable in $Ca(OH)_2$ solution[5]and therefore developed a method for the synthesis of nano-$CaCO_3$ particles by the chemical method[7]. In this thesis, the effect of some cations, anions, and stabilization conditions were studied on the formation of nano-$CaCO_3$ particles to be produced in the chemical method.

CHAPTER 2

LITERATURE REVIEW

2.1. $CaCO_3$ as Filling Material

The $CaCO_3$ is widely utilized as filling material in a variety of products, including paper, paint, plastic, packaging, polyurethane foam, and pigments. $CaCO_3$ also utilized in medical; drug delivery, anti-acid and bone rehabilitation, as well as the cosmetics and food industries. The filling material can increase the mechanical and physicochemical properties of the composite material as well as significantly reduce the manufacturing costs. Therefore, $CaCO_3$ is used in a wide range of products including coating materials, pigments and inks, paper, lubricating oils, and plastic and rubber materials.

$CaCO_3$ is used as a filler in paper to increase the quality of the paper to retain dye, brilliance, and waterproofing. The porous surfaces in calcium carbonate grains improve the absorption of oils and inks [8]. Also, excellent light dispersion was attained with the paper when combined the precipitated calcium carbonate and Aluminum-Magnesium–silicate compounds [10]. In addition, water resistance is greatly increased by the introduction of $CaCO_3$, which assists in increasing the opacity, whiteness, and printing performance of the paper.

The presence of $CaCO_3$ particles enhances the structural, durability, and morphological properties of a series of polymeric plastic products, including polyvinyl chloride[9–11], polypropylene[12], PMMA[13], acrylonitrile-butadiene-styrene[14], high-density polyethylene. Nano-size $CaCO_3$ particles were found to be more effective than the micro-sized particles due to an excellent distribution within the matrix phase of the polymers. Another application of $CaCO_3$ is that heptade-cafuorodecyl-trimethoxy silane and regular polyacrylate have been shown to have antifreeze properties, especially when combined with their super-hydrophobicity in nano-$CaCO_3$[15].

Due to CaCO3's compatibility with the body, $CaCO_3$ is employed as a calcium substitute and antacid categorization in medicinal applications because of its non-toxicity and excellent solubility in acidic environments. $CaCO_3$ particles are capable of being used in biomedical applications such as crystals of aragonite form bone components with integrated gentamicin formulations for the prevention or treatment of osteomyelitis[16]. $CaCO_3$ is used as filling material in toothpaste with the appropriate amount of pigment or dentine abrasiveness[17]. $CaCO_3$ is also used in transdermal insulin injections into the blood[18].

2.2. Polymorphs of Calcium Carbonate

There are basically two forms of CaCO3 present. These are anhydrous and hydrous forms. The anhydrous crystalline polymorphs are spheroidal vaterite, dendritic or orthorhombic aragonite, and rhombohedral or scalenohedral calcite[19–21]. The hydrous crystalline polymorphs for $CaCO_3$ are calcium carbonate monohydrate, calcium carbonate hexahydrate (ikaite, $CaCO_3 \cdot 6H_2O$) and amorphous calcium carbonate (ACC)[21–24]. The most stable form of $CaCO_3$ is calcite at atmospheric temperature and pressure. Figure 2.1 shows the polymorphs of $CaCO_3$ as the unstable – amorphous calcium carbonate, ACC[25]; metastable - vaterite; metastable - aragonite[26]; and stable-calcite (this work).

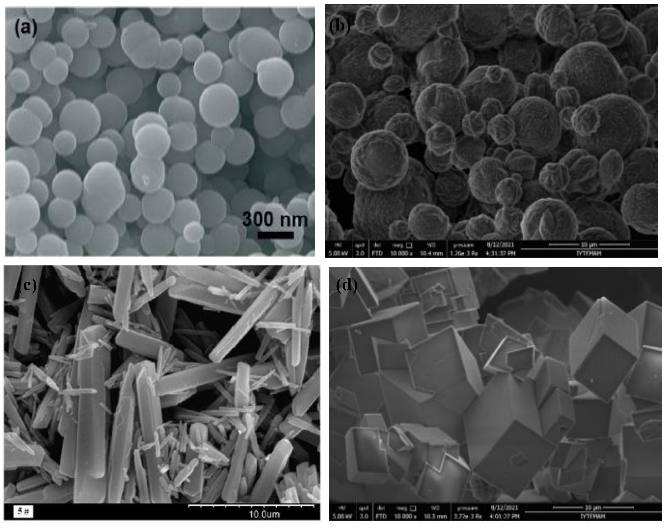

Figure 2.1. Polymorphs of $CaCO_3$ as the unstable – amorphous calcium carbonate, ACC[25]; metastable - vaterite; metastable - aragonite[26]; and stable-calcite (this work).

Polymorphs of $CaCO_3$ is a rather common form of calcium carbonate that occurs naturally as a transformation of its polymorphic components. Figure 2.2 shows the $CaCO_3$ formation pathways at high supersaturation[27]. As shown in the figure, the amorphous phase of $CaCO_3$ forms rapidly from its constitutes generating a colloidal-based amorphous phase. Because of their poor colloidal stability, it is impossible to prevent aggregation in these systems. Aggregation develops a gel formation in the reaction medium as a result of the high-density distribution of particles and the ionic force of the mixture in the solution. The gel's quick morphological failure occurs as a result of the gel becoming colloidally less stable since the gel is linked to each other only by van der Waals interactions. While the amorphous phase dissolves, it may recrystallize into the metastable vaterite before dissolving and transforming into the most stable calcite[27]. Apart from the transformation of ACC to Vaterite and vaterite to calcite, the metastable-aragonite can form under specific conditions especially when the temperature is higher than 40 ^{o}C and in the presence of certain additives. The transformation of $CaCO_3$ polymorphs can occur by the precipitation of a less soluble or stable polymorph from the dissolution of less stable metastable phase under the supersaturated conditions in solution. The least soluble phase initially precipitates, dissolves, and then recrystallizes to a much more stable form as dominated by the Ostwald Stage Rule[21,28–30].

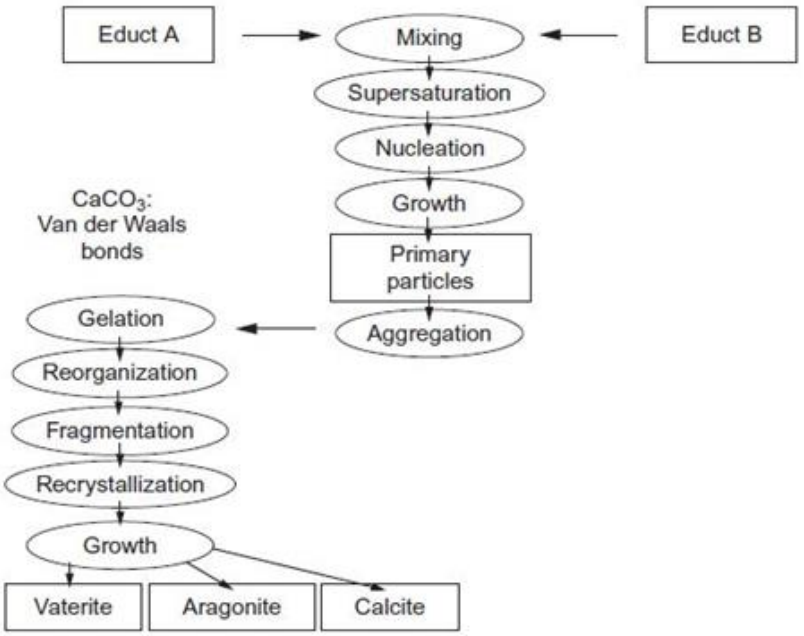

Figure 2.2. Calcium Carbonate formation pathways at high supersaturation [27]

2.3. Nucleation and Growth of CaCO3 crystals

$CaCO_3$ crystallization happens via various steps, each resulting in a different polymorph. Polymorphism may be observed in a solution depending on the conditions and composition. pH, ion concentration, and Temperature can all play a role in the formation of polymorphs. The first stage is the formation of the least thermodynamically stable ACC in solution. The second is the transformation of AAC into the metastable-vaterite. Then, vaterite can transform into the most stable form of calcite. As shown in the figure, this process took minutes to hours. Unstable-Amorphous $CaCO_3$ may transform into metastable-aragonite at temperatures equal to or higher than 40°C or in the presence of certain additive ions [1,21,31,32]

Rodriguez-Blanco et al[31] previously investigated the mechanism of $CaCO_3$ crystallization as shown in Figure 2.3. Their study concentrated on the development of $CaCO_3$ crystals by the chemical method by mixing $CaCl_2$ and Na_2CO_3 solutions. Their results indicated that the formation of $CaCO_3$ particles could be classified into two stages. The process begins with formation of unstable-ACC, which is rapidly converted to metastable-vaterite. Finally, vaterite is converted into stable calcite in the second stage.

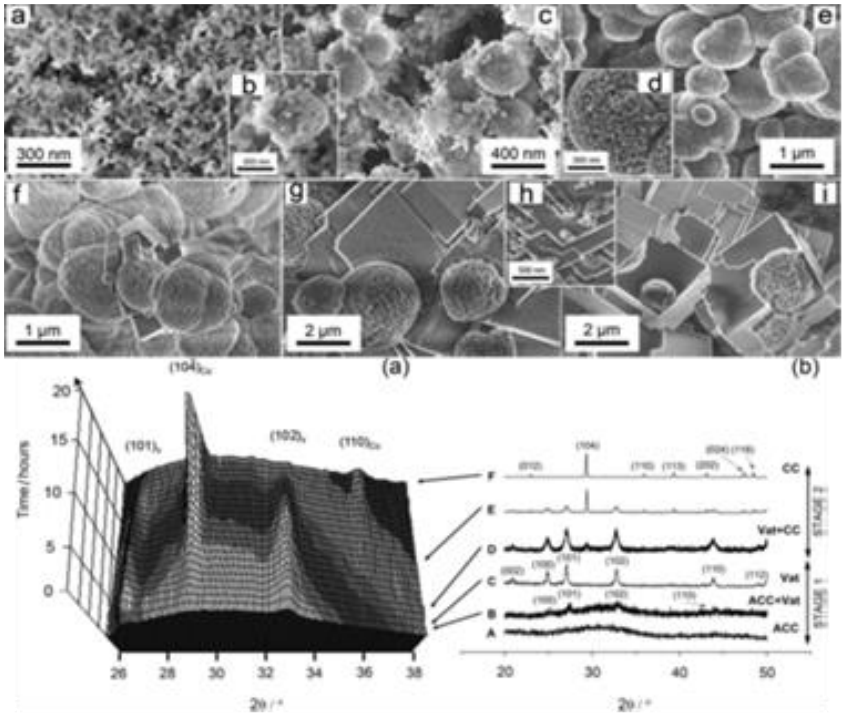

Figure 2.3. $CaCO_3$ crystallization occurs in two stages

According to Ogino et al.[33], a similar result was achieved when they studied the process of vaterite transformation into calcite. This process is characterized by the simultaneous dissolution of metastable-vaterite and the formation of stable calcite, which was the rate-determining process. Bots et al[21]., investigated the mechanism for the transformation of ACC into vaterite and vaterite to calcite as shown in Figure 2.4. As shown in the figure, the transformation of $CaCO_3$ into different polymorphs has three stages: first, the formation of unstable-ACC and a spherulitic growth of metastable-vaterite; second, repining of aggregated vaterite; and third, dissolution of vaterite and reprecipitation into stable-calcite. This is a time-dependent process as shown in Figure 2.4. Interesting to note that, the formation of ACC took about 1 minute and started to dissolve. The dissolution of ACC and formation of vaterite started at about 1.2 minutes and completed total dissolution and reformation by 5 minutes. Dissolution of vaterite and recrystallization of calcite started at about 16 minutes. The transformation was only 20% at about 100 minutes. Then, the transformation accelerated at about 100 minutes and completed the dissolution and recrystallization in about 350 minutes.

This was the starting point to our design on the synthesis of nano-calcite particles with the chemical method. We argued that nano-ACC particles occurred in the first 2 minutes and they can be stabilized for nano-$CaCO_3$ production.

2.4. Influence of Ions on $CaCO_3$ Crystallization

The crystallization of CaCO3 is governed by processes of nucleation and growth. The existence of impurity ions has a major impact on the $CaCO_3$ crystallization process. Certain ions have major effects, such as increasing or decreasing nucleation and growth rates or delaying the transformation to another phase, or on the size and morphology of particles. Wada et al.[34] reported that cations with a divalent charge such as Co^{++}, Cu^{++}, Fe^{++}, Ni^{++}, Mg^{++}, and Zn^{++} are prone to forming aragonite phases, while Cd^{++} shows no significant influence. Furthermore, a recent study has demonstrated[35,36] that Zn^{++} and Cu^{++} may lower the growth rate of calcium carbonate. Moreover, cations with a divalent charge such as Ba^{++}, Ca^{++}, Mn^{++}, Pb^{++}, and Sr^{++} have an affinity for calcite formation[37].

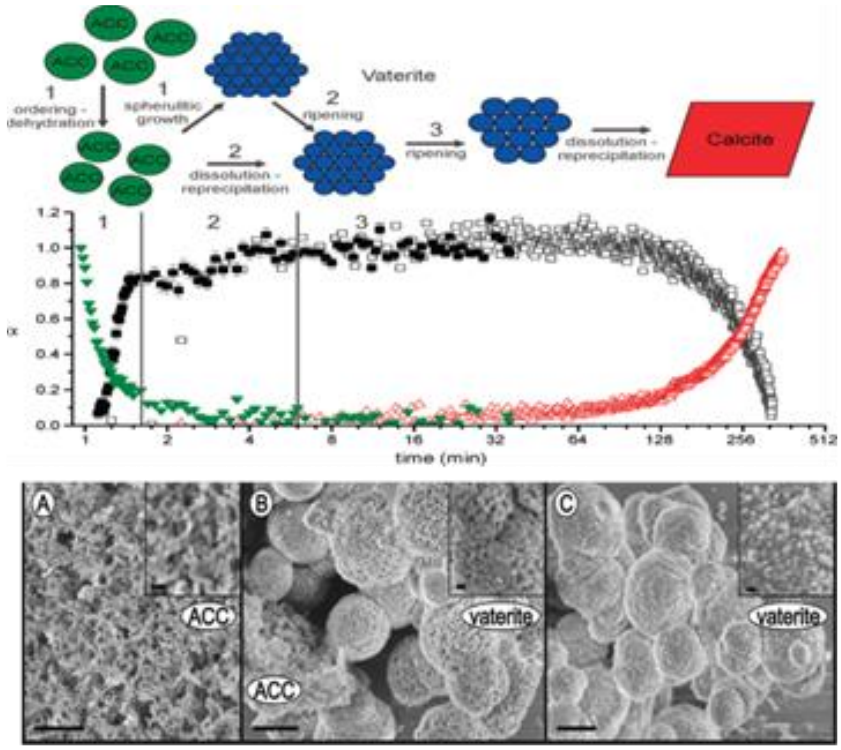

Figure 2.4. The three stages of the crystallization of CaCO3[21].

2.5. Influence of Organic and Inorganic additives on $CaCO_3$

The particles of $CaCO_3$ are formed in the presence of foreign materials and ions that have a direct effect on the shape and size of $CaCO_3$ particles by forming an unusual structure rather than a typical morphology. Additives may be synthetic or natural polymers, inorganic, organic, as well as biologic. Numerous studies have shown the production of $CaCO_3$ particles with novel morphologies by including a variety of additives[2838,39]. For instance, using an organic addition (e.g., carboxylic acid), the size of the $CaCO_3$ particle reduced to submicron proportions; whereas, using an inorganic additive (e.g., ammonium chloride), the particle sizes increased by 1.5 to 2 times proportionally[40]. Furthermore, nonionic materials such as starch and dextran had a significant impact on the size of $CaCO_3$ particles. Kontrec et al.[41] discussed the effect of nonionic additives, when dextran was utilized, the calcite was predominant and inhibited the growth rate of $CaCO_3$ resulting in a decrease in particle size.

2.6. Zeta potential of $CaCO_3$ and electrical double layer theory

The zeta potential, or electrodynamic potential, is the reflection of surface charge from a potential difference between the particles' surface and the dispersion liquid. It may be assessed in a variety of ways and is also used to estimate the electrical surface of suspended particles. As seen in Figure 2.5, the film or interface of the liquid layer is classified into two parts: the diffuse layer, which contains fewer bound ions, and the Stern layer which contains ions that are closely coupled to the particles' surfaces. The Stern's layer has the largest concentration of ions, whereas concentrations are very low at considerable distances from the particle surface[42]. The boundary is defined as the surface of the hydrodynamic slip or slip plane and is dependent on the non-slip conditions being used in the model development of the flowing fluid at the liquid-solids interface[43]. The particles that have low absolute value of the zeta potential are unstable and vulnerable to aggregate. The particles that have a high value of zeta potential are demonstrated as stable particles because they tend to repel each other. This value of zeta potential is ±30 mV[44]. The pH of suspended particles is a crucial factor that influences the value of zeta potential. When more acid is utilized to dissolve the suspended particles in aqueous media, the charge of zeta potential will be more likely to be positive. When base is utilized in increasing quantity, it will reach a point where it reaches the isoelectric point at which the net charge is zero[45]. Further addition of base will result in a negative charge on the surface and the zeta potential vale will be negative.

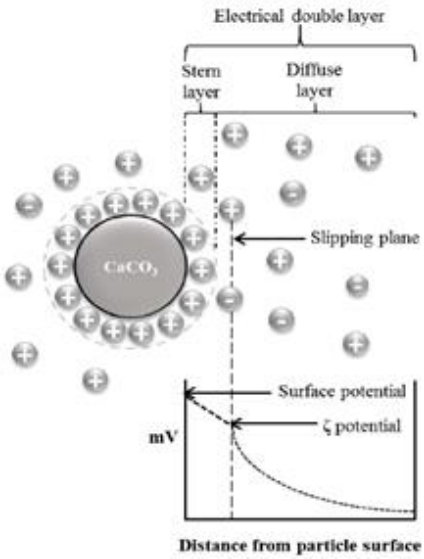

Figure 2.5. Electrical double layer of $CaCO_3$ particles[4742]

2.7. Problem Statement

The development of new possibilities for the synthesis of nanoparticle materials and the control of their size has been the subject of an increasing majority of research in recent decades[46]. As a consequence of technological studies revealing that nano-$CaCO_3$ may greatly enhance the mechanical and physical properties of composite materials in a range of applications[2,47]. Instances of such uses include using $CaCO_3$ nanoparticles in concrete to increase the mechanical durability of concrete[48], and in the medical field as a carrier particle for pharmaceuticals, genetic material, antiviral therapy, and other biotechnological applications[46,49]. The challenge here is the possibility of obtaining nano-$CaCO_3$ particles using the chemical method.

Crushing the ground calcium carbonate may reduce the particle size of $CaCO_3$ to about 1 micron[50], however, impurities from the natural sources would make the approach unattractive considering the medical and food sectors [46,49,51,52 21]. $CaCO_3$ particles have a rapid crystallization rate, which leads to an increase in their size growing once the chemical method is utilized in aqueous systems[41,53–55], which causes nano-$CaCO_3$ synthesis impossible under high supersaturation conditions.

2.8. Aim of the Study

The present study aimed at establishing a concrete knowledge on how certain cations such as sodium (Na^{+}), potassium (K^{+}), calcium (Ca^{++}), barium (Ba^{++}) and anions such as sulfate ($SO_4^{=}$), nitrate (NO_3^{-}), carbonate ($CO_3^{=}$) and bisphosphate ($HPO_4^{=}$) affect the $CaCO_3$ crystal formation, and develop a method to synthesize nano-$CaCO_3$ particles by the chemical method, which is rare or none in the current literature.

CHAPTER 3

MATERIALS AND METHODS

3.1. Materials

The reagents such as Na_2CO_3 (assay ≥ 99.5-100.5%, Sigma-Aldrich), $CaCl_2.2H_2O$ (assay ≥ 98%, Sigma-Aldrich), Barium hydroxide octahydrate ($Ba(OH)_2{\cdot}8H_2O$) (assay ≥ 98%, Merck), sodium hydroxide (NaOH) (assay ≥ 98%, Sigma-Aldrich), potassium hydroxide (KOH) (assay ≥ 85.0-100.5 % %, PanReac), hydrochloric acid (HCl) (37% w/w, Sigma-Aldrich), and acetone (CH_3COCH_3); assay ≥ 99%, Carlo Erba Reagents), Sodium phosphate dibasic (Na_2HPO_4) (assay ≥ 99.0%, Sigma-Aldrich), sodium nitrate ($NaNO_3$) (assay ≥ 99.0 - 100.5 %,Merck), sodium sulphate (Na_2SO_4) (assay ≥ 99.0 %,Merck), $Ca(OH)_2$ (assay ≥ 96.0 %) were all analytical grade and used as-received without further purification. Calibrations of pH and conductivity probes were carried out using the pH buffer and conductivity solutions. Solutions were prepared using ultrapure deionized water from the Milli-Q water purification system with a resistivity of 18.2 MΩ·cm.

3.2. Experimental Setup for a Semi-Batch Reactor

The experimental setup used in the $CaCO_3$ crystallization is shown in Figure 3.1. Unless otherwise mentioned, stock solutions of $CaCl_2$ and Na_2CO_3 were prepared in glass bottles and capped in order to seal from the atmospheric CO_2. The two solutions were send to a Tee valve through a peristaltic pump and mixed in a tubular tubing as a plug flow reactor (PFR). The retention time in the tubular reactor, defined as the ratio of the volume of the tubular reactor to the flow rate, was calculated to be 9 seconds, unless otherwise indicated. The content in the tubular reactor was fed into a 5-neck stirred reactor containing either DI water or a stabilizing solution. The stirred reactor was sealed from the atmosphere. Any pressure buildup was eliminated by attaching a balloon to the

reactor. The pH and conductivity in the stabilizing solution were monitored by the installed pH and conductivity probes through Orion 5-Star software application by a computer. Samples were taken at each minute or at the indicated time intervals.

In crystallization experiments, equimolar concentrations of calcium chloride ($CaCl_2$) and sodium carbonate (Na_2CO_3) were taken from stock solutions using a peristaltic pump at a constant flow rate of 7.5 mL/min each, mixed in a Tee valve, and reacted in a model tubular reactor. The total flow rate of the reaction mixture in the tubular reactor was maintained constant at 15 mL/min. Following contacting in the mixing tee, the reaction content including precipitated calcium carbonate, Ca^{++}, $CO_3^{=}$, and other ions such as $CaOH^+$, $CaHCO_3^+$, Na^+ and Cl^-, were poured into the 5-neck semi-batch reactor containing the stabilizing solution and stirred continuously. The experiment was run at atmospheric pressure and ambient temperature of 24±1 °C. The pH and conductivity of the stabilizing suspension were measured continuously using a glass pH electrode and a metallic conductivity probe attached to the Thermo Scientific Orion 5-Star meter. The Orion 5 Star meter software keeps a continuous record of the sensor's signals shown on the computer screen.

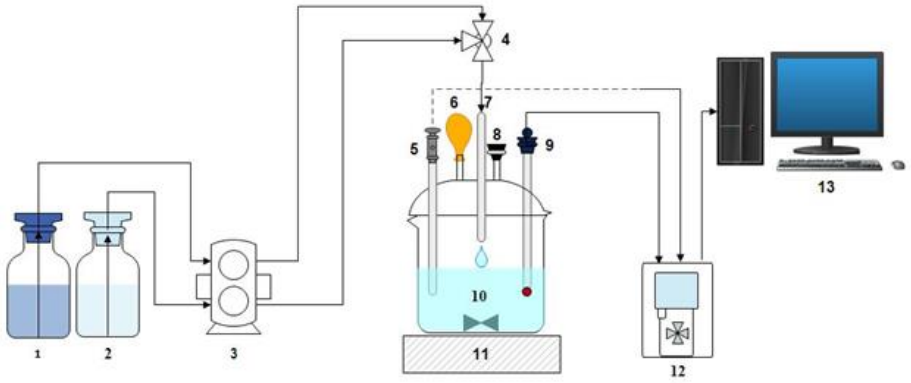

where: 1. Solution of $CaCl_2$ 2. Solution of Na_2CO_3; 3. Peristaltic pump; 4. Tee valve for mixing; 5. Conductivity probe; 6. A balloon.; 7. Tubular reactor; 8. The sample neck; 9. glass pH electrode; 10. 500 mL vessel with stabilizer solution; 11. Magnetic stirrer 12. Conductivity and pH meter; 13. Computer.

Figure 3.1. Semi-batch crystallization reactor

3.3. Experimental Setup for a Continuous Stirred Reactor (CSTR)

Nano-$CaCO_3$ particles were synthesized using a continuous stirred tank reactor as shown in Figure 3.2. In the developed set-up, a previously prepared $Ca(OH)_2$ solution was pumped into the CSTR reactor at a constant flow rate of 20 mL/min, synchronized with the withdrawal of $CaCl_2$ and Na_2CO_3 at 10 mL/min from each stock solutions. The reactant solutions were integrated with a Tee Valve. By-products of the crystallization occurring in the model tubular reactor (PFR) included precipitated $CaCO_3$ along with sodium, chloride, and otherf ions. Immediately after coming into contact with the mixing tee, the flow rate of the reaction mixture was kept constant at 20 mL/min and supplied into the CSTR, which also supplied with a constant flow rate of $Ca(OH)_2$ solution, constantly stirred at 500 revolutions per minute (RPM). The volumetric flow rate in the output of CSTR was maintained at 40 ml/min with the peristaltic pump. The pump was calibrated for the reactant flow rates and $Ca(OH)_2$ flow rate. A larger diameter pipe is used in the peristaltic pump to achieve higher flow rates. For the exit stream, a different pump was used at 40 ml/min flow rate in total. The experiment was run at ambient temperature of 24±1 ℃ and atmospheric pressure. The conductivity and pH of the stabilizing suspension was monitored continuously by the glass pH electrode and a metallic conductivity detector in the CSTR by using an Orion 5-Star pH and conductivity meter (Thermo Scientific, Inc.). The Orion 5-Star meter software keeps a continuous record of the sensor's signals on a computer screen as shown in Figure 3.2.

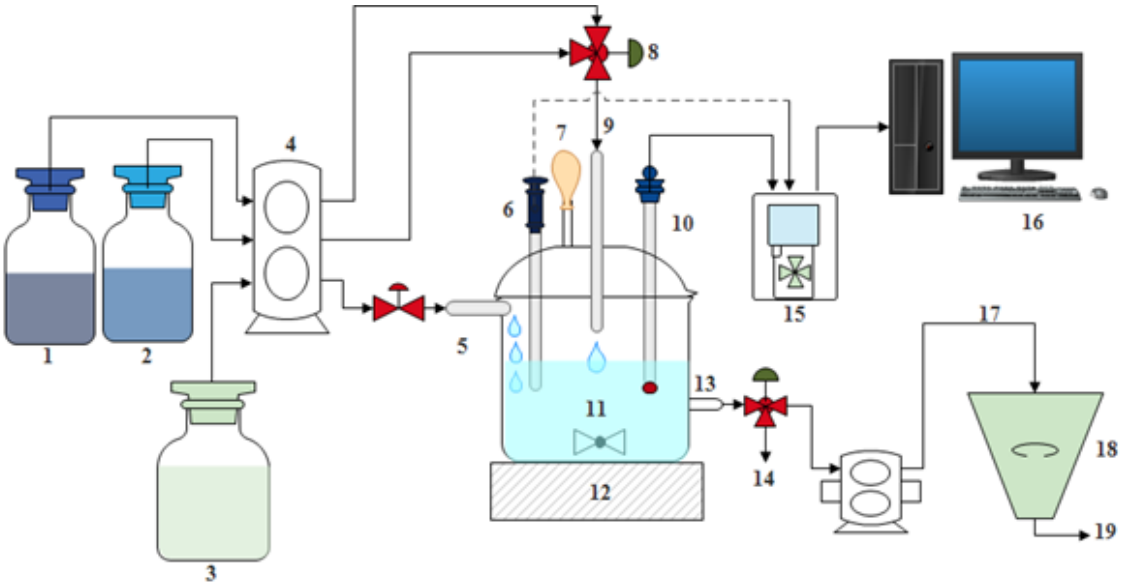

Where:1. Solution of $CaCl_2$ 2. Solution of Na_2CO_3; 3. Solution of Ca $(OH)_2$ 4. Peristaltic pump; 5. The input of Ca (OH)2; 6. Conductivity probe; 7. A balloon.; .8 Tee valve for mixing; 9. PFR as tubular reactor; 10. Glass pH electrode; 11. The CSTR with stabilizer solution of Ca $(OH)_2$; 12. Magnetic stirrer;13. The output of suspended solution; 14. The sample valve;15. Conductivity and pH meter; 16. Computer; 17. Suspended particles; 18. Centrifuges; 19. Produced Particles.

Figure 3.2. Continuous Stirred Tank Reactor (CSTR) for nano-$CaCO_3$ production by the chemical method

3.4. Experimental Variables Studied

The main experimental parameters studies were listed in Table 3.1. The effect of anions, cations, concentration of reactants, concentration of stabilization solution, pH of Na_2CO_3 as the stabilizing solution, pH of Na_2CO_3 in the reactant solution, and the ratio of Ca^{++} and $CO_3^{=}$ ion concentrations were studied.

Table 3.1. The parameters studied

Parameter	Range
Anions	$CO_3^{=}$, NO_3^{-}, $PO_4^{=}$, $SO_4^{=}$
Cations	Ca^{++}, Ba^{++}, Na^{+}, K^{+}
Reactor type	Semi-Batch and CSTR
Concentration of Reactants (CR)	4-160 mM
Concentration of stabilizing solution (Cs)	0-15 mM
Space time	9 seconds - 2 mins
The pH of Na_2CO_3 as stabilizing solution	7.5-12
The pH of Na_2CO_3 in reactant solution	7-12
Volumes of solutions	30-250 ml
Collected time of $CaCO_3$ particles	5 min-1 hours
$[Ca^{++}]/[CO_3^{=}]$ Ratio	10%-100%

3.6. Particle Characterization

Particle size and zeta potential of particles were determined with dynamic light scattering (DLS) using Nano-ZS (ZEN3600, Malvern) instrument. Samples with a volume of 1 ml were withdrawn for each minute and average particle size, particle size distribution, and particles' zeta potential values were estimated. Malvern Nano-ZS instrument can detect particle sizes ranging from 0.3 nm to 10 µm. The Zeta potential values were measured using a hybrid measuring method including the principles of Laser Doppler Velocimetry (LDV) and Laser Doppler Electrophoresis (LDE). The results were auto calculated and recorded by its software on the computer.

In order to detect the effect of Ba^{++} on the $CaCO_3$ crystal synthesis, the concentrations of ions in the stabilizing solution were estimated using the Thermo Scientific Dionex ICS 5000+ instrument to perform Ion Chromatography and Elemental Analysis with ICP-OES Quantitation. Samples were taken from the stabilization solution at each minute and passed through a 0.22 µm membrane filter to separate the suspended particles from the rest of the liquid solution. The instrument works on the concept of

excited atoms and ions with wavelength characteristics that are unique to each element. The same instrument was used to continuously measure the concentrations of Ba^{+2}, Na^{+}, and Ca^{+2} in suspension solution with conductivity detection at each time interval.

The crystalline form and the morphologies of the solid particles were characterized using X-ray diffraction (XRD) and scanning electron microscope (SEM), respectively. Samples were withdrawn from the suspension and centrifuged to separate the particles from solutions at each minute to ensure there were enough samples for analysis. The solid particles were then washed with pure acetone and vacuum-dried for overnight at 85 ^{o}C to remove any remaining moisture. An X-ray diffraction (XRD) analysis with Cu-K radiation was used to determine the forms of particles. There was a step size of 0.013 degrees between the 2θ scans, with a range of 10 to 80 degrees. The Rietveld technique was used to enhance the data using X'Pert Highscore Plus and to refine the diffraction data in order to determine the relative quantity of each crystalline phase in the samples. The scanning electron microscope (SEM) (Carl Zeiss 300VP) was used to study the morphologies of the particles. The particles were gold-coated before imaging and their images were recorded at multiple magnifications.

CHAPTER 4

RESULTS AND DISCUSSION

4.1. Chemical Synthesis of $CaCO_3$

Calcium carbonate, $CaCO_3$, can be synthesized by chemical method using $CaCl_2$ and Na_2CO_3 as reactants. $CaCO_3$ particles were synthesized using our developed experimental set up shown in Figure 3.1 with different concentrations of $CaCl_2$ and Na_2CO_3 from 20 mM up to 160 mM each. Samples were taken at the exit of the tubular plug flow reactor after 9 seconds of crystallization time, centrifuged for 20 minutes, dried in the oven overnight, and obtained their SEM images. Figure 4.1.(a) shows the produced $CaCO_3$ particles at increasing reactant concentrations with a 30 μm magnification. Figure 4.1.(b) shows the average sizes of these particles. And, Figure 4.1.(c) shows their XRD patterns indicating their crystal forms. As shown in the figure, the particle sizes are always larger than 3 μm produced from the chemical method. Vaterite and calcite forms were discerned. ACC forms are hardly seen or detected since the crystallization time was 9 seconds and centrifugation time was 20 minutes, therefore, it was expected that the ACC forms were almost totally converted to vaterite or calcite as indicated in Figure 2.4.

The newly synthesized $CaCO_3$ particles were added into DI water for stabilization. Figure 4.2.(a) shows the SEM images of the newly synthesized $CaCO_3$ particles from 75 mM and 60 ml of $CaCl_2$ and Na_2CO_3 each. These particles are composed of vaterite and calcite with sizes larger than 3 μm. Figure 4.2.(b) shows the stabilization of these particles in 250 ml of DI water for stabilization. The XRD peaks (data not shown) were identical for these two images indicating vaterite and calcite polymorphic forms of $CaCO_3$. As can be seen in the figure, the number of vaterite forms in the water stabilized SEM image is seen highly increased comparing to the particles produced in the tubing indicating that these particles are still converting to each other. It took about 8 minutes to add 60 ml of one reactant solution to the tubular reactor with a flow rate of 7.5 ml/min and a total of 15 ml/min for both reactant solutions. The change in pH and conductivity in the DI water were shown in Figure 4.2.(c) during $CaCO_3$ stabilization.

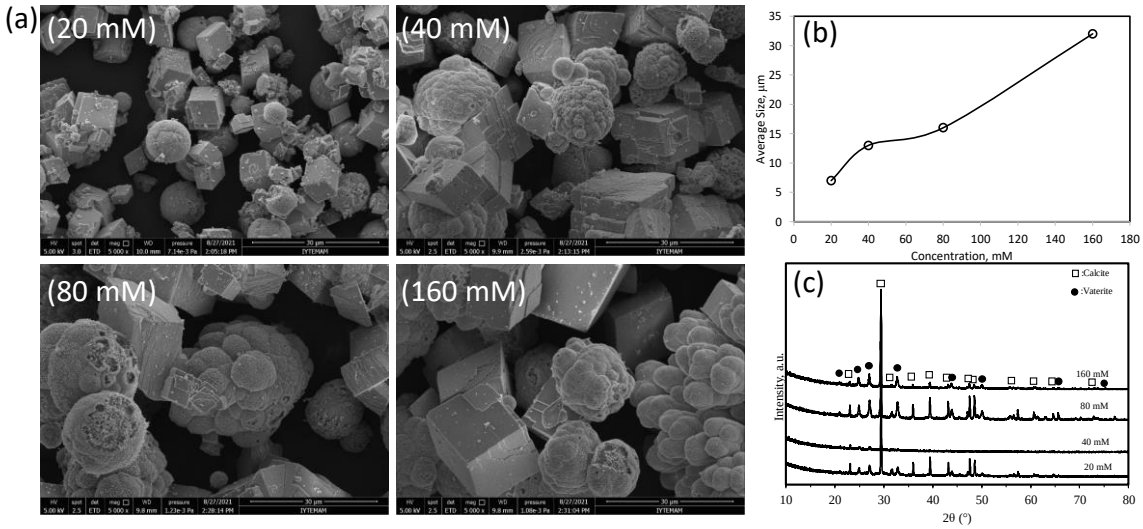

Figure 4.1. (a) Chemical synthesis of $CaCO_3$ in tubular plug flow reactor, (b) average particles size with increasing reactant concentrations, (c) crystal forms of these particles.

The pH was bout 6.3 for the DI water initially and it suddenly jumped to 9.8 upon addition of the newly synthesized $CaCO_3$ particles. Conductivity also increased as particles were added to the DI water. Steady increase in conductivity and pH with the addition of newly synthesized particles indicated an increase in the Ca^{++}, OH^- and $CO_3^=$ ions in the DI water. It is interesting to note that when addition was stopped at the 8th minute, the conductivity was seen still increasing for almost 2 minutes and then started to decrease indicating that the newly synthesized $CaCO_3$ particles dissolved and reprecipitated. When the SEM image and the decrease in pH and conductivity were considered together, it is clear that these newly synthesized particles were dissolved and reprecipitated into more vaterite particles, and therefore, the number of vaterite particles were increased.

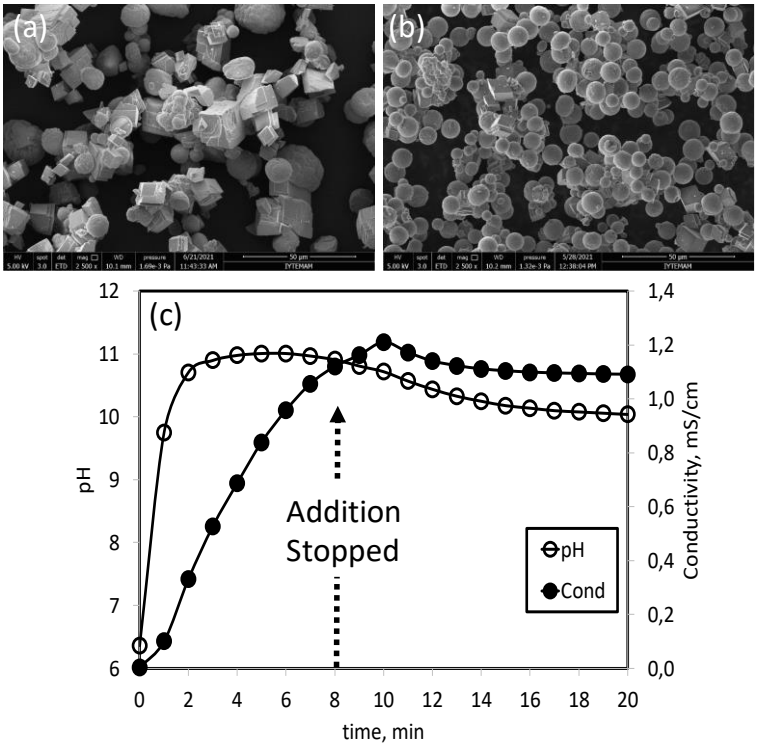

Figure 4.2. SEM images of (a) newly synthesized $CaCO_3$ particles, (b) stabilized in DI water, and pH and conductivity changes in the DI water during $CaCO_3$ stabilization.

4.2. Effect of Anions on Precipitated $CaCO_3$

In order to understand more about the effects of anions on freshly precipitated $CaCO_3$, four anions such as $HPO_4^{=}$, $CO_3^{=}$, $SO_4^{=}$, and NO_3^{-} were investigated. Both $CaCl_2$ and Na_2CO_3 with 25 mM and 60 ml each were reacted in the PFR tubular reactor with a total flow rate of 15 ml/min and the newly synthesized $CaCO_3$ particles were sent to the stabilization tank containing 10 mM and 250 ml of the indicated stabilizing solution. pH and conductivity of the stabilizing solutions were monitored. Samples were taken at each minutes and average size and zeta potential values were measured. One milliliter of samples was withdrawn from the stabilization solutions within the semi-batch reactor at the end of one hour and XRD patterns and SEM images were obtained.

Figure 4.3 is pH and conductivity change in stabilizing solution containing sodium salts of these anions. As can be seen in the figure, $CO_3^{=}$ ion seems ineffective on the newly synthesized $CaCO_3$ particles, during which neither pH nor conductivity changed

up on addition of particles. pH of the $SO_4^{=}$ and NO_3^{-} solutions was about 5.73 initially and it suddenly jumped to about 10.2 altogether. Conductivity also slightly increased for these two anions. However, the pH almost slightly increased with $HPO_4^{=}$ ion from 4.6 to 5.9 and did not change afterwards.

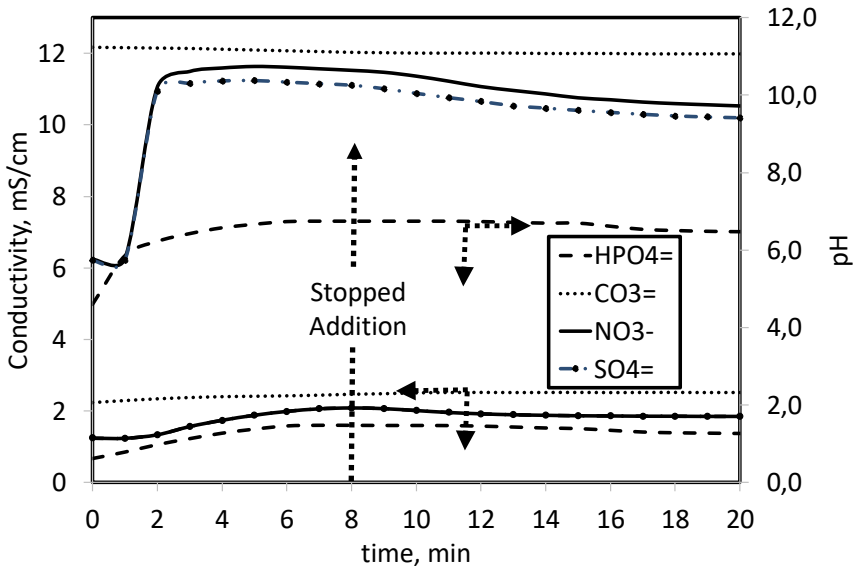

Figure 4.3. pH and conductivity change in stabilizing solution containing sodium salts of anions.

Figure 4.4 shows the average particle size and zeta potential for the CaCO3 particles stabilized in solutions containing sodium salts of anions of $HPO_4^{=}$, $CO_3^{=}$, $SO_4^{=}$, and NO_3^{-}. As shown in Figure 4.4. (a), the stabilization solutions had some impurities as such the initial average particle size ranged from ~500 nm up to 1.4 µm, confirming the presence of 1% contaminants as inorganic salt impurities. The five-minute dispersion of $CaCO_3$ particles in each anionic liquid was demonstrated. Particle sizes changed slightly for 2 minutes for the addition of newly synthesized $CaCO_3$ into the stabilization solution. As more $CaCO_3$ precipitates were dispersed, the average particle size increased over time in anionic solutions from about 1 µm to about 3.5 µm. While using $SO4^{=}$ ions as stabilizer, the largest hydrodynamic sizes of about 4 µm were obtained.

The zeta potential of the particle varies over time during $CaCO_3$ precipitation in stabilizer solutions, as shown in Figure 4.4.(b). Zeta potential values was negative in all of the stabilizing solutions containing anions. The zeta potential values for CaCO3 particles were -7 mV for $HPO_4^{=}$and NO_3^{-} anions, -10 mV for $SO_4^{=}$, and about 20 mV for $CO_3^{=}$ anion. In each of the cases studied, the presence of impurity ions has an effect on

the zeta potential of calcium carbonate particles[56]. In the case of the carbonate ion, when freshly precipitated $CaCO_3$ was added to an existing $CO_3^{=}$ ion solution, more $CO_3^{=}$ was adsorbed to the surface of the calcium carbonate layer, decreasing the zeta potential and increasing its negative value. Moreover, the zeta potential of $CaCO_3$ decreased over time from approximately -5 mV to -22 mV, which is in accordance with a previous study in which the zeta potential of $CaCO_3$ decreased from -10mV to -25 mV when excess $CO_3^{=}$ was present[51]. Particles in anionic environment seem to have a negative surface charge due to the adsorption of these ions on their surfaces.

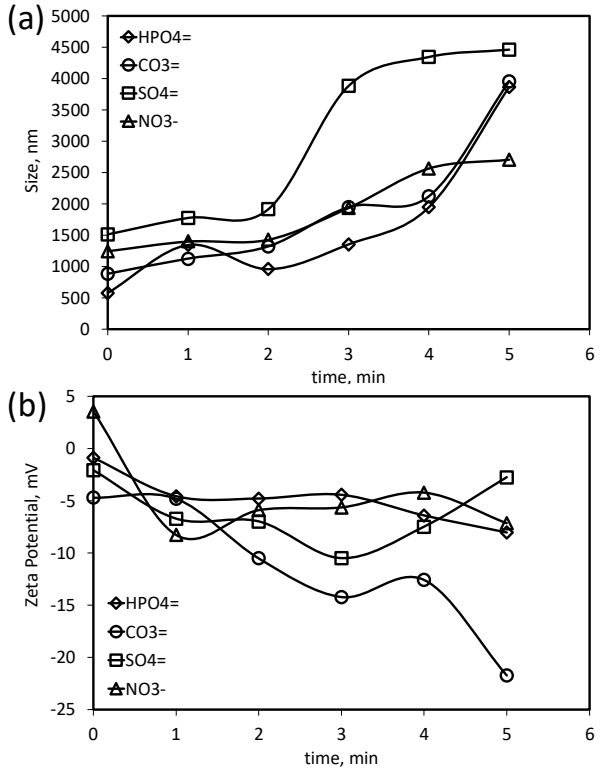

Figure 4.4. (a) Average particle size and (b) zeta potential for the $CaCO_3$ particles stabilized in solutions containing sodium salts of anions of $HPO_4^{=}$, $CO_3^{=}$, $SO_4^{=}$, and NO_3^{-}.

Figure 4.5 shows the SEM images of precipitated $CaCO_3$ particle stabilized in solutions containing sodium salts of anions of $HPO_4^{=}$, $CO_3^{=}$, NO_3^{-}, and $SO_4^{=}$. As shown in the figure, the image obtained in the solution containing $HPO_4^{=}$ ions are different than the images obtained from $CO_3^{=}$, NO_3^{-}, and $SO_4^{=}$ solutions. When the particles were analyzed with the XRD patterns as shown in Figure 4.6, the particles seen in Na_2HPO_4 were seen to be rod-like monetite and plate-like hydroxylapatite obtained as a result of fully dissolution of $CaCO_3$ particles at the initial low pH of 4.6 and then react with the

$HPO_4^{=}$ ions to crystallize into these new crystal forms. There is no effect on $CaCO_3$ particles in $CO_3^{=}$, NO_3^{-}, and $SO_4^{=}$ solutions and appeared as spherical vaterite and cubical calcite.

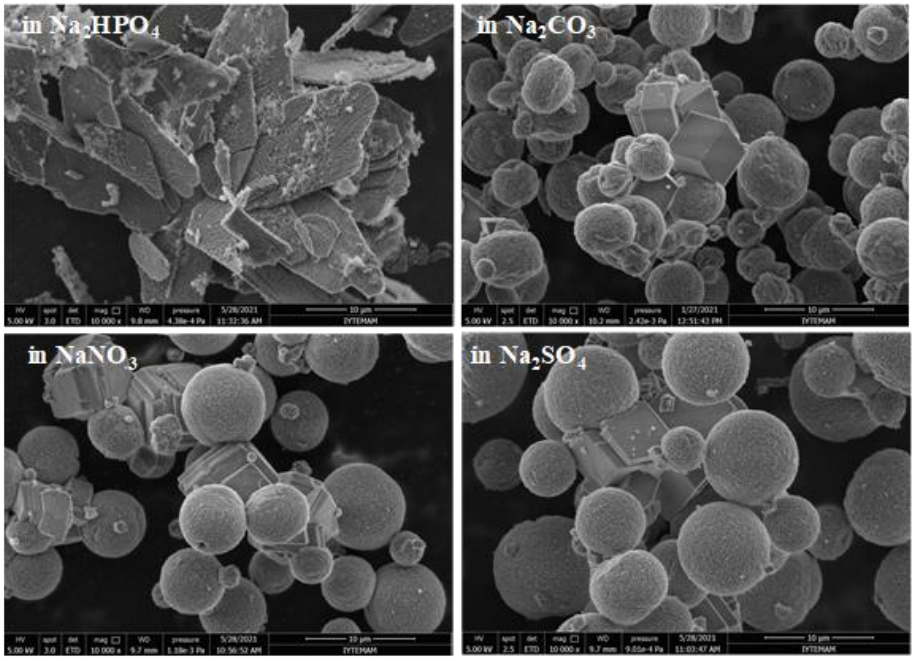

Figure 4.5. SEM images of precipitated $CaCO_3$ particles stabilized in solutions containing sodium salts of anions of $HPO_4^{=}$, $CO_3^{=}$, NO_3^{-}, and $SO_4^{=}$.

Figure 4.6 shows the XRD patterns and the percent crystal forms of precipitated $CaCO_3$ stabilized in solutions containing sodium salts of anions of $HPO_4^{=}$, $CO_3^{=}$, NO_3^{-}, and $SO_4^{=}$. It is clearly seen that 77% of monetite and 23% of hydroxylapatite forms when $CaCO_3$ particles were stabilized in $HPO_4^{=}$ solution. The $CO_3^{=}$ ions enhance vaterite formation over calcite or inhabit the vaterite to calcite transformation such that 70% of vaterite and 30% of calcite formed in the $CO_3^{=}$ solution. From vaterite to calcite transformation increased in NO_3^{-}, and $SO_4^{=}$ solutions, respectively.

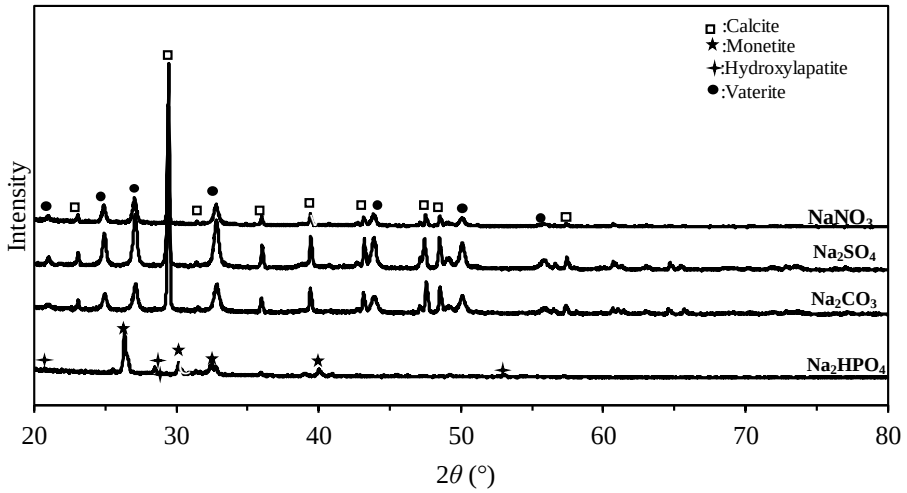

10mM of Anions	Calcite %	Vaterite %	Monetite %	Hydroxylapatite %
$HPO_4^{=}$	-	-	77	23
$CO_3^{=}$	30	70	-	-
$SO_4^{=}$	56	44	-	-
NO_3^{-}	65	35	-	-

Figure 4.6. XRD patterns of precipitated $CaCO_3$ particles stabilized in solutions containing sodium salts of anions of $HPO_4^{=}$, $CO_3^{=}$, NO_3^{-}, and $SO_4^{=}$.

4.3. Effect of Cations on Precipitated $CaCO_3$

The effects of cations on the freshly precipitated $CaCO_3$ were investigated using the OH^- ions of NaOH, KOH, $Ca(OH)_2$, and $Ba(OH)_2$. The starting concentrations of $CaCl_2$ and Na_2CO_3 were 25 mM and their volume were 60 ml each. Both reactants were send to the PFR tubular reactor with a flow rate of 7.5 ml/min and a total flow rate of 15 ml/min. The residence time were calculated to be 9 seconds for the crystallization in the tubular reactor. The newly synthesized $CaCO_3$ particles were added directly to the stabilization tank containing 250 ml of cationic stabilization solutions with a concentration of 10 mM. Therefore, the effect of Na^+, K^+, Ca^{++}, and Ba^{++} on the newly synthesized $CaCO_3$ particles were investigated. pH and conductivity of the stabilizing

solutions were monitored. Samples were taken at each minutes and average size and zeta potential values were measured with the DLS method. Samples of 1 ml were withdrawn from the stabilization solutions within the semi-batch reactor at the end of 1 hr and XRD patterns and SEM images were obtained.

Figure 4.7 shows the pH and conductivity change in stabilizing solution containing hydroxyl forms of these cations. As can be seen in the figure, Ca^{++}, and Ba^{++} ions showed very slightly decrease in conductivity or almost insensitive to the conductivity change, however, decrease in pH were discerned upon addition of particles in these solutions containing Ca^{++}, and Ba^{++} ions. There was slight increase in conductivity and decrease in pH for stabilizing solutions containing Na^{+} and K^{+} ions indicating that there were dissolutions and increase in Ca^{++} ions as well as consumption in OH^{-} ions upon addition of $CaCO_3$ particles in the stabilization solutions.

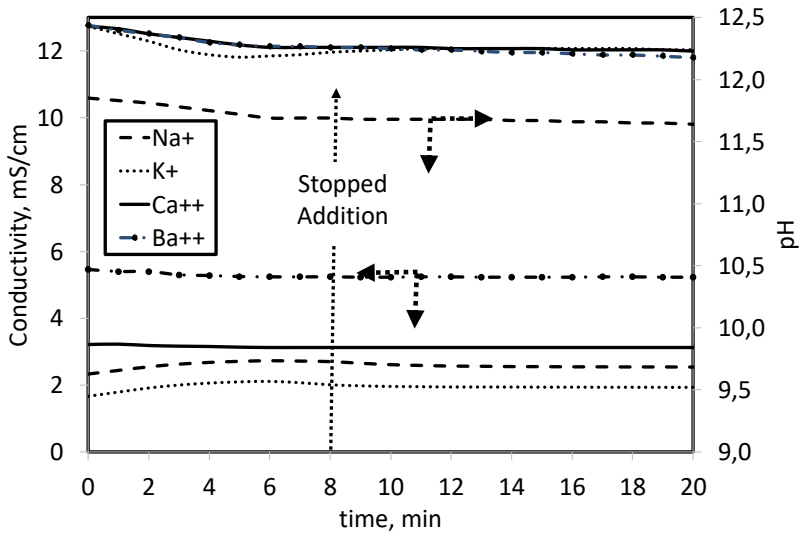

Figure 4.7. pH and conductivity change in stabilizing solution containing OH^{-} ions of cations.

Figure 4.8 shows the average particle size and zeta potential for the $CaCO_3$ particles stabilized in solutions containing hydroxyl forms of Na^{+}, K^{+}, Ca^{++}, and Ba^{++} ions. As shown in Figure 4.8(a), the stabilization solutions had some impurities as such the initial average particle size ranged from ~300 nm up to 1.4 μm, confirming the presence of impurities. The particle sizes changed slightly for 2 minutes for the addition of newly synthesized $CaCO_3$ into the stabilization solutions. As more $CaCO_3$ precipitates were dispersed, the average particle size increased over time in cationic solutions about 2.5 μm in 5 minutes except for the Ca^{++} ions. According to the findings shown in the

figure, the particle size of the freshly dispersed $CaCO_3$ was more than 2 μm in diameter and the particle size became larger when the Na^+, K^+, and Ba^{++} ions were used. However, submicron sized $CaCO_3$ particles ranging from 300 nm to 500 nm were obtained when Ca^{++} ions were in the stabilization solution. It is obvious that there was a significant size difference when $CaCO_3$ particles were stabilized in the stabilization solution containing Ca^{++} ions.

The zeta potential of the particle almost unchanged over time during $CaCO_3$ precipitation in stabilizer solutions, as shown in Figure 4.8(b). Zeta potential values stayed negative in the stabilizing solutions containing Na^+ and K^+ ions and the zeta potential were positive for Ca^{++} and Ba^{++} ions. The zeta potential value was about -7 mV for the stabilization solution containing K^+ ion, -20 mV that for Na^+ ion, about +12 mV that for Ba^{++} ion, and about +24 mV that for Ca^{++}ion. The zeta potential of precipitated $CaCO_3$ surfaces almost unchanged in each of the calcium or barium ions, and the positive zeta potential of the $CaCO_3$ particles was detected, which agreed with[1,44,56–58] that the Ca^{+2} and Ba^{+2} have a propensity to adsorb on the surface of calcium carbonate. In the case of sodium and potassium ions, results showed that they have a poor or negligible affinity for adsorption on the surface of $CaCO_3$, lowering their zeta potential and increasing their negative value, which was consistent with the previous findings[58]. The capacity to aggregate (become unstable) is greater when the absolute value of the zeta potential is low, whereas particles with a high zeta potential were shown to be stable due to their tendency to repel one another when the zeta potential is greater than ±30 mV[44]. One element affecting particle aggregation is the solution's saturation concentration. Other critical variables include temperature and chemical composition[59]. When Na^+ and K^+ were present, the particles aggregated (becoming unstable), but when Ba^{++} was present, they aggregated uniformly throughout the particle size range due to a chemical reaction between Ba^{++} and $CaCO_3$, resulting in the formation of Barytocalcite, a new material. It seems that particles in cationic environment seem to have a positive surface charge due to the adsorption of these ions on their surfaces.

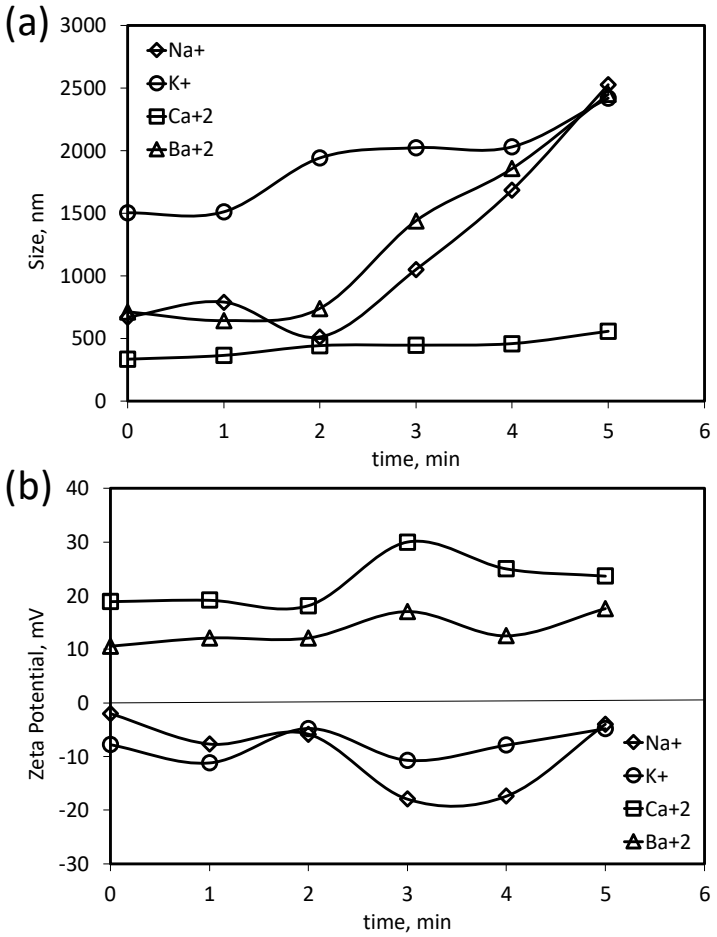

Figure 4.8. (a) Average particle size and (b) zeta potential for the $CaCO_3$ particles stabilized in solutions containing hydroxyl form of cations of Na^+, K^+, Ca^{++}, and Ba^{++}.

The SEM images of precipitated $CaCO_3$ particle stabilized in solutions containing hydroxyl form of cations of Na^+, K^+, Ca^{++}, and Ba^{++} were shown in Figure 4.9. As shown in the figure while anion stabilizers had a minimal impact on the size and morphology of $CaCO_3$, cations had a substantial effect on both the size and morphology. The presence of hydroxyl ions in the solution contributed to the transition of $CaCO_3$ into the formation of a stable form at high pH values[1,60] When Na^+ and K^+ ions were employed as stabilizer in solutions, the SEM and DLS findings indicated that the particles were larger than 3 μm in size, and calcite crystals with an asymmetrical morphology, in excellent agreement with earlier findings[61]. When Ca^{++} ions were present, the average particle size was about less than 400 nm. It can be seen from the SEM images that nano-$CaCO_3$ particles could be synthesized in $Ca(OH)_2$ solution as the stabilizer[5].

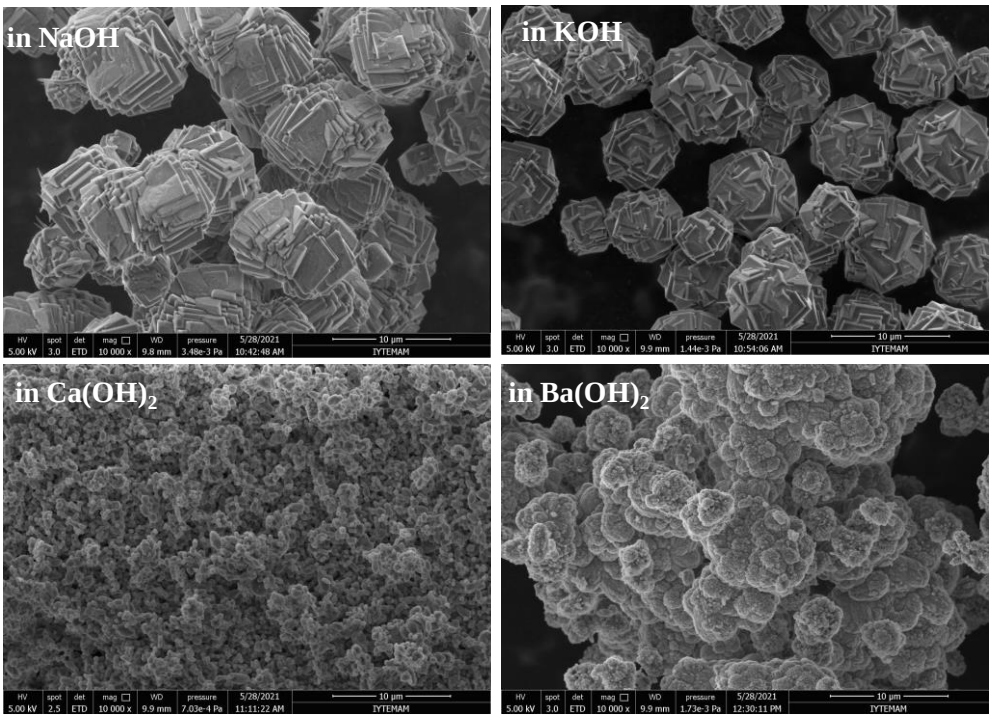

Figure 4.9. SEM images of precipitated $CaCO_3$ particles stabilized in solutions containing hydroxyl form of cations of Na^+, K^+, Ca^{++}, and Ba^{++}.

Figure 4.10 shows the XRD pattern of the particles obtained in the stabilization solutions containing Na^+, K^+, Ca^{++}, and Ba^{++} cations. the only form present was calcite in the instances of Na^+, K^+, and Ca^{++}. Whereas when Ba^{++} ions were utilized, precipitated calcium carbonate was mainly converted to 81% of Barytocalcite and 10% of witherite of $BaCO_3$, a compound with a size larger than 3µm and aggregated.

It can be suggested that when certain ions such as Ba^{++} or Ca^{++} ions were added to the freshly precipitated $CaCO_3$, the particles, larger than 3 µm, dissolves in the solution and then recrystallizes to a different size and morphology, a process known as post-precipitation. The overabundance of the free ions might adsorb on the surface of the $CaCO_3$ particles, thus delaying their growth while boosting the nucleation rate, which results in the formation of smaller particles. However, when Ba^{++} ions were used, another unique compounds were formed such as barytocalcite and witherite[57].

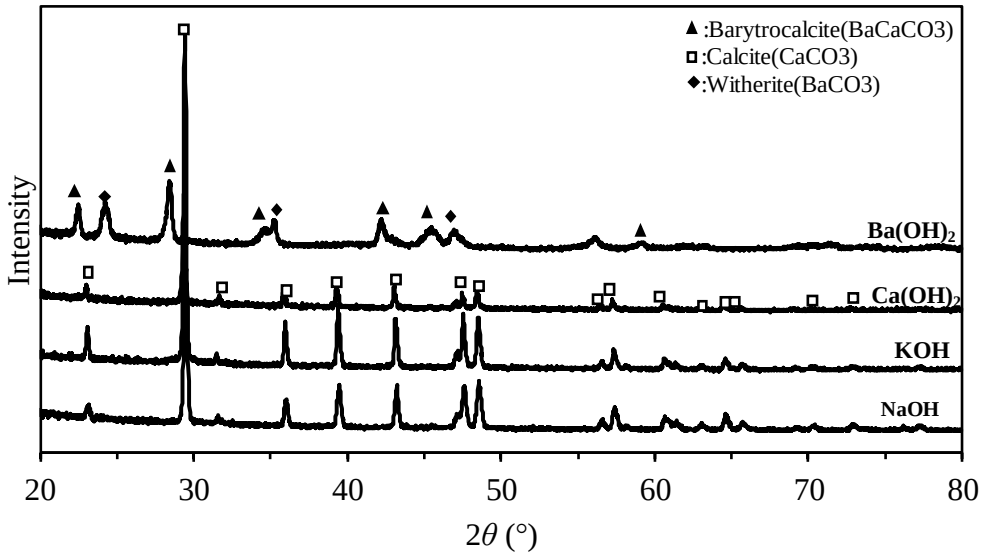

10mM of Cations	Vaterite %	Calcite %	Barytocalcite %	Witherite %
Na^{+}	-	100	-	-
K^{+}	-	100	-	-
Ca^{+2}	-	100	-	-
Ba^{+2}	-	9	81	10

Figure 4.10. XRD patterns and crystal refinement results of precipitated $CaCO_3$ particles stabilized in solutions containing hydroxyl form of cations of Na^{+}, K^{+}, Ca^{++}, and Ba^{++}.

4.4. Effect of pH Variation in Reactant Na_2CO_3 Solution on $CaCO_3$

It is important to know which variables influence the precipitated $CaCO_3$ crystallization process, the polymorphism, and the final form of the crystal. The main parameters could be super saturation, pH, additive concentration, and temperature [1,60]. In most previous studies, the pH was shown to strongly influence the $CaCO_3$ polymorphism[62]. Here, the effects of pH variations in reactant Na_2CO_3 solution were studied on the development and shape of $CaCO_3$ particles using our set-up. The pH of the Na_2CO_3 solution was adjusted by concentrated 5 M of HCl and 1 M of NaOH and varied

from 7.5 up to 12, whereas the pH of the $CaCl_2$ solution unchanged. Both solutions containing 75 mM and 60 mL each were reacted in a PFR tubular reactor with a space-time of 9 seconds before being distributed in a stirred reactor containing DI water having a volume of 250 mL.

Adjusting the pH of Na_2CO_3 resulted in several new ions for $CaCO_3$ crytstallizations. For instance, dissolution of Na_2CO_3 produced Na^+ ion and $CO_3^=$ ion at the same time as shown in Eq.(4.1). Adding more HCl to the solution converts $CO_3^=$ ion into HCO_3^- ion as shown in Eq.(4.2). When HCl was continued to be added, the HCO_3^- ions became converted into CO_2 as shown in Eq.(4.3). However, since the pKa for HCO_3^- /CO_2 is about 6.3, the formation of CO_2 seems to be rare. Therefore, there are HCO_3^- ions which would be effective at low pHs and $CO_3^=$ ions which would be effective at higher pHs.

$$Na_2CO_{3(aq)} \leftrightarrow 2\ Na^+ + CO_3^= \quad (4.1)$$

$$CO_3^= + H^+ \leftrightarrow HCO_3^- \quad (4.2)$$

$$HCO_3^- + H^+ \leftrightarrow CO_2 + H_2O \quad (4.3)$$

Figure 4.11 shows the ionic species in a Na_2CO_3 solution at different pHs. When Na_2CO_3 solution was prepared, the pH was about 11.3. In order to increase pH to 12, concentrated NaOH solution of 1 M was added and considered in the PHREEQC calculations. For lower pHs, concentrated HCl solution of 5 M was added to the Na_2CO_3 solution and considered in the PHREEQC calculations. Because the value for the Cl- ion is so small, about $2.61.10^{-17}$ molality, therefore, it is not included in the figure. As shown in the figure, $CO_3^=$ ions almost totally converted into HCO_3^- ions at lower pHs. When the pH increases, both $CO_3^=$ ions and HCO_3^- ions are present and these ions also make complexes with Na^+ ions to form $NaCO_3^-$ ion and $NaHCO_3$ ion although the $NaHCO_3$ ion is pretty low in quantity. At higher pHs, there are Na^+, $CO_3^=$, $NaCO_3^-$, and OH^- ions, which were thought to be effective in $CaCO_3$ crystallization.

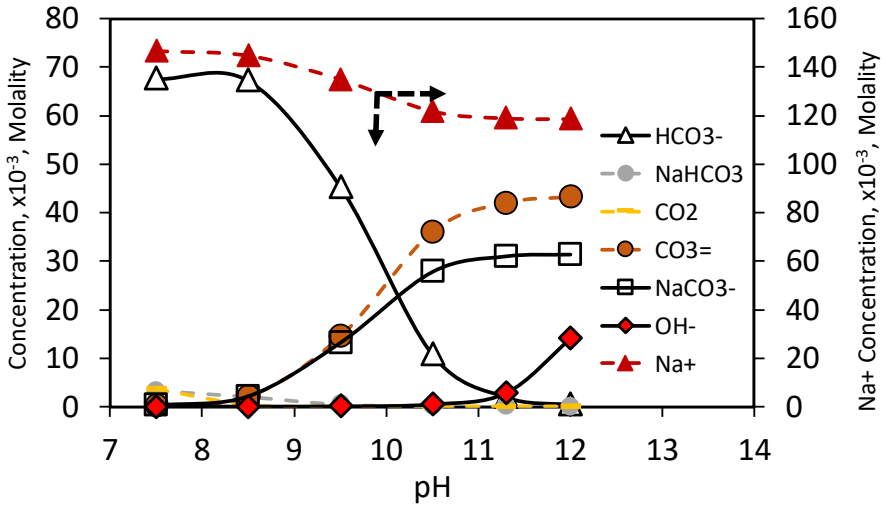

Figure 4.11. The ionic compositions in 75 mM of Na_2CO_3 solution at different pH adjusted by concentrated HCl and NaOH solutions estimated by the PHREEQC program.

The Na_2CO_3 solutions at different pHs shown in Figure 4.11 above was mixed with $CaCl_2$ solution in a PFR tubular reactor, crystallized during the retention time of 9 seconds, and added into DI water as the stabilization solution in a semi-batch reactor. The PHREEQC program was used to estimate the saturation index of $CaCO_3$ under ambient conditions as a function of the 8-minute process time as shown in Figure 4.12. As shown in the y-axis of the figure, the saturation index values were higher than 1.0 at all pHs including at pH 7.5. When they first added into the DI water at a flow rate of 15 ml/min, they undergo a dilution, therefore, their SI index became lower than 1.0. It was expected that the initial particles dissolved in the solution and no crystallization was seen. Indeed, there was a clear solution in the semi-batch reactor initially, and up to 2 minutes when pH was 7.5, then became a white precipitate was observed. At high pHs, this stage was very short. Decrasing the supersaturation may dominate the nucleation of calcite particles. Kranj at al.[59] suggest that when the pH and supersaturation decrease, calcite predominates, facilitating the nucleation of stable crystal forms. They found that recently created nuclei keep growing at greater supersaturation degrees following nucleation[63].

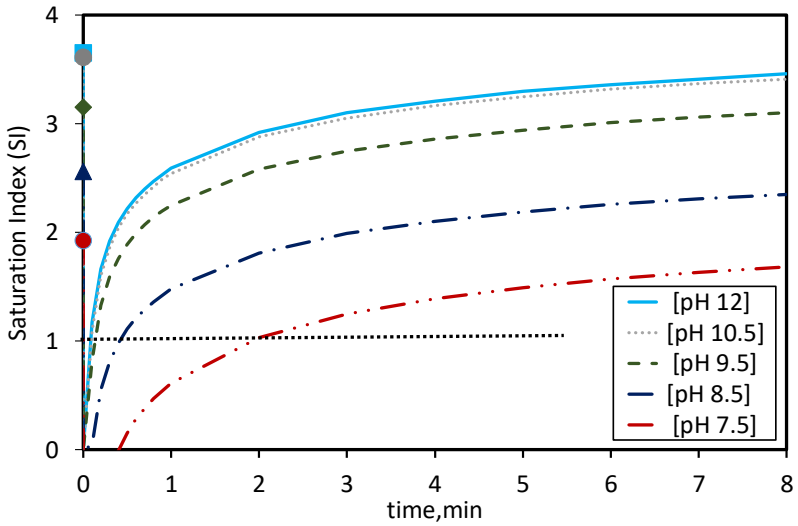

Figure 4.12. Changes in saturation index over time in the semi-batch reareacor containing DI water as the stabilization solution with varied pH of Na_2CO_3 solution using PHREEQC program.

The ionic compositions in the semi-batch reactor for crystallization at different pH values of Na_2CO_3 solutions were given in Figure 4.13 as estimated by the PHREEQC program. The Na^+ ion was almost 74.10^{-3} molality in the PFR tubular reactor, which was shown in y-axis in the figure, and its concentration dropped to about zero at the beginning of the dispersion in the DI water as the stabilization solution and steadily increased as more crystallization medium was added. The concentration of HCO_3^- ion is higher at lower pHs and it diminished at higher pHs. On the contrary, there was no $CO_3^=$ ions at lower pHs and it appeared in the stabilization solution at higher pHs. The Ca^{++} ions were higher at lower pHs and it was persistently present in the solution at also higher pHs with a decreasing concentrations. Interestingly, an uncharged form of $CaCO_3^o$ complex appeared at pHs greater than 8.0 and its concentrations increased pH icreased. The concentration of $CaHCO_3^+$ ion is higher at lower pHs and diminishes as pH increased. The concentration of $NaCO_3^-$ ion is increased as pH increased. It was clearly shown from the PHREEQC calculations that the crystallization medium contained mostly Na^+, Ca^{++}, HCO_3^-, $CaHCO_3^+$ at lower pHs. On the other hand, Na^+, Ca^{++}, $CO_3^=$, CaCO3^o, HCO_3^-, $NaCO_3^-$, OH^- ions are mostly contained by the crystallization medium at higher pHs. We believe that these ions are effective in synthesizing different forms of $CaCO_3$ such as ACC, aragonite, vaterite, and/or calcite.

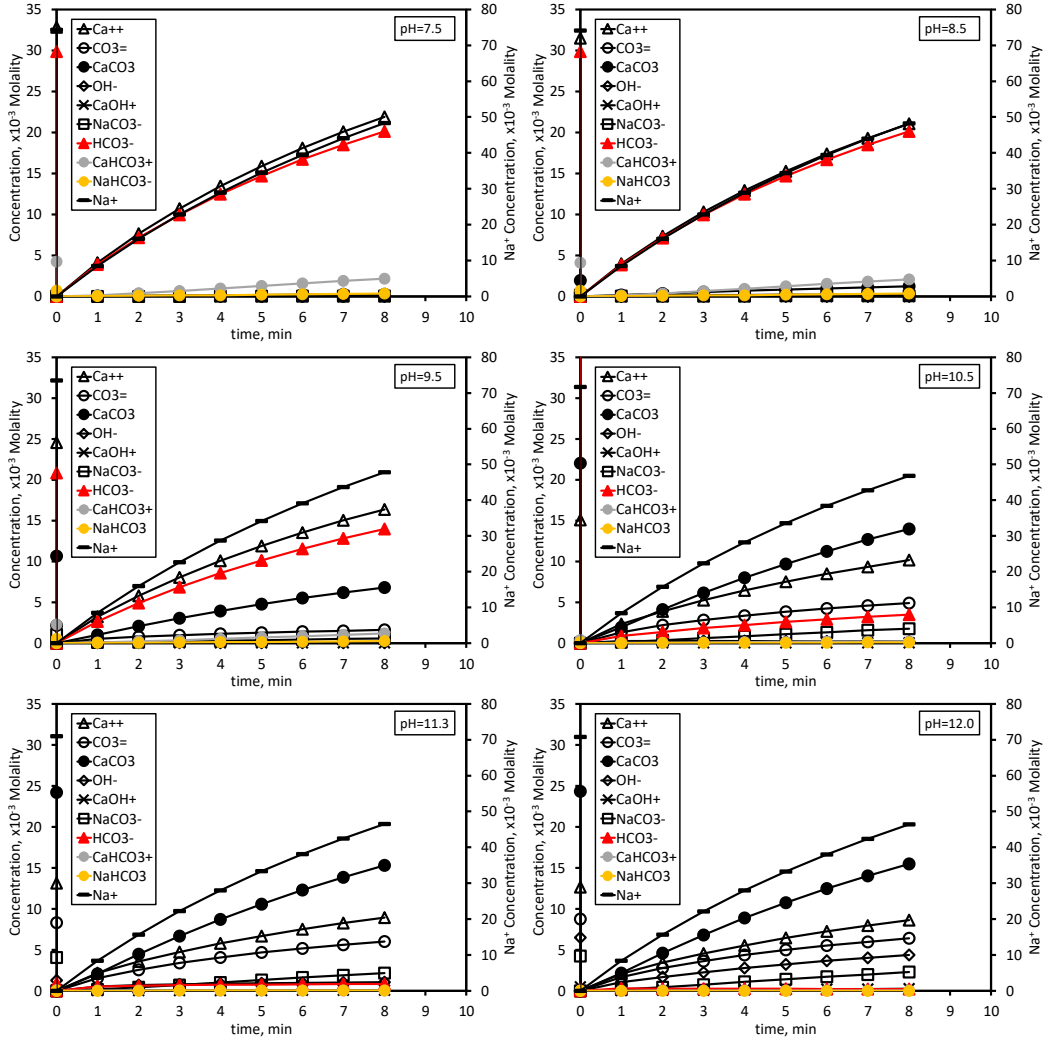

Figure 4.13. The ionic compositions in semi-batch stabilization solution after additions from the PFR tubular reactor contained $CaCl_2$ solution and Na_2CO_3 solution which is at different pH estimated by the PHREEQC program.

Figure 4.14 shows the pH and conductivity changes of 250 ml of DI water used as stabilizer solution in the semi-batch reactor for the $CaCO_3$ particles formed by mixing of Na_2CO_3 solution at various pHs and $CaCl_2$ solution in the PFR tubular reactor throughout a one-hour time period and shown only in 20 minutes period. As shown in Figure 4.14(a), the pH of solutions changed from about 6 (the pH of pure water) to more than 8 as soon as the initial droplets of $CaCO_3$ and its moieties were distributed in the DI water, then started to decrease upon addition. Although the pH values almost did not change in the stabilization solution when the pH of Na_2CO_3 solution was higher than 11.3, the pH values decreased when the initial pH value in Na_2CO_3 solution was below 11.3.

When the addition stopped at 8th minutes, the pH was seen to stabilize to about 7 or to about 8 when the initial pH value in Na_2CO_3 solution was below 11.3. It seems that the $CO_3^{=}$ ions were consumed high enough during the $CaCO_3$ dissolution-reprecipitation process in the semi-batch reactor so that the pH decreased in the medium to an equilibrium value due to the $CO_3^{=}/HCO_3^{-}$ chemistry. On the other hand, when the initial pH value in Na_2CO_3 solution was above 11.3, the stoichiometric consumption of $CO_3^{=}$ ions were surpassed by the OH^{-} ions, therefore, the pH stayed high throughout the stabilization stages.

Figure 4.14(a) shows the conductivity in DI water as the stabilizing solution. As shown in the figure, the conductivity increased steadily until the addition of $CaCO_3$ crystallization medium stopped. The conductivity values were higher at lower pHs and lower at higher pHs indicating that higher amount of ions were converted into solid $CaCO_3$ particles. It was thought that HCO_3^{-} ions are predominant at low pHs, less than 8, while $CO_3^{=}$ ions are dominant at higher pH values, greater than 10.3, where $NaCO_3^{-}$ and $CO_3^{=}$ ions become dominant[61]. The solution's conductivity decreased when the majority of its OH^{-} ions were consumed. Also, increasing pH may lead to higher OH^{-} ion consumption by HCO_3^{-} ions as occurred in $OH^{-} + HCO_3^{-} \leftrightarrow H_2O + CO_3^{=}$, which further decrease the conductivity due to OH^{-} ions' higher ionic mobility than $CO_3^{=}$ ions [64–66].

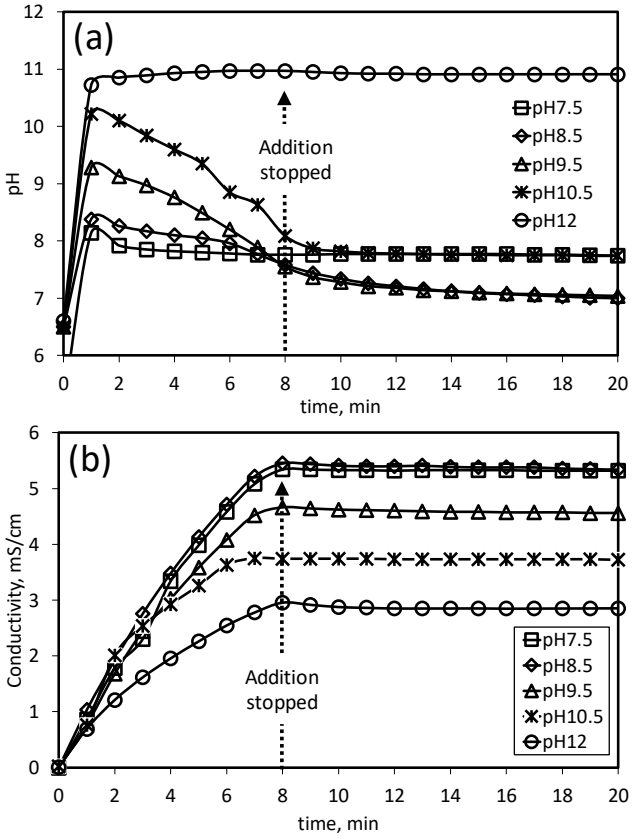

Figure 4.14. pH and conductivity changes of 250 ml of DI water used as stabilizer solution in the semi-batch reactor for the $CaCO_3$ particles formed by mixing of Na_2CO_3 solution at various pH and $CaCl_2$ solution in the PFR tubular reactor throughout a one-hour time period.

Figure 4.15 shows the SEM images of particles obtained in the semi-batch reactor in DI water after one hour of stabilization with varying pH values of Na_2CO_3 as reactant and the pH of the $CaCl_2$ solution was not altered. As shown in the figure, the $CaCO_3$ particles were larger than 3 μm as generally occurred in the chemical method. Some of the particles obtained when the pH of Na_2CO_3 solution was lower, 7.5 or 8.5, plate-like, lens-like, and ellipsoidal-like vaterite particles were observed. When pH of Na_2CO_3 solution n was 9.5 to 10.5, spherical-like vaterite particles were obtained. Higher pH values of Na_2CO_3 solution resulted in cubical calcite and spherical vaterite particles.

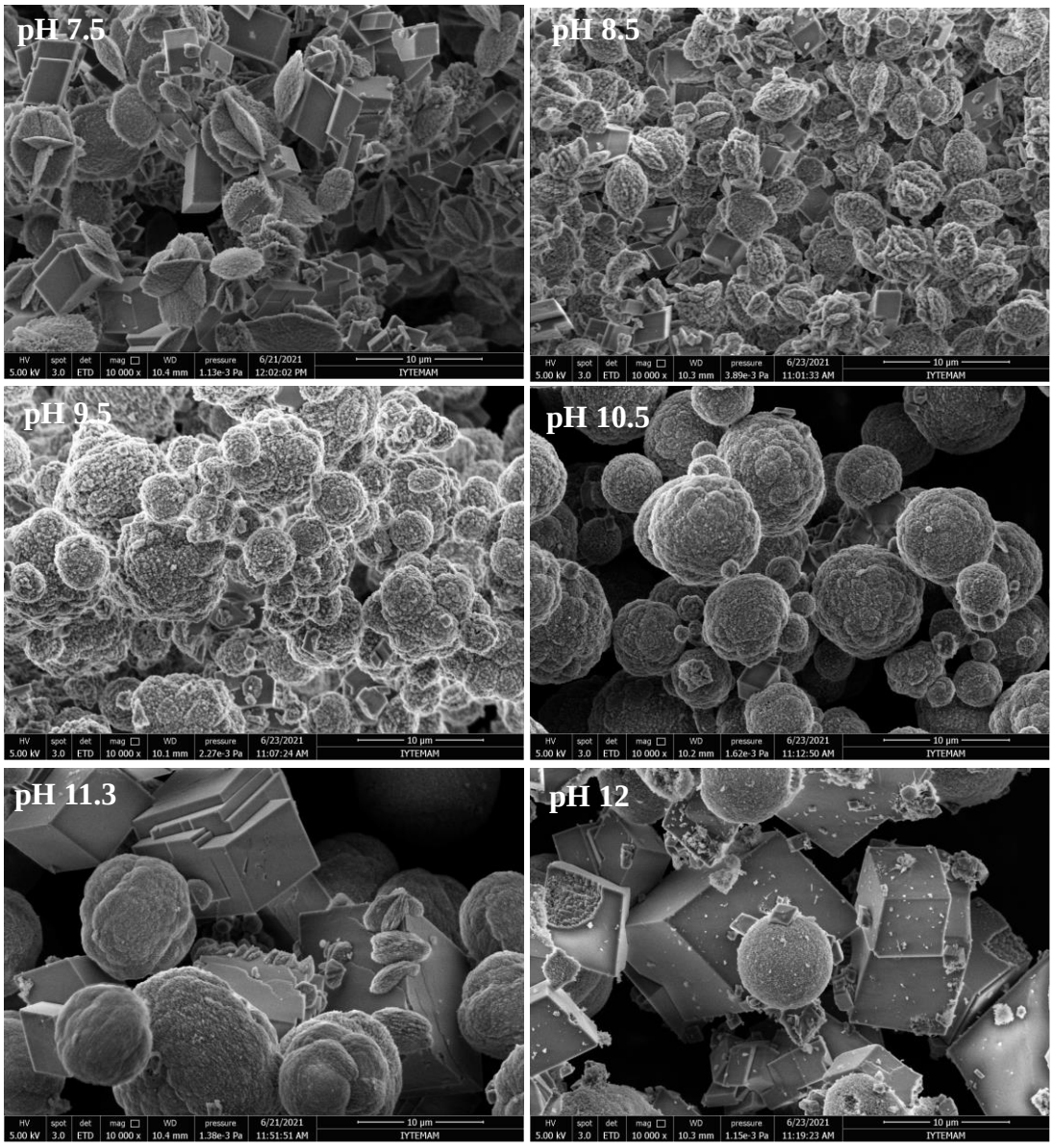

Figure 4.15. SEM images of $CaCO_3$ particles (CR=75mM) obtained in semi-batch reactor in DI water after one hour of stabilization with varying pH values of Na_2CO_3 as reactant.

The X-ray crystallographic patterns for the $CaCO_3$ particles were shown in Figure 4.16. The refinement results also shown in the Table. As shown in the figure and in the table, there were both vaterite and calcite forms were present in the suspension. It was observed that the pHs of Na_2CO_3 solution were between 9.5 and 10.5, 85% of particles were composed of vaterite. There seems to be a transformation from vaterite to stable calcite after one hour of suspension in DI water. It seems that when vaterite was

suspended in DI water for an extended period of time, it has the ability to transform into the most stable form of calcite[5,38,40,65]. Therefore, both vaterite and calcite forms were present in the synthesis of $CaCO_3$ crystallization by varying the pH of the Na_2CO_3 solution.

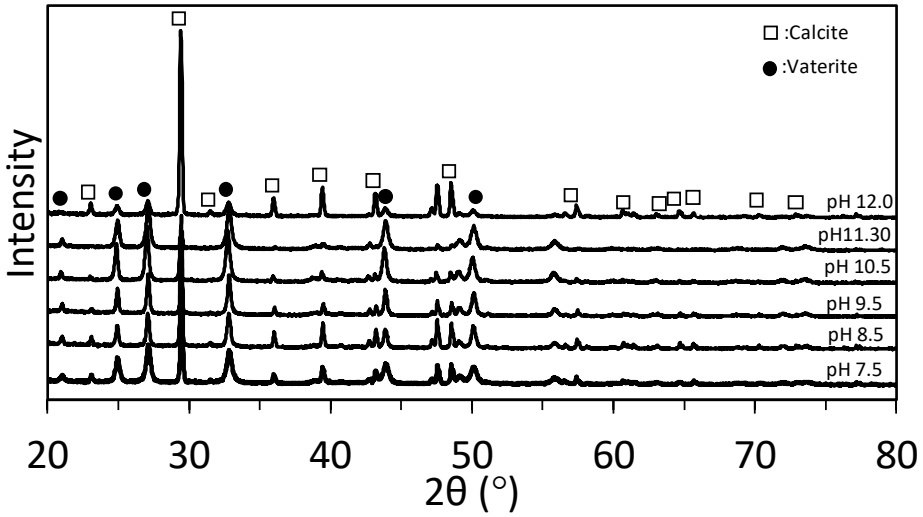

Initial pH of Na_2CO_3	Calcite %	Vaterite %
11.3 (in PFR)	51	49
7.5	58	42
8.5	40	60
9.5	20	80
10.5	15	85
12	86	14

Figure 4.16. X-ray crystallographic patterns on $CaCO_3$ particles obtained when initial pH of Na_2CO_3 solution varied. The refinement results also shown in the Table.

Figure 4.17 shows the vaterite and calcite compositions in $CaCO_3$ crystallization when varying the pH of Na_2CO_3 solution. As shown in the figure, there were almost 60% of calcite formed when the pH of the Na_2CO_3 solution was 7.5. Indeed, the $CaCO_3$

particles were only seen after 2 minutes of stabilization since the particles were dissolved at such low pH values of 7.5. As the concentrations of ions increased, particles were seen to form in the stabilization medium. These particles were mostly calcite and its formation decreased as more vaterite partcles were present in the stabilization solution when the initial pH of the Na_2CO_3 solution was higher. When the pH of the Na_2CO_3 solution was higher than 10.5, the presence of calcite form in in the stabilization medium were seen to increase. It seems that the ionic species play a critical role in the medium for the formation of different forms of $CaCO_3$ in the crystallization. While Na^+, Ca^{++}, HCO_3^-, and $CaHCO_3^+$ play a critical role in calcite formation at lower pHs, Na^+, Ca^{++}, $CO_3^=$, $CaCO3^o$, $NaCO_3^-$, and OH^- ions play important role in dissolution-recrytallization of calcite from vaterite at higher pHs.

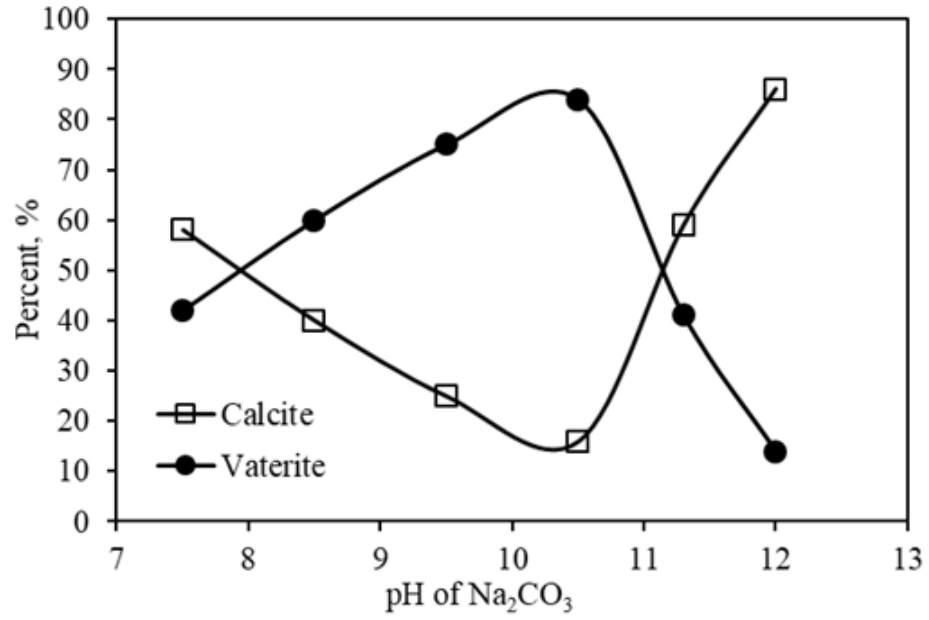

Figure 4.17. Vaterite and calcite composition in CaCO3 crystallization when varying the pH of Na_2CO_3 solution.

4.5. Use of Na_2CO_3 as Stabilizing Solution at Different pH

The effect of pH and ions generated from the Na_2CO_3 solution on the crystal form of $CaCO_3$ were investigated. Both Na_2CO_3 and $CaCl_2$ solutions were prepared to a

reactant concentration (CR) of 25 mM and a volume of 50 ml for each and $CaCO_3$ particles were crystallized in the PFR tubular reactor for which the total flow rate was 15 ml/nin and the tubing length was 27 cm, and therefore, the residence time was calculated to be 7.5 seconds. The precipitated particles were added directly into a semi-batch reactor containing 250 ml of Na_2CO_3 stabilization solution with concentration of 10 mM. For each run, the pH of Na_2CO_3 stabilization solution was adjusted beforehand either with 1 M of concentrated NaOH solution or 5M of HCl solutions. The ionic species of Na_2CO_3 solution at different pH was calculated with PHREEQC program and shown in Figure 4.11. The pH of Na_2CO_3 solution was measured as 11.14 without any pH adjustment.

Figure 4.18 shows the pH and conductivity changes in the Na_2CO_3 stabilization solution at different pHs during the addition of precipitated $CaCO_3$ medium. As shown in the figure, both pH and conductivity were increased steadily at lower pHs, lower than 11.1, when freshly precipitated $CaCO_3$ particles and its crystallization medium was added into the Na_2CO_3 stabilization solution. At higher pHs, pH higher than 11, pH almost did not vary significantly or their change were almost negligible when precipitated $CaCO_3$ medium was added. Conductivity is a good indicator for increasing or decreasing of the concentrations of ionic species. As can be seen in the figure, the conductivity of the Na_2CO_3 solution as the stabilization solution increased steadily during the addition of the $CaCO_3$ medium indicating that either accumulation of ions was added into the solution with the crystallization medium or there might be a dissolution of precipitated $CaCO_3$ particles which increased their concentrations in the solution. When the additions were stopped at the 5^{th} minutes, both the pH and conductivity values were seen to decrease at all pHs indicating that reprecipitation occurred on the surfaces of the particles.

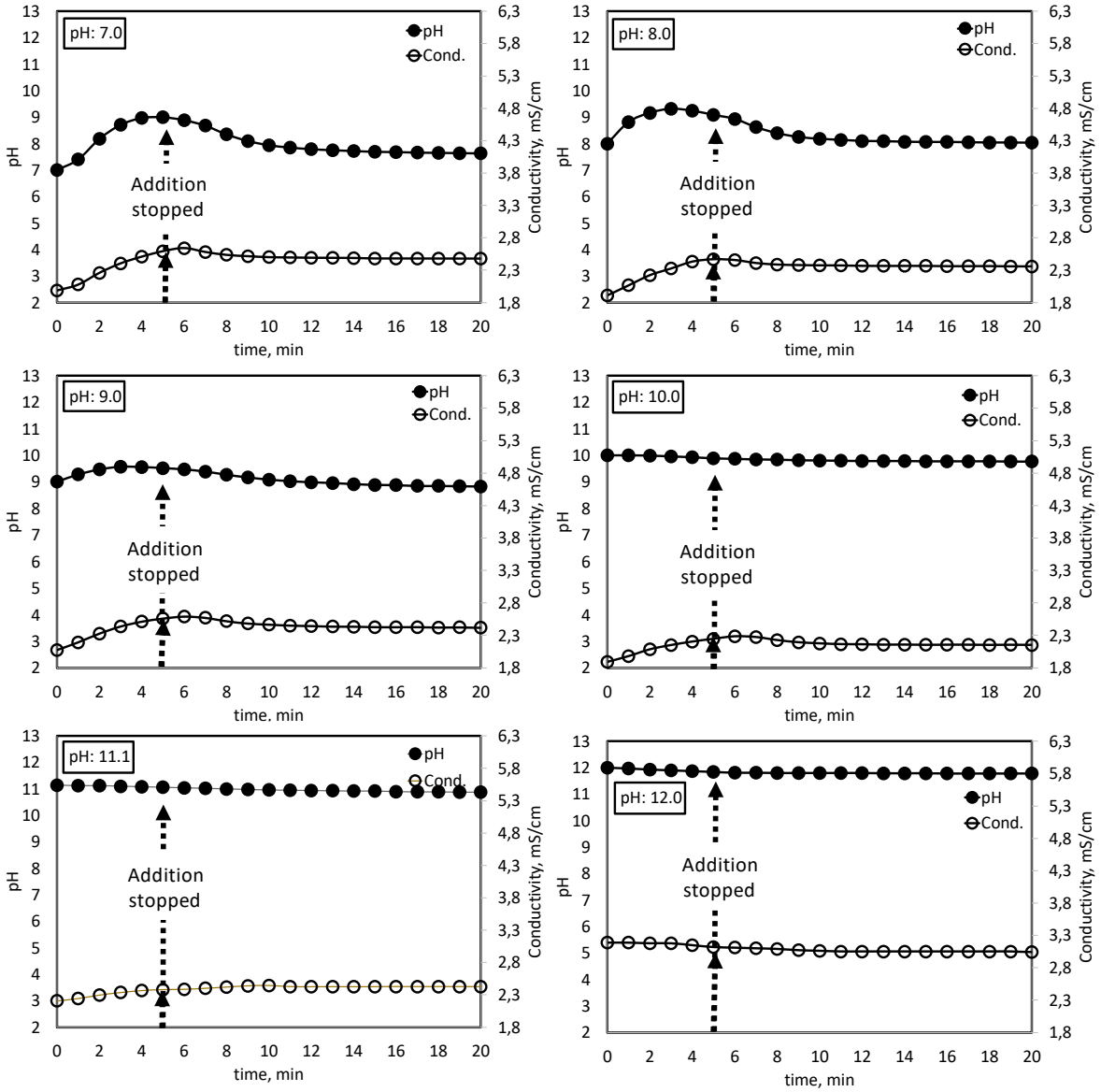

Figure 4.18. pH and conductivity changes in the Na_2CO_3 stabilization solution at different pHs during the addition of precipitated $CaCO_3$ medium.

After one hour, the $CaCO_3$ particles were collected by centrifugation and subjected to further analysis. Figure 4.19 shows the SEM images of the particles stabilized in Na_2CO_3 solution at different pHs. At lower pHs, mostly HCO3- ions were present in the stabilization solution, and at higher pHs, mostly CO3= ions were present in the stabilization solution. Both vaterite and calcite particles formed and stabilized in the Na_2CO_3 solution at different pHs. As shown in the figure, the sizes and morphologies of

the particles were not significantly varied, except that almost all of the vaterite particles converted into calcite particles at pH of 12.

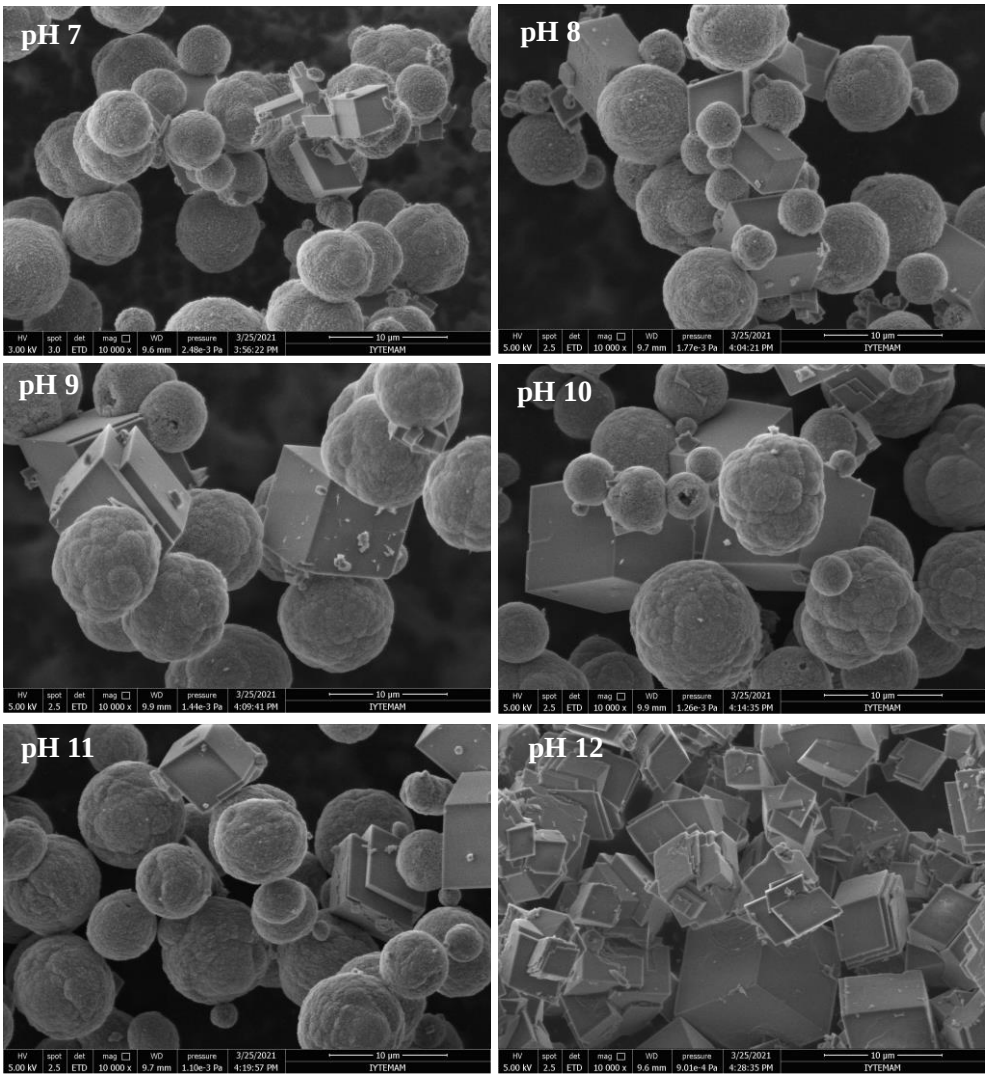

Figure 4.19. SEM images of $CaCO_3$ particles stabilized in Na_2CO_3 solution adjusted to different pH.

Figure 4.20 shows the XRD patterns and refinement results of $CaCO_3$ particles stabilized in Na_2CO_3 solution at different pH values. As shown in the figure, both vaterite and calcite forms of $CaCO_3$ were present in the Na_2CO_3 stabilization solution at pH lower than 11 and totally calcite at pH of 12.

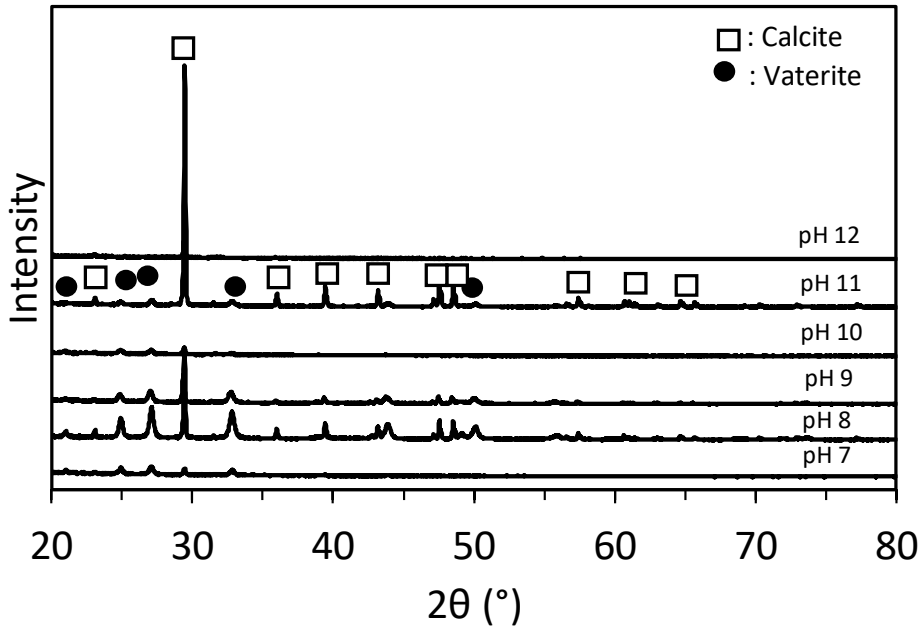

pH of Stabilizer Na_2CO_3	Calcite (%)	Vaterite (%)
7	21	79
8	44	56
9	47	53
10	64	36
11	69	31
12	100	0

Figure 4.20. XRD patterns and refinement results of $CaCO_3$ particles stabilized in Na_2CO_3 solution at different pH values.

The forms of CaCO3 were clearly shown in Figure 4.21. As shown in the figure, the vaterite form is almost 80% and calcite form is almost 20% in Na^+, Ca^{++}, HCO_3^-, and $CaHCO_3^+$ rich solution at pH of 7.0. While the vaterite content was decreasing, the calcite content increased at increasing pHs where additional ions appeared in the Na_2CO_3 stabilization solution such as $CO_3^=$, $NaCO_3^-$, and $CaCO3^o$. At higher pHs, pH of 12, vaterite totally converted into calcite in the presence of Na^+, Ca^{++}, $CO_3^=$, $CaCO3^o$, $NaCO_3^-$, and OH^- ions. This is consistent with the findings that the pace at which vaterite transforms into calcite is proportional to the pH of the solution [1,44,56–58].

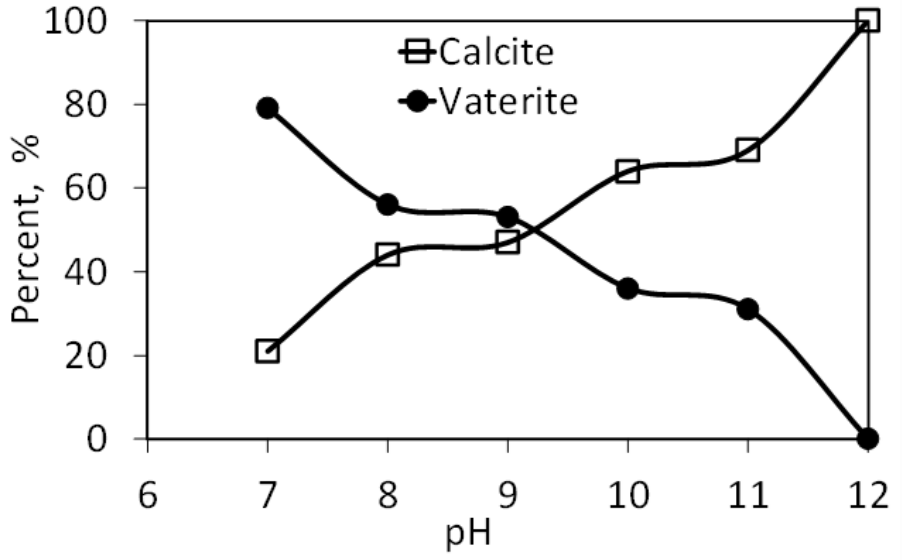

Figure 4.21. Forms of $CaCO_3$ particles stabilized in Na_2CO_3 solution at different pH values.

4.6. Effects of Barium Ions (Ba^{++}) on Freshly Precipitated $CaCO_3$ Particles

Effects of Ba^{++} ions on the $CaCO_3$ crystallization was investigated. Solutions of Na_2CO_3 and $CaCl_2$ of 75 mM and 60 ml each were prepared andmixed in the PFR tubular reactor having a diameter and length of 0.3 cm and 425 cm, respectively, therefore, the retention time was calculated to be 2 minutes for a flow rate of 7.5 ml/min for each. The crystallization medium was added into a semi-batch stirred reactor containing 250 ml and 10 mM of $Ba(OH)_2$ solution. pH and conductivities were monitored continuously. One milliliter of samples was withdrawn from the semi-batch reactor and particle size and zeta potential values were estimated at each minute of additions. Separate runs were conducted in order to obtain enough samples for the SEM imaging and XRD patterning measurements. In each run, fresh solutions were prepared; the $CaCO_3$ mediums were added to the $Ba(OH)_2$ stabilization solution, and the additions were stopped at each minutes up to 8 minutes. Then, whole suspensions were centrifuged for 20 minutes, washed with acetone, and dried in a vacuum oven at 85 ^oC overnight.

Figure 4.22 shows the SEM image of $CaCO_3$ particles in vaterite and calcite forms obtained in the PFR tubular reactor with a retention time of 2 minutes. The average sizes

of these cubical calcite and spherical vaterite particles were more than 13 μm. Their XRD patterns indicated that the compositions of the samples were about 82% cubical-calcite and 18% spherical-vaterite. These crystallization medium was added into Ba(OH)2 stabilization solution and the progress in stabilization were observed.

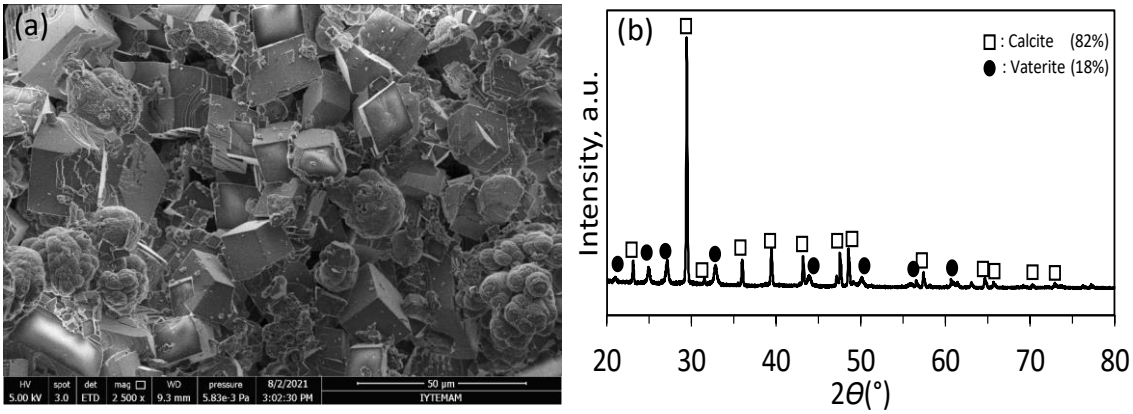

Figure 4.22. (a) SEM image of $CaCO_3$ particles in vaterite and calcite forms obtained in the PFR tubular reactor with a retention time of 2 minutes, and (b) XRD pattern showing a composition of 82% cubical calcite and 18% spherical vaterite.

Figure 4.23(a) shows the pH and conductivity change during the adiition of $CaCO_3$ crystallization medium into the $Ba(OH)_2$ stabilization solution. As shown in the figure, pH slightly decreased while conductivity increased during the addition of $CaCO_3$ medium indicating that some or all of the $CaCO_3$ crystals in the form of vaterite and calcite were dissolved in the stabilization medium. Therefore, there were a dynamic variation in the concentrations of the ions in the stabilization medium where OH^- ions seemed to be consumed, and there was an accumulation in Ca^{++} ions in the solution.

Figure 4.23(a) shows the average particle size and zeta potential of particles in the stabilization medium. As can be seen in the figure, particle size increased continuously from 1.2 μm to 4 μm upon addition of $CaCO_3$ medium. The zeta potential of the particles were all positive and almost constant at +15 mV indicating that these particles were covered by either Ca^{++} and Ba^{++} ions.

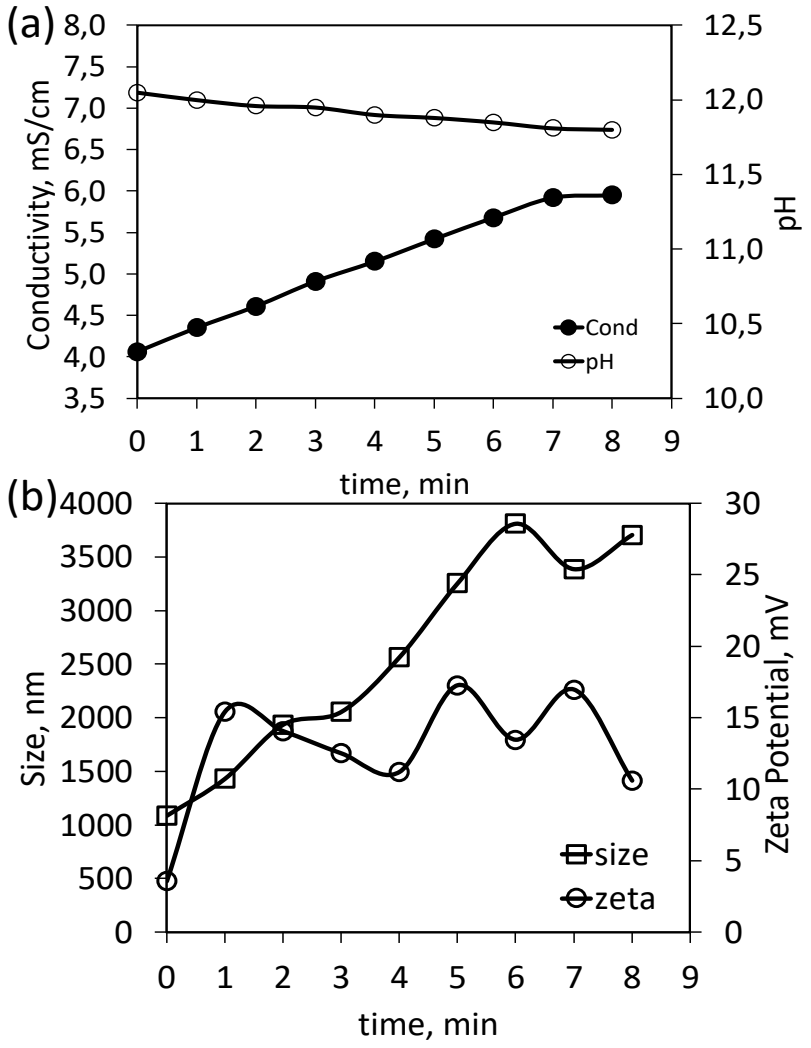

Figure 4.23. (a) pH and conductivity values (b) particle size and zeta potential values for the $CaCO_3$ stabilization in 10 mM and 250 ml of $Ba(OH)_2$ solution.

Figure 4.24 shows the changes in [Ba^{++}] and [Ca^{++}] ion concentrations during the stabilization of $CaCO_3$ particles in $Ba(OH)_2$ solution measured by the ion chromatography and compare them with the theoretically calculated values from PHREEQC program. After taking the samples from the stabilization solution, the particles suspended in liquids were filtered using a 0.22 µm filter, and the concentration of cations Ba^{++} and Ca^{++} ions were measured using ion chromatography. The theoretical cation concentrations were estimated in the stabilizing solution using the PHREEQC program, considering the introduction of volumes at each minutes. As shown in the figure, the Ba^{++} ion concentration initially declined from 10 mM to roughly 7.4 mM after the first minute and the final concentration was about 2.4 mM at the end of 8th minute, which

suggests that the consumption of Ba^{++} ion is either absorbed onto the $CaCO_3$ surfacew or iinvolved in producing a complexation ions which lead to the dissolution of $CaCO_3$ particles Ba^{++} ion concentrations measured by the ion chromatography decreased substantially in the first 4 minutes and almost slightly changed afterwards. On the other hand, Ca^{++} ion concentrations increased to about 2.5 mM at the end of the first minute in the stabilization medium indicating that some or all of the $CaCO_3$ particles dissolved in the stabilization medium. The Ca^{++}ion concentrations increased as more $CaCO_3$ particles dispersed throughout the stabilizing solution, reaching around 4.7 mM at the end of the 4^{th} minute. The final concentration reached to about 5 mM at the end of the 8^{th} minute showing a slight increase, probably due to recrystallization. The measured concentrations were lower than the estimated concentrations by the PHREEQC program, because, we think that, there were different form of crystals that PHREEQC program did not account such as BarytoCalcite ($BaCa(CO_3)_2$).

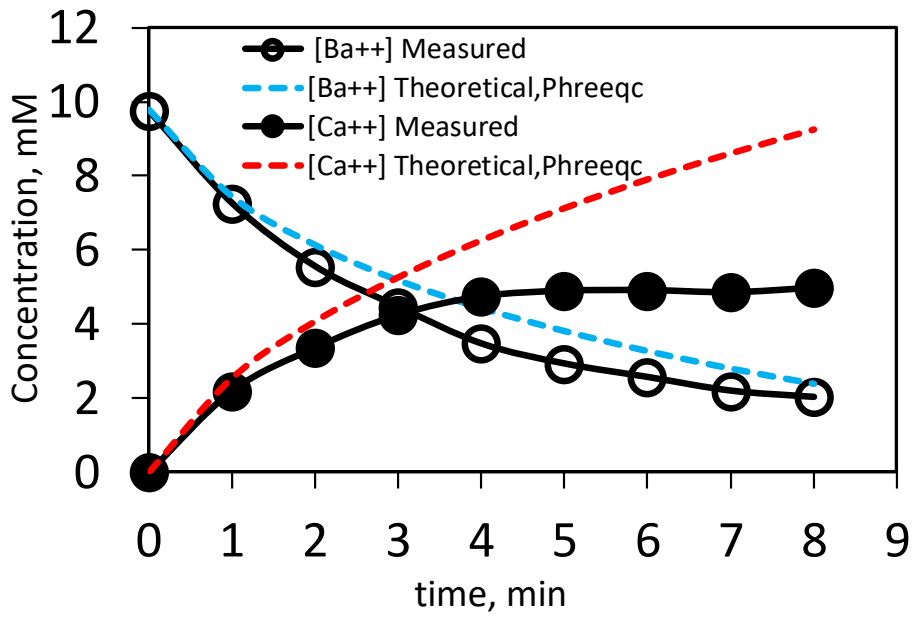

Figure 4.24. Change in [Ba^{++}] and [Ca^{++}] ion concentrations during the stabilization of $CaCO_3$ particles in $Ba(OH)_2$ solution measured by the ion chromatography and compare them with the theoretically calculated values from PHREEQC program.

Figure 4.25 shows the SEM images showing the progress of freshly formed particles when stabilized in $Ba(OH)_2$ solution. As shown in the figure, all of the particles

added into the stabilization solution were seen to dissolve at the first minute where the $[Ca^{++}]/[Ba^{++}]$ ratio was 0.225 which is much less than 1. The mean hydrodynamic size of these particles were about more than 13 μm and they were cubical-calcite and spherical-vaterite $CaCO_3$ particles before introducing the crystallization medium from the PFR tubular reactor. When these particles were dispersed in the $Ba(OH)_2$ solution, they dissolved and recrystallized into new forms of crystals, such as mostly BarytoCalcite, $BaCa(CO_3)_2$, Barium carbonate, $BaCO_3$, and Calcite, $CaCO_3$, but not Vaterite. In the first two minutes, barytocalcite particles were dominant in the medium with an oval-shape or rice-like shape with an average diameter of 1 μm to 3 μm. At third mimute, when the $[Ca^{++}]/[Ba^{++}]$ ratio was 0.63, large crystalline particles were appeared and grown on the surfaces of the Barytocalcite particles. These crystallines covered all around the surface of the particles and grew to a larger globular aggregates. As more $CaCO_3$ particles were introduced into the stabilizing solution, small cubical calcite particulates at about 350 nm in size appeared on the surfaces of the large particles at 5^{th} or 6^{th} minutes when the $[Ca^{++}]/[Ba^{++}]$ ratio was greater than 1. This was probably the start of the dissolution of the Barytocalcite crystals and convertion into the smaller calcite particles. As shown in Figure 4.23(a), addition of Ba^{++} ions influenced the colloidal stability of particles. Low zeta potential of about 15 mV may have been caused high aggregation, which in turn, increased the average particle size. When the addition of CaCO3 medium progressed, mostly cubical calcite particles were seen to accumulate on the surfaces of the old particles suggesting these nano cubical calcite particles nucleate on the surfaces of these particles and grow by a dissolution-recrystallization mechanism.

Figure 4.26 shows XRD patters for the progress of the particles obtained during the addition of $CaCO_3$ crystallization medium into the $Ca(OH)_2$ stabilization solution. The refinement results were also obtained using the X'Pert Highscore Plus XRD analyzing program and also shown in the table. According to X-ray crystallographic patterns, the crystal forms of particles were seen to be Barytocalcite ($BaCa(CO_3)_2$), calcite ($CaCO_3$), and witherite ($BaCO_3$). No vaterite form was detected in the XRD analysis. As shown in the figure, the calcite peak did not develop during the 1^{st} minute to 4 minutes. The calcite peaks first appeared on the 5^{th} minute when $[Ca^{++}]/[Ba^{++}]$ ratio was 1.125 and the peak intensity increased for the following minutes with addition of the $CaCO_3$ medium. The refinement results derived from crystal structures of particles indicated

calcite form was seen in the structure but the XRD patterns did not clearly show the peak intensity.

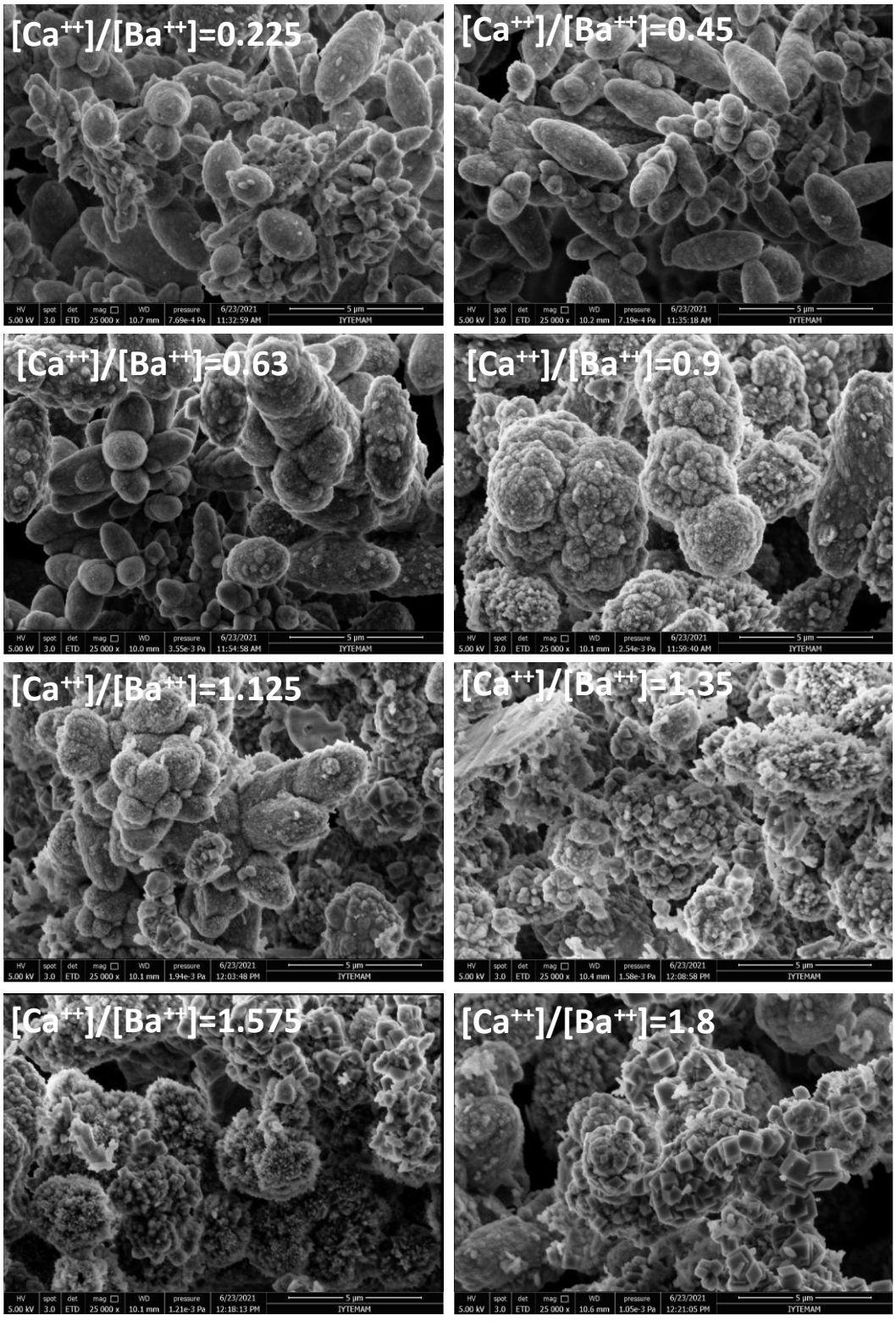

Figure 4.25. SEM images showing the progress of freshly formed particles stabilized in $Ba(OH)_2$ solution.

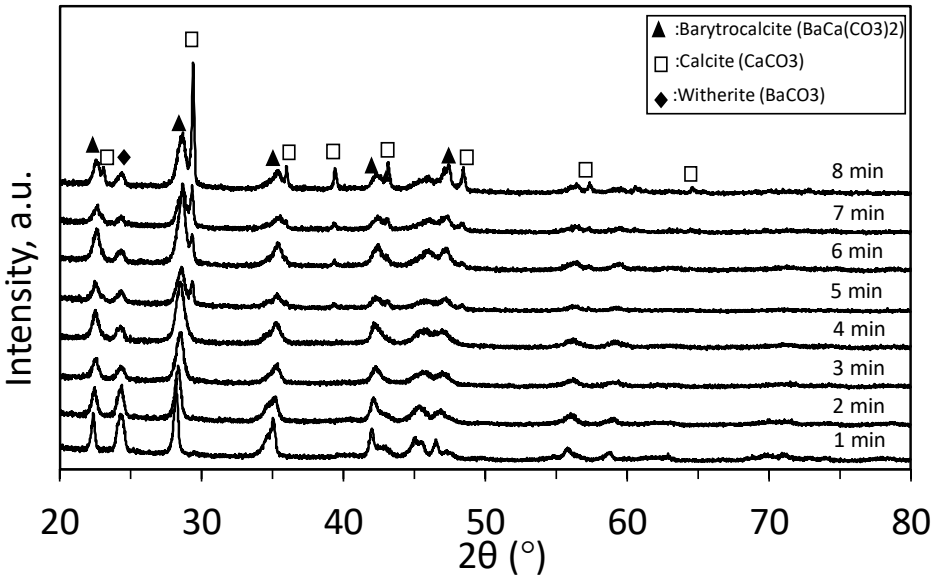

time (min)	Barytocalcite ($BaCa(CO_3)_2$) (%)	Calcite ($CaCO_3$) (%)	Witherite ($BaCO_3$) (%)
1	80	7	13
2	75	16	8
3	58	25	17
4	45	28	27
5	53	33	14
6	44	47	9
7	23	63	15
8	21	76	3

Figure 4.26. XRD patters and the refinement results for the progress of the particles obtained during the addition of $CaCO_3$ crystallization medium into the $Ca(OH)_2$ stabilization solution.

Figure 4.27(a) shows the percent distribution of crystal forms for the progress of particle development during the addition of $CaCO_3$ medium into the $Ba(OH)_2$ solution. As shown in the figure, initially, large calcite and vaterite $CaCO_3$ particles obtained from

the crystallization medium dissolved as soon as the $CaCO_3$ particles were added into the $Ba(OH)_2$ solution and formed mostly Barycalcite, about 80%, calcite, about 7%, and witherite, about 13%. Figure 4.27(b) shows saturation index calculated for $CaCO_3$ and $BaCO_3$ using the PREEQC program indicating the possibility of dissolution of particles at the very early stages. However, the dissolution of these particles at the late stages proving that the Ba(OH)2 solution is the medium for dissolution of $CaCO_3$ particles and is a good medium for recrystallization of new forms of particles such as Barytocalcite.

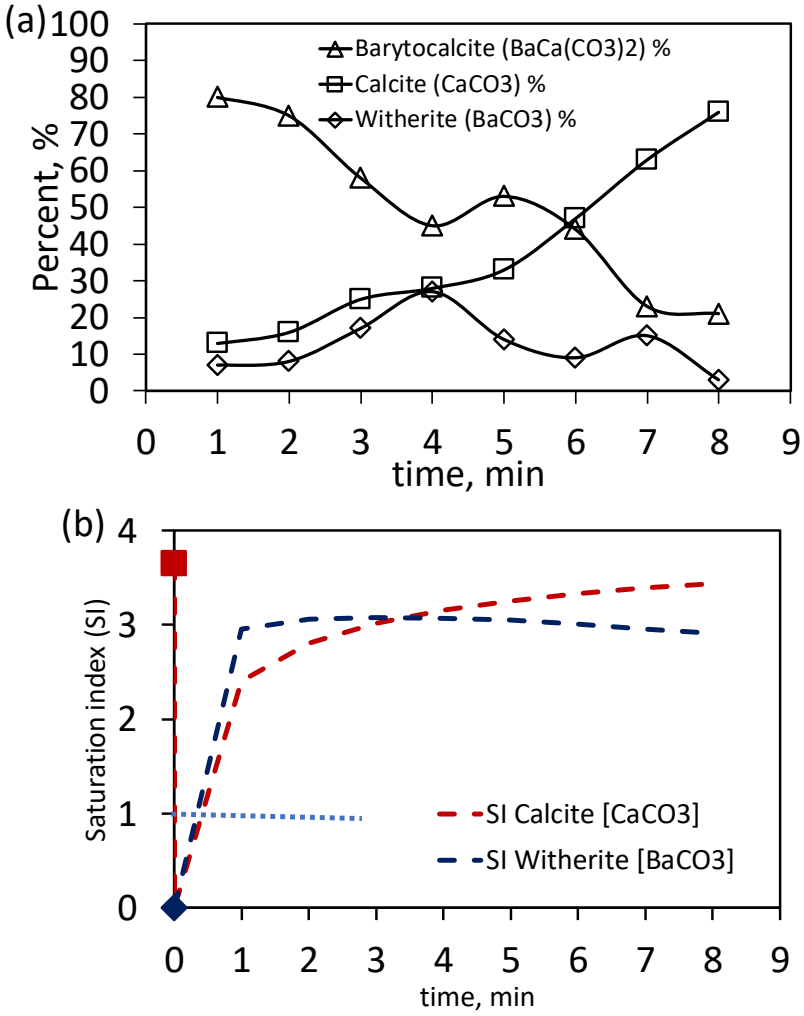

Figure 4.27. (a) Distribution of percent crystal forms for the progress of particle development during the addition of $CaCO_3$ medium into the $Ba(OH)_2$ solution, (b) saturation index calculated for $CaCO_3$ and $BaCO_3$ using the PREEQC program.

Ba^{++} ion effect on the $CaCO_3$ crystallization was also investigated with the crystallization and addition of higher concentrations of reactants to the $Ba(OH)_2$ solution. Solutions of Na_2CO_3 and $CaCl_2$ were prepared at different concentrations from 25 mM to 100 mM. Both components were mixed in the PFR tubular reactor with as a diameter and length of 0.3 cm and 32 cm, respectively, therefore, the retention time was calculated to be 9 seconds for a flow rate of 7.5 ml/min for each. The outcome of the crystallization medium was added into a semi-batch stirred reactor containing 250 ml and 10 mM of $Ba(OH)_2$ solution. In such cases, $[Ca^{++}]/[Ba^{++}]$ Ratios were varied from 0.6 to 2.4.

Figure 4.28 shows the pH and conductivity changes in the $Ba(OH)_2$ solution during the addition of precipitated $CaCO_3$ medium at different concentrations. As shown in the figure, pH slightly decreased from about 12.3 to about 12 and the decrease was in the order of the increasing concentrations of reactant solutions. On the other hand, conductivities showed a different trend, decreased when the $[Ca^{++}]/[Ba^{++}]$ ratio was below 1 and increased when $[Ca^{++}]/[Ba^{++}]$ ratio was greater than 1. It seems that ions, especially Ca^{++} and Ba^{++} ions consumed when $[Ca^{++}]/[Ba^{++}]$ ratio was less than 1, and these ions may accumulate in the solution when the $[Ca^{++}]/[Ba^{++}]$ ratio was higher than 1.

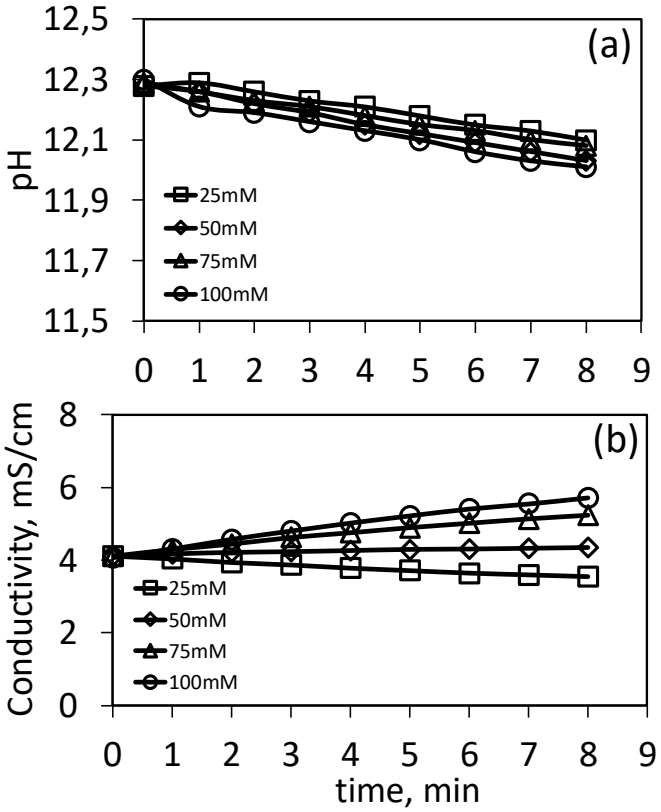

Figure 4.28. pH and conductivity changes in the $Ba(OH)_2$ solution as stabilizer during the addition of precipitated $CaCO_3$ medium at different concentrations.

Figure 4.29 shows changes in particle size and zeta potential during the addition of $CaCO_3$ medium into the stabilizer $Ba(OH)_2$ solution. As shown in Figure 4.29(a), there were initially big particles of about 1 μm to 2.2 μm in size indicating that there were impurities in the $Ba(OH)_2$ solution, mostly $BaCO_3$ to about 2%. When $CaCO_3$ medium was added into the stabilization solution, particles sizes were slightly increased in the first 2 minutes, almost unchanged between 2 to 5 minutes and thereafter, the particle sizes increased much faster. As shown in Figure 4.29(b), zeta potential values were positive, about 10 mV and 5 mV for the reactant concentrations of 25 mM and 50 mM, where the $[Ca^{++}]/[Ba^{++}]$ ratios were 0.6 and 1.2, respectively. When the reactant concentration increased, the zeta potential values turned into negative, about -2 mV at the reactant concentration of 75 mM with a $[Ca^{++}]/[Ba^{++}]$ ratio of 1.8 and about -10 mV at the reactant concentration of 100 mM with the $[Ca^{++}]/[Ba^{++}]$ ratio of 2.4. It seems that when the $[Ca^{++}]/[Ba^{++}]$ ratio was less than 1, the particles mostly covered by Ba^{++} and Ca^{++} ions and became positively charged. When excess reactants were introduced to the stabilizing solution, the particles were totally covered by $CO_3^{=}$ ions, therefore, the surface charge became negative.

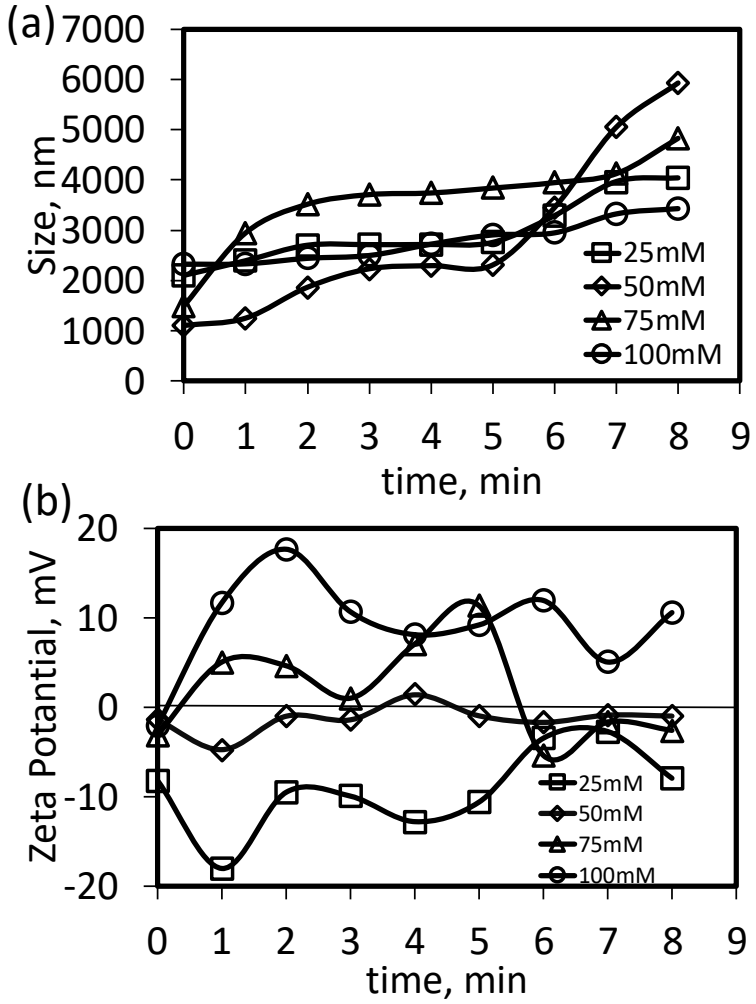

Figure 4.29. Changes in particle size and zeta potential during the addition of $CaCO_3$ medium into the stabilizer $Ba(OH)_2$ solution.

Figure 4.30 shows SEM images of particles synthesized using 60 ml of different concentrations of reactants each and stabilized in 10 mM and 250 ml of $Ba(OH)_2$ solution. As shown in the figure, addition of $CaCO_3$ medium into the $Ba(OH)_2$ stabilizing solution resulted in dissolution of vaterite and calcite particles synthesized in the PFR tubular reactor and reprecipitate into new forms of rice-like or elipsodial-like $BaCa(CO_3)_2$, rod-like $BaCO_3$, and cubical-like $CaCO_3$ as calcite. At low concentrations, when the $[Ca^{++}]/[Ba^{++}]$ ratio was below 1, $BaCa(CO_3)_2$ was dominant. When the reactant concentrations were higher, when the $[Ca^{++}]/[Ba^{++}]$ ratio was much above 1, $CaCO_3$ in calcite form was dominant. These particles were larger than 2 μm, which is in contrast to the literature's assertion that crystal size and rate of growth increase with increasing lattice ion concentration[54].

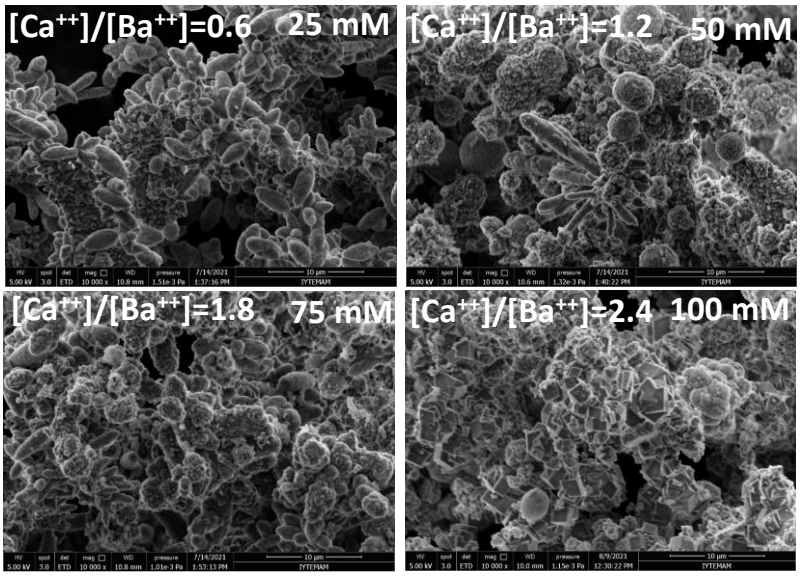

Figure 4.30. SEM images of particles synthesized using 60 ml of different concentrations of reactants each and stabilized in 10 mM and 250 ml of $Ba(OH)_2$ solution.

Volumetric mixing ratios were studied. Solutions of both $CaCl_2$ and Na_2CO_3 reactants were prepared with concentrations of 75 mM called CR and volmes of 60 ml. A stabilizer solution of $Ba(OH)_2$ was also prepared with a concentration of 10 mM called as Cs and a volume of 240 ml for a volumetric ratio of 0.5 called as VR. For different volume ratios, the volume of $Ba(OH)_2$ solution as the stabilizer solution decreased in half such as 120 ml and 60 ml for volumetric ratio of VR=1 and VR=2, respectively. Equal amount of $CaCl_2$ and Na_2CO_3 were send to the PFR tubular reactor with a flow rate of 7.5 ml/min each, where $CaCO_3$ crystallization took place a with a retention time of 9 seconds. Then, a 120 ml of $CaCO_3$ medium was added into a stirred semi-batch reactor containing $Ba(OH)_2$ solution to obtain different volume ratios. At the end of 8 minutes of addition, the contents of the semi-batch reactor were centrifuged, washed with acetone, and dried overnight at 85 ^oC under vacuum.

Figure 4.31(a) shown SEM images of synthesized $CaCO_3$ particles obtained in PFR tubular reactor obtained from $CaCl_2$ and Na_2CO_3 with concentrations of 75 mM and volumes of 60 ml. As shown in the figure, the produced $CaCO_3$ particles were composed of only vaterite and calcite with a composition of 48% and 51%, respectively. It was predicted that the $CaCO_3$ particles would become larger in size as the reactants supersaturation increased because the growth rate of crystal improves at increasing levels of supersaturation, which agrees with our findings and previous findings[31,54,55,67].

Addition of these $CaCO_3$ media into the $Ba(OH)_2$ stabilization solution of 10 mM and different volumes of 240 ml, 120 ml, and 60 ml to yield a volume ratios of VR=0.5, VR=1, and VR=2, respectively. Particles obtained in the stabilization solutions were shown in Figure 4.31(b), Figure 4.31(c), and Figure 4.31(d) for different volume ratios. As shown in the figure, the particles were much smaller than the particles produced in the PFR tubular reactor.

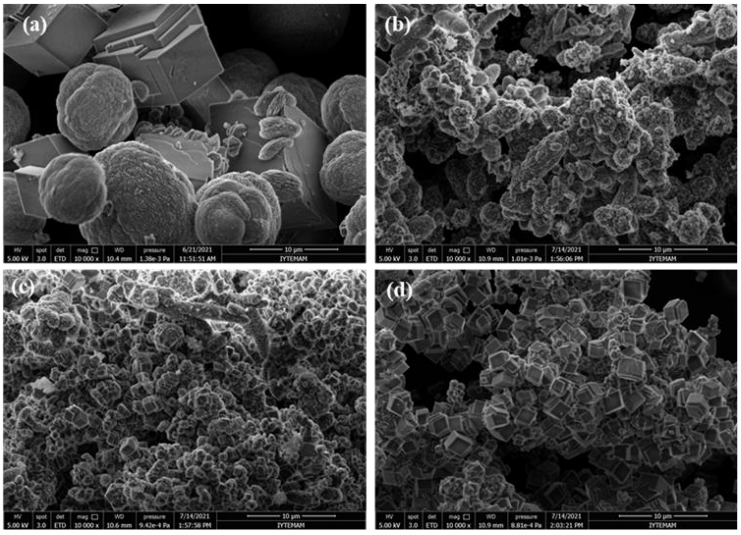

Figure 4.31. SEM images of (a) synthesized $CaCO_3$ particles obtained in PFR tubular reactor from 75 mM and 60 ml of each reactants of $CaCl_2$ and Na_2CO_3 and particles stabilized in 10 mM and different volumes of 240 ml, 120 ml, and 60 ml of $Ba(OH)_2$ solution to yield a volume ratios of (b) VR=0.5, (c) VR=1, and (d) VR=2.

Figure 4.32 shows XRD patterns and refinement results from crystal structures for the particles obtained in PFR tubular reactor as well as the particles stabilized in 10 mM of $Ba(OH)_2$ solution at different volumes to yield different volume ratios of VR=0.5, VR=1, and VR=2. The volume ratio is defined as the volume of $CaCO_3$ media added from the PFR tubular reactor per the volume of the $Ba(OH)_2$ stabilization solution in the semi-batched reactor. As shown in the figure, mixing of reactants produced only Vaterite and calcite whereas the addition of the $CaCO_3$ media into the $Ba(OH)_2$ solution yielded Barytocalcite ($BaCa(CO_3)_2$), Witherite ($BaCO_3$), calcite, and vaterite. However, vaterite was rare or almost none in $Ba(OH)_2$ stabilization solution indicating that all vaterite was dissolved and converted into Barytocalcite, calcite, and witherite.

The XRD patterns and refinement results also demonstrated that barytocalcite formed in the stabilization solution decreased from 63% to 7% while the portions of calcite reproduced increased from 30% to 89% as volume ratio was increased when higher amount of $CaCO_3$ media was added into the $Ba(OH)_2$ stabilization solution. The witherite was present in small quantities, about 7%. And, no vaterite were detected.

The stabilizer concentration of $Ba(OH)_2$ was reduced in half to 5 mM and the same runs were repeated. As shown in Figure 4.33, large chunks of vaterite and calcite particles were seen in the PFR plug flow reactor. When the $CaCO_3$ media was added into the 5 mM $Ba(OH)_2$ stabilizer solution, much smaller cubicle particles were seen at volume ratios of 0.5 and 1. At volume ratio of 2, vaterite particles were seen.

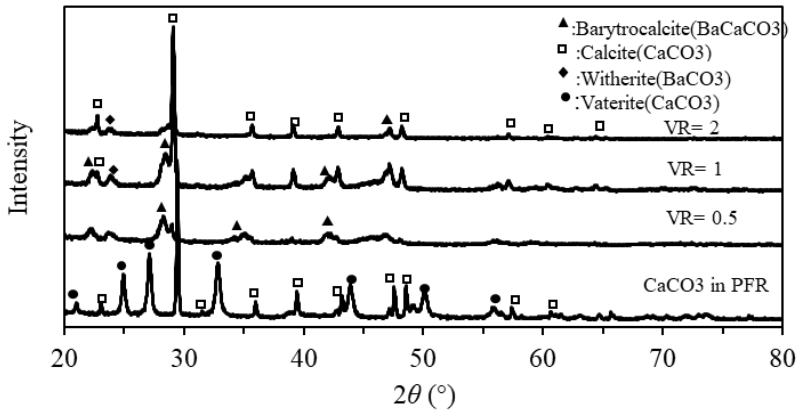

Volume Ratio VR	Barytocalcite %	Calcite %	Witherite %	Vaterite %
75mM in PFR	-	51	-	49
0.5	63	30	7	-
1	22	73	5	-
2	7	89	4	-

Figure 4.32. XRD patterns and refinement results from crystal structures for the particles (a) obtained in PFR tubular, and the particles stabilized in 10 mM of $Ba(OH)_2$ solution at different volumes to yield different volume ratios of (b) VR=0.5, (c) VR=1, and (d) VR=2.

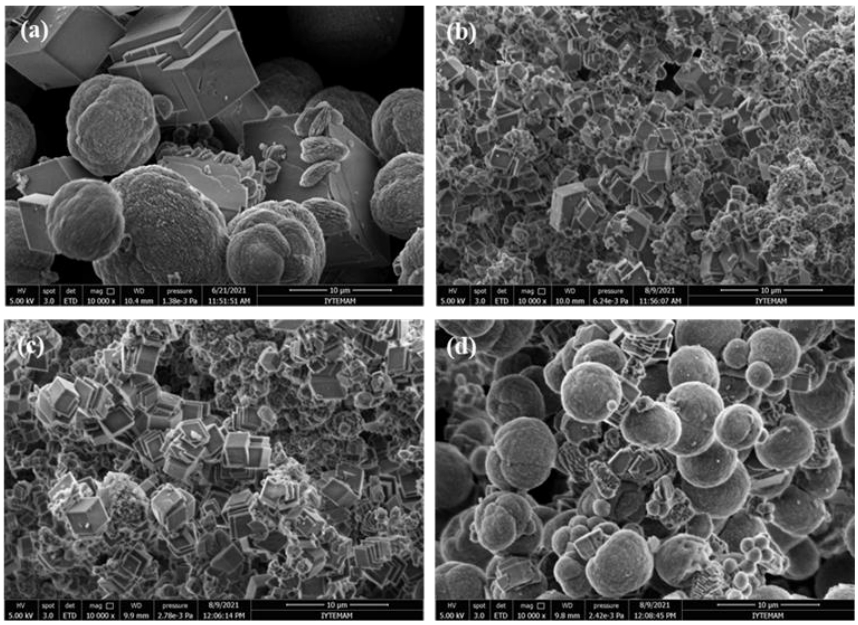

Figure 4.33. SEM images of particles obtained in (a) PFR tubular reactor when $CaCl_2$ and Na_2CO_3 reactant concentrations were 75 mM and 60 ml, stabilized in 5 mM of $Ba(OH)_2$ solution at different volumes to yield a volume ratios of (b) VR=0.5, (c) VR=1, and (d) VR=2.

The XRD patterns and refinement results for the crystals obtained in PFR tubular reactor with 75 mM and 60 ml of reactants and particles obtained in 5 mM of $Ba(OH)_2$ stabilized solution at different volume ratios were shown in Figure 4.34. As shown in the figure, most of the particles were calcite about 82% when VRs were 0.5 and 1. Barytocalcite was present only in small quantities when the VR=0.5. The witherite was also present in small quantities of about 6% and 18% at VRs of 0.5 and 1, respectfully. When VR was 2, there were only vaterite and calcite particles in the medium. As shown in the SEM image in Figure 4.33(d), large calcite particles were dissolved in the $Ba(OH)_2$ solution and recrystallized into much smaller calcite particles. When higher amounts of $CaCO_3$ medium from the PFR plug flow reactor was mixed with the 5 mM of stabilizer solution, when VR=2, the Ba^{++} ions were ineffective dissolving all these $CaCO_3$ particles and, to the end, the vaterite particles were distributed in the stabilization solution without further structural changes.

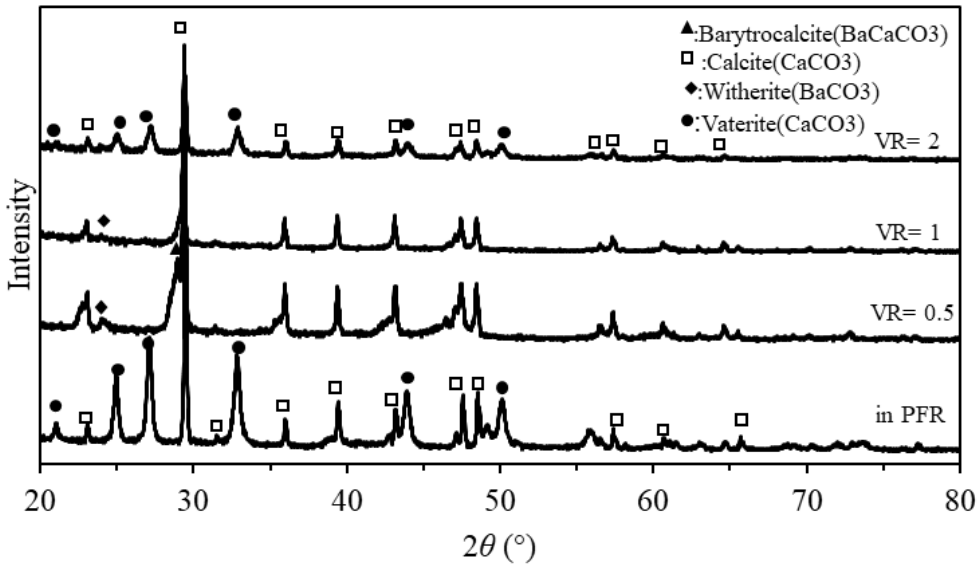

Volume Ratio	Barytocalcite %	Calcite %	Witherite %	Vaterite %
75mM in PFR	-	51	-	49
0.5	11	83	6	-
1	-	82	18	-
2	-	63	-	37

Figure 4.34. XRD patterns and refinement results for the crystals (a) obtained in PFR tubular reactor with 75 mM and 60 ml of reactants, (b) stabilized in 5 mM $Ba(OH)_2$ at different volume ratios yielding (b) VR=0.5, (c) VR=1, and (d) VR=2.

$CaCO_3$ crystallization is primarily concerned with the growth and nucleation processes. Thus, the rate at which the $CaCO_3$ particles dissolve is determined by the degree of supersaturation present in the system. Precipitation of $CaCO_3$ particles may occur if the saturation index is higher than 1. There ought to be the dissolution of $CaCO_3$ particles if the saturation index is less than 1[58,68]. According to previous studies, the precipitation of additives and impurities can decrease the rate of growth[67,69,70]. A 60 ml + 60 ml of reactants were utilized in the $CaCO_3$ crystallization medium in total. The

crystallization reaction occurred in PFR plug flow reactor. The crystallization products were poured into the stirred semi-batch reactor containing 250 ml of $Ba(OH)_2$ stabilization solution at a rate of 15 ml/min. The saturation index was determined using the PHREEQC computer model as shown in Figure 4.27(b).

$$CaCO_{3(s)} \leftrightarrow CaCO_{3(aq)} \quad (4.4)$$

$$CaCO_{3(aq)} \leftrightarrow Ca^{++} + CO_3^{=} \quad (4.5)$$

$$Ba^{++} + CO_3^{=} \rightarrow BaCO_{3(aq)} \quad (4.6)$$

$$CaCO_{3(aq)} + BaCO_{3(aq)} \rightarrow BaCa(CO_3)_{2\,(s)} \quad (4.7)$$

Figure 4.35(a) shows the compositions of ionic species as a function of pH for 10 mM and 250 ml of $Ba(OH)_2$ solution estimated using the Hydra–Medusa program[71]. There are basically Ba^{++}, OH^- and $BaOH^+$ ions produed in $Ba(OH)_2$ solution. The compositions of ionic species after the addition of the $CaCO_3$ crystallization media containing 75 mM and 60 ml each of reactants were also shown in Figure 4.35(b). After being poured the $CaCO_3$ particles into the 10 mM of $Ba(OH)_2$ solution, the $CaCO_3$ saturation index decreased from 3.65 to less than 1 initially, as shown in Figure 4.27(b), suggesting that the $CaCO_3$ particles had already dissolved and dissociated into Ca^{++} and $CO_3^{=}$ ions in the $Ba(OH)_2$ solution. The free Ba^{++} ions then formed a covalent bond with $CO_3^{=}$ ions, whereas the free Ca^{++} ions formed a covalent bond with OH^-ions, resulting in the formation of $CaOH^+$ complation ions, which is a recognized Lewis acid[72,73] to comprehend ionic electrochemistry and hadrochemical equilibrium. When $CaCO_3$ media was added into the $Ba(OH)_2$ solution, complex ions were produced such as OH^-, Ca^{++}, Ba^{++}, $CaOH^+$, $BaOH^+$, $CO_3^{=}$, $CaCO_{3(aq)}$, $BaCO_{3(aq)}$ at higher pHs. It was inferred that especially CaOH+ and BaOH+ play a major role in the dissolution of $CaCO_3$ particles before proceeding into newly formed recrystallized particles.

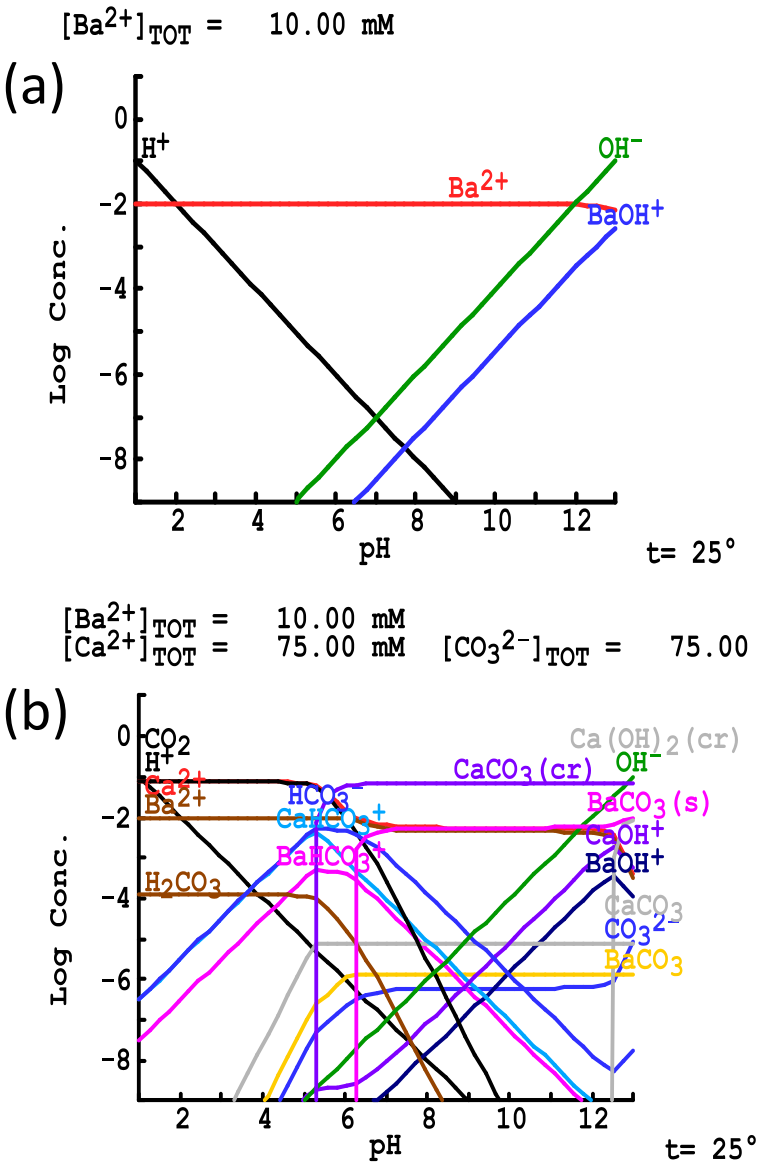

Figure 4.35. Compositions of ionic species as a function of pH (a) before and (b) after addition of $CaCO_3$ media into 10 mM of $Ba(OH)_2$ solution estimated using the Hydra–Medusa program[76].

Similar effects were seen when higher concentrations of reactant solutions were used. Figure 4.36 shows the SEM images of synthesized $CaCO_3$ particles obtained in PFR tubular reactor from 100 mM and 60 ml of each reactants of $CaCl_2$ and Na_2CO_3 and particles stabilized in 10 mM and different volumes of 240 ml, 120 ml, and 60 ml of $Ba(OH)_2$ solution to yield volume ratios of 0.5, 1, and 2. When the concentration of reactants were increased, larger vaterite and calcite particles were peoduced in the PFR plug flow reactor. These particles were seen to dissolve in Ba(OH)2 solution and

recrystallize into much smaller particles and most of it were calcite as indicated in the XRD patterns as shown in Figure 4.37. Barytocalcite particles formed when the vaolume ratio was 0.5, they were disappeared when the volume ratios were 1 and 2, indicating that the Barytocalcite particles were dissolved and recrystallized into the calcite particles.

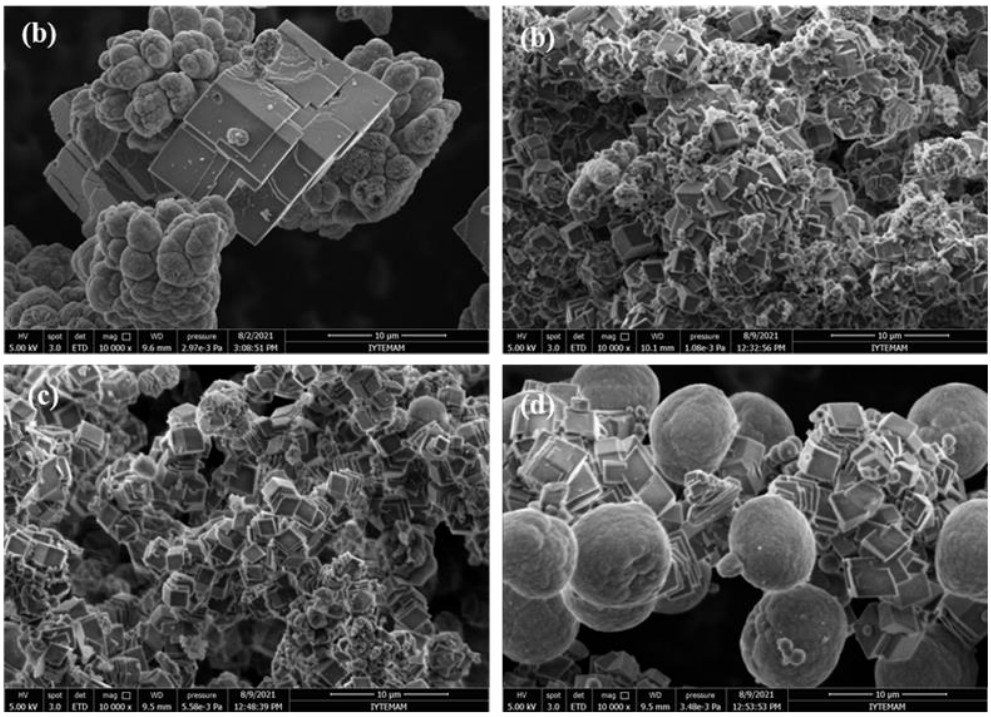

Figure 4.36. SEM images of (a) synthesized $CaCO_3$ particles obtained in PFR tubular reactor from 100 mM and 60 ml of each reactants of $CaCl_2$ and Na_2CO_3 and particles stabilized in 10 mM and different volumes of 240 ml, 120 ml, and 60 ml of $Ba(OH)_2$ solution to yield volume ratios of (b) VR=0.5, (c) VR=1, and (d) VR=2.

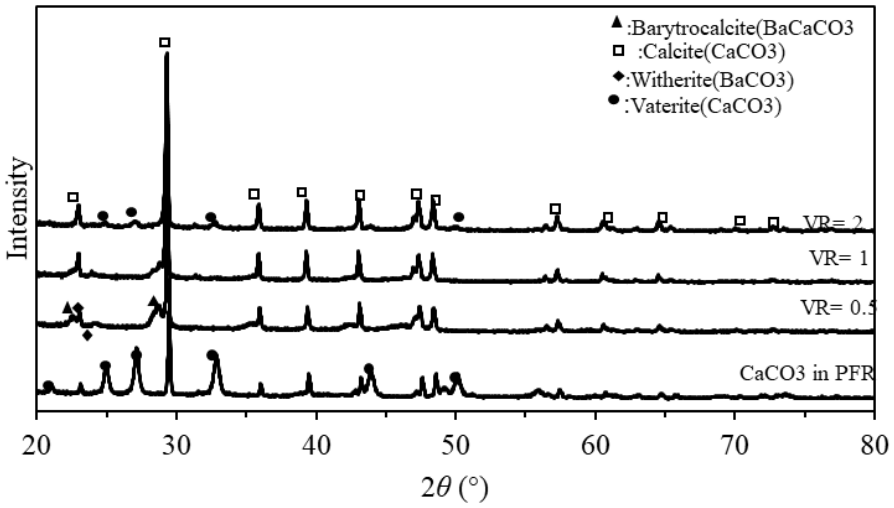

Volume Ratio	Barytocalcite %	Calcite %	Witherite %	Vaterite %
100mM in PFR	-	50	-	50
0.5	11	81	8	0
1	-	84	16	-
2	-	79	-	21

Figure 4.37. XRD patterns and refinement results for the crystals (a) obtained in PFR tubular reactor, (b) stabilized in 10 mM $Ba(OH)_2$ at different volume ratios yielding (b) VR=0.5, (c) VR=1, and (d) VR=2.

Smaller particles were formed at very low $Ba(OH)_2$ concentration of 5 mM with a volume ratio of VR = 0.5 and reactants concentrations of CR = 100 mM with a volume of 60 ml each, as revealed by the SEM results as shown in Figure 4.38. The XRD patterns and refinement results for the crystals obtained in PFR tubular reactor and stabilized in 5 mM $Ba(OH)_2$ at different volume ratios yielding VR=0.5, VR=1, and VR=2 were also shown in Figure 4.39. As shown in the figures, no Barytocalcite and witherite were obtserved in the crystals. Instead, a new form of Paralstonite was obtained ina very small quantity of about 4%. In each mixture, mostly recrystallized calcite with maller size were obtained when the VR=0.5 and 1. Small amout of vaterite was seen when VR=2, indicating that vaterite particles were distributed in the stabilization solution without

dissolution at such high volume ratios. According to the results of a recent study[57], Ba^{++} ions have both a strong bonding strength and high adsorption energy. When reactants were utilized in higher concentrations together with two times the reactants volume (VR=2), a vaterite morphology formed, implying that either a high amount of Ba^{++} ions in solution consumed or that a substantial quantity of lattice ions was present throughout the nucleation and growth process, preventing the Ba^{++} ions from adsorbing on the surface of the crystals. As understood from these results, the Ba^{++} ions have a massive effect on freshly produced $CaCO_3$ particles. At low concentrations of stabilizer solution, nano-calcite particles were produced at higher concentrations of reactants and lower concentrations of stabilizer solution when the volume ratios equal 0.5 and 1. While the volume ratio was greater than 2, there was no Barytocalcite, only vaterite and calcite, which indicated that the number of Ba^{++} ions were consumed to obtain submicron calcite.

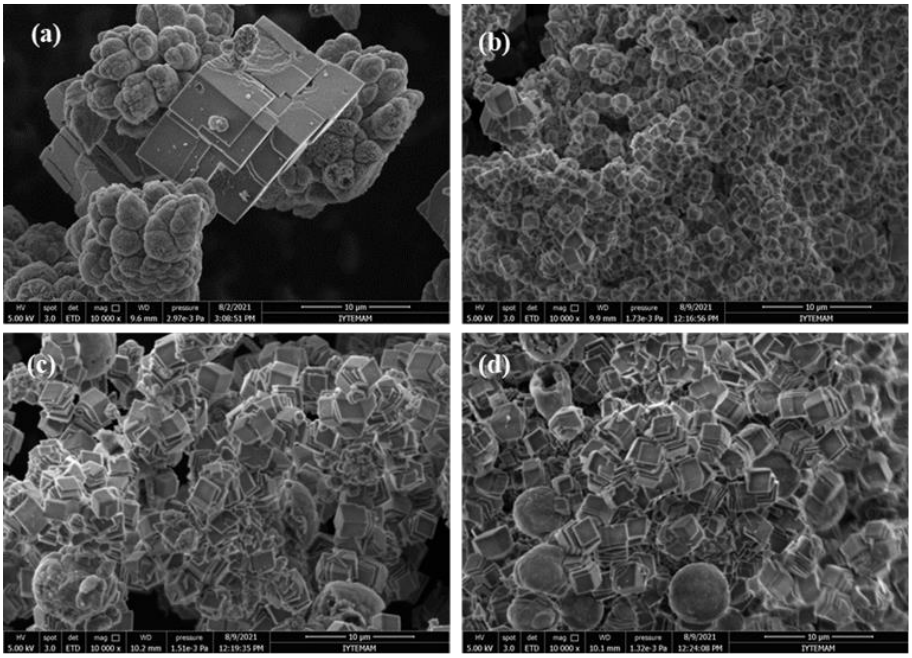

Figure 4.38. SEM images of particles obtained in (a) PFR tubular reactor when $CaCl_2$ and Na_2CO_3 reactant concentrations were 100 mM and 60 ml, stabilized in 5 mM of $Ba(OH)_2$ solution at different volumes to yield a volume ratios of (b) VR=0.5, (c) VR=1, and (d) VR=2.

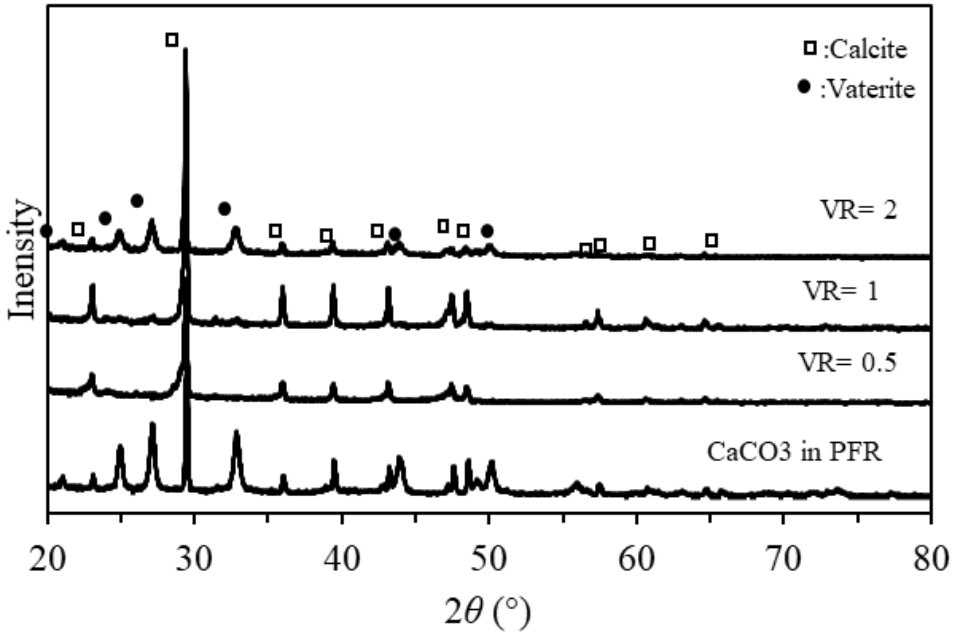

Volume ratio VR	Calcite %	Paralstonite %	Vaterite %
100mM in PFR	50	-	50
0.5	96	4	-
1	98	2	-
2	44	-	56

Figure 4.39. XRD patterns and refinement results for the crystals (a) obtained in PFR tubular reactor, (b) stabilized in 5 mM $Ba(OH)_2$ at different volume ratios yielding (b) VR=0.5, (c) VR=1, and (d) VR=2.

4.7. Method Development for Nano-$CaCO_3$ synthesis with Chemical Method

Effect of mole ratio of reactants were studied. The effect of the initial molar concentration ratio on the nucleation and growth processes is critical because it has a significant impact on the shape and size of particles that form as a result of an excess of

ions adsorbed on the crystal surface. Reactants of $CaCl_2$ and Na_2CO_3 were prepared with a volume of 60 ml at different concentrations from 4 mM to 40 mM so that the mixing $Ca^{++}/CO_3^{=}$ mole ratio would change from 0.1 up to 10. Reactant solutions were fed to the PFR tubular reactor with a volumetric flow rate of 7.5 ml/min each and crystallized with a retention time of 9 seconds. The $CaCO_3$ particles formed in the PFR tubular reactor were added into a stirred semi-batch reactor containing 250 ml and 10 mM of $Ca(OH)_2$ solution. For each run, samples were taken at the exit of the PFR tubular reactor and from the semi-batch reactor. Particles were separated, washed with acetone, and dried at 85 ^oC under wacuum. Then, the SEM images and XRD diffraction peaks were obtained for these particles. Figure 4.40(a) shows SEM images of $CaCO_3$ particles synthesized in the PFR tubular reactor using different reactant $Ca^{++}/CO_3^{=}$ mole ratios at the same volumetric flow rates. As shown in the figure, the sizes of the $CaCO_3$ particles were larger than 10 μm. These particles were typical vaterite and calcite particles as indicated from the XRD patterns as shown in Figure 4.40(b). Interestingly, as shown in the figure with the arrows, when the $Ca^{++}/CO_3^{=}$ ratio was lower at 4mM/40mM, needle-like crystals were seen. These needle-like crystals were neither aragonite nor calcite nor vaterite as the diffraction peak could not be identified clearly with the Expert-HighScore Plus program. The amount of needle-like crystals decreased as Ca^{++} ion concentration increased to 16mM/40mM and they diminished at higher concentrations. It was thought that the $CO_3^{=}$ ions may have aided in speeding up the growth rate of $CaCO_3$[71,73,74]. When the $CO_3^{=}$ ion concentrations were lower, when the $Ca^{++}/CO_3^{=}$ ratio was lower than 40mM/28mM, the surfaces of vaterite particles were seen to be eroded. We think that the erosion from the vaterite surfaces was probably due to the adsorption of Ca^{++} ions to these surfaces and detachment of coupling ions from the surfaces such as $CaCO_3^o$, $CaOH^+$.

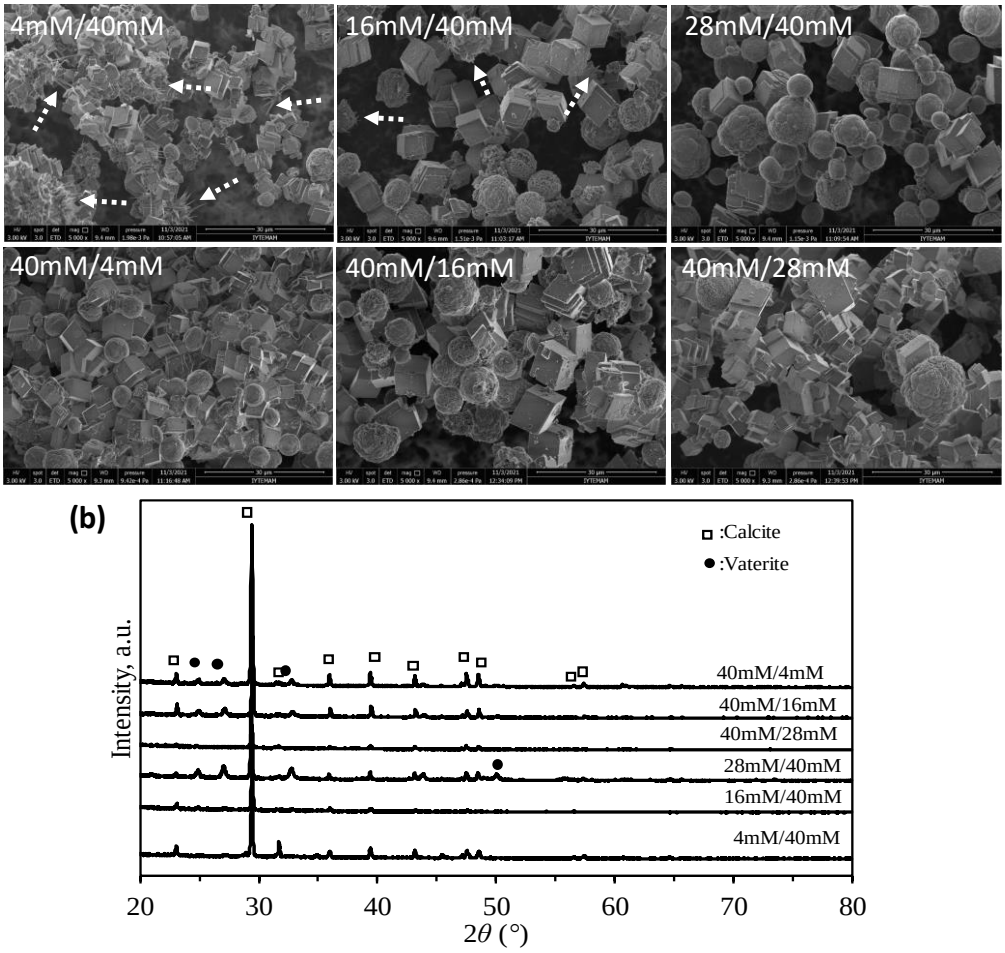

$[Ca^{++}]/[CO_3^{=}]$ Ratio	Calcite %	Vaterite %
40mM/4mM	76	24
40mM/16mM	85	15
40mM/28mM	90	10
4mM/40mM	63	37
16mM/40mM	66	34
28mM/40mM	45	55

Figure 4.40. (a) SEM images of CaCO3 particles synthesized in the PFR tubular reactor using different reactant mole ratios at the same volumetric flow rates, (b) XRD patterns for the crystal structures and the refinement results for the synthesized $CaCO_3$ crystals. Arrows show needle-like crystals.

The calcite and vaterite compositions were estimated for different $Ca^{++}/CO_3^{=}$ mole ratios studied. As shown in Figure 4.41, the calcite compassion was always higher than the vaterite compassion produced in the PFR tubular reactor. Considering the retention time in the tubular reactor of 9 second and the time for centrifugation was 20 minutes, the main composition of the particles was supposed to be vaterite and little calcite were expected as indicated in Figure 2.4[21]. In our experimental design, both calcite and vaterite particles were synthesized with a particle size larger than 10 μm by the chemical method.

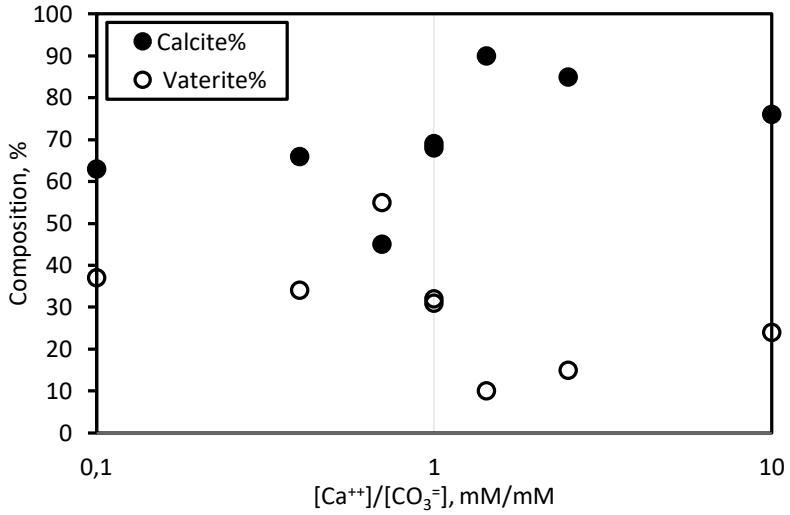

Figure 4.41. Calcite and vaterite compositions estimated for different $Ca^{++}/CO_3^{=}$ mole ratios.

The CaCO3 media from the PFR tubular reactor were added into the stirred semi-batch reactor containing 250 ml and 10 mM of $Ca(OH)_2$ solution as the stabilization solution. pH and conductivity values were monitored continuously within the satiation solution. Samples were taken at each minute and particle size and zeta potential values were estimated using Malvern ZS Zeta Sizer. Figure 4.42 shows the pH and conductivity values monitored in the stirred semi-batch reactor during the addition of $CaCO_3$ media from the PFR tubular reactor when Ca^{++} ions were higher in the crystallization media, and when $CO_3^{=}$ ions were higher in the crystallization media. As shown in Figure 4.42(a) and Figure 4.42(c), pH slightly decreased with the addition of $CaCO_3$ media from the PFR tubular reactor. The conductivity did not change when $Ca^{++}/CO_3^{=}$ mole ratios was

higher in the crystallization media as shown Figure 4.42(b). When the $Ca^{++}/CO_3^{=}$ mole ratios was lower, that is, the Ca^{++} ion concentration is lower than $CO_3^{=}$ ion concentration, the conductivity values slightly decreased as shown in Figure 4.42 (d) indicating that more Ca^{++} ions were consumed in the $Ca(OH)_2$ solution.

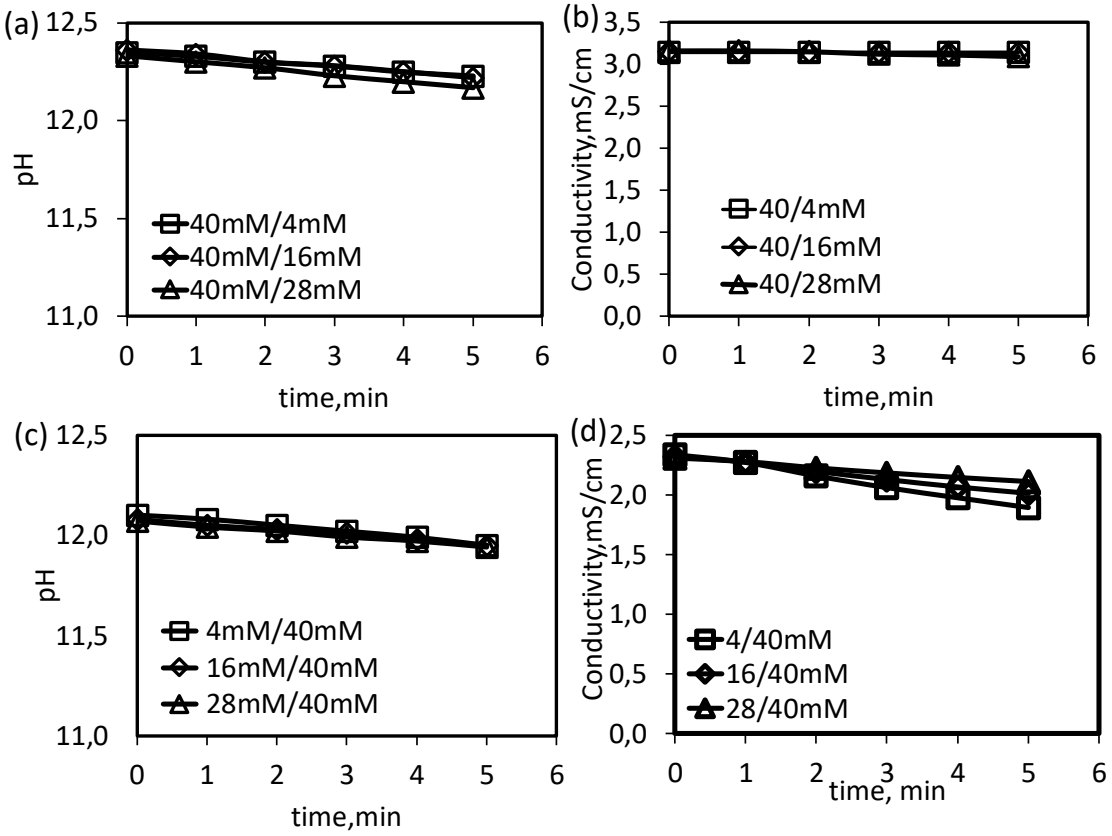

Figure 4.42. (a) pH and (b) conductivity values monitored in the stirred semi-batch reactor during the addition of $CaCO_3$ media from the PFR tubular reactor when Ca^{++} ions were higher in the crystallization media, (c) pH and (d) conductivity values when $CO_3^{=}$ ions were higher in the crystallization media.

Figure 4.43(a) and (b) show the average particle size and zeta potential values measured for the particles in the stirred semi-batch reactor when Ca^{++} ions were higher in the crystallization media. The average particle size and zeta potential values were also shown in Figure 4.43(c) and (d) when $CO_3^{=}$ ions were higher in the crystallization media. The average particle sizes were found to be about from 200 nm to about 450 nm in the $Ca(OH)_2$ solution as shown in Figure 4.43(a) and (c). As shown in Figure 4.43(b) and

(d)., the zeta potential values were positive at about +27 mV indicating that these particles were stable in the $Ca(OH)_2$ solution.

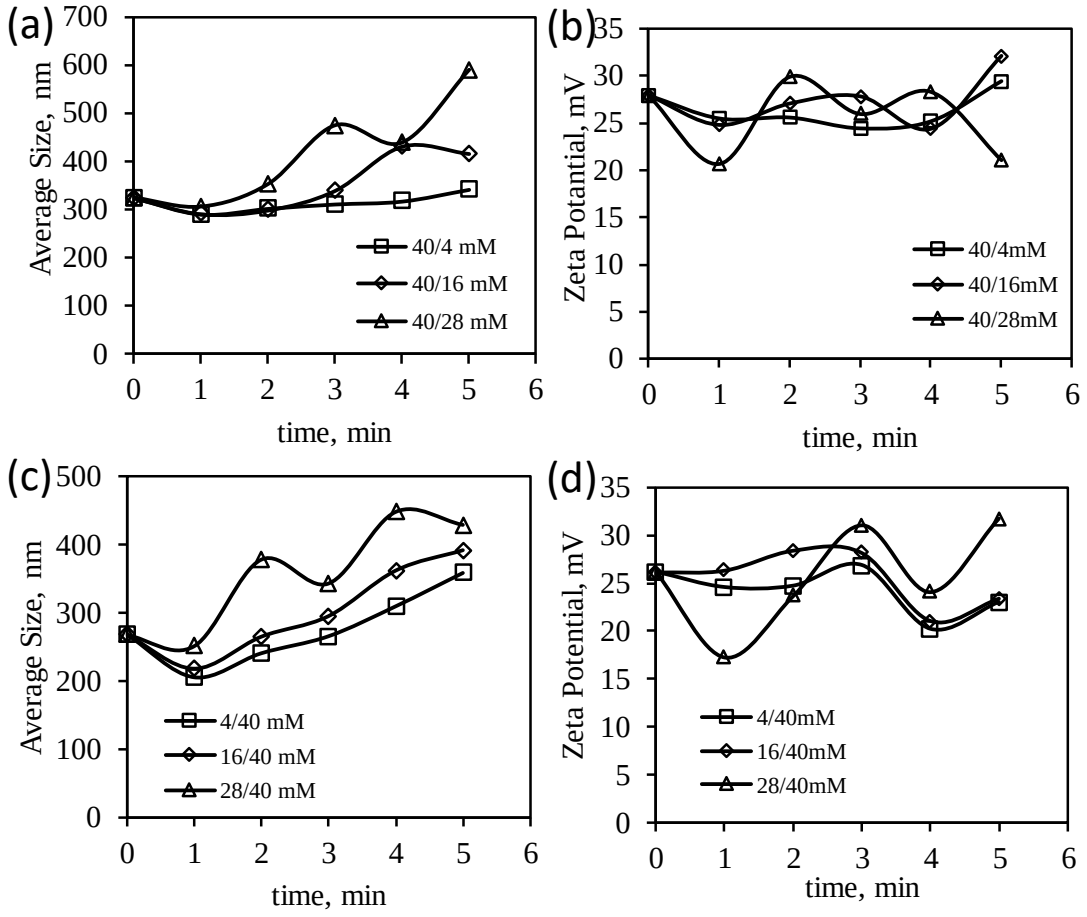

Figure 4.43. (a) Average particle size and (b) zeta potential values measured for the particles in the stirred semi-batch reactor when Ca^{++} ions were higher in the crystallization media, (c) Average particle size and (d) zeta potential values when $CO_3^{=}$ ions were higher in the crystallization media.

Figure 4.44 shows SEM images of particles synthesized in $Ca(OH)_2$ solution as the stabilizer medium by the chemical method when different $Ca^{++}/CO_3^{=}$ mole ratios used, and their XRD diffraction peaks. As shown in Figure 4.44(a), all the $CaCO_3$ particles stabilized in the $Ca(OH)_2$ solution were in nano sizes of about 350 nm regardless of $Ca^{++}/CO_3^{=}$ mole ratios used. Hollow nano-CaCO3 particles were also discerned when the $Ca^{++}/CO_3^{=}$ mole ratio was 16mM/40mM. These particles were not aggregated and almost homogenously size distributed. The XRD diffraction peaks indicated that these particles

were all in calcite form although their shapes are rice-like and elliptical. It is clearly demonstrated that nano-calcite particles could be synthesized by the chemical method with an average size of 350 nm and homogenous size distribution when stabilized in $Ca(OH)_2$ solution.

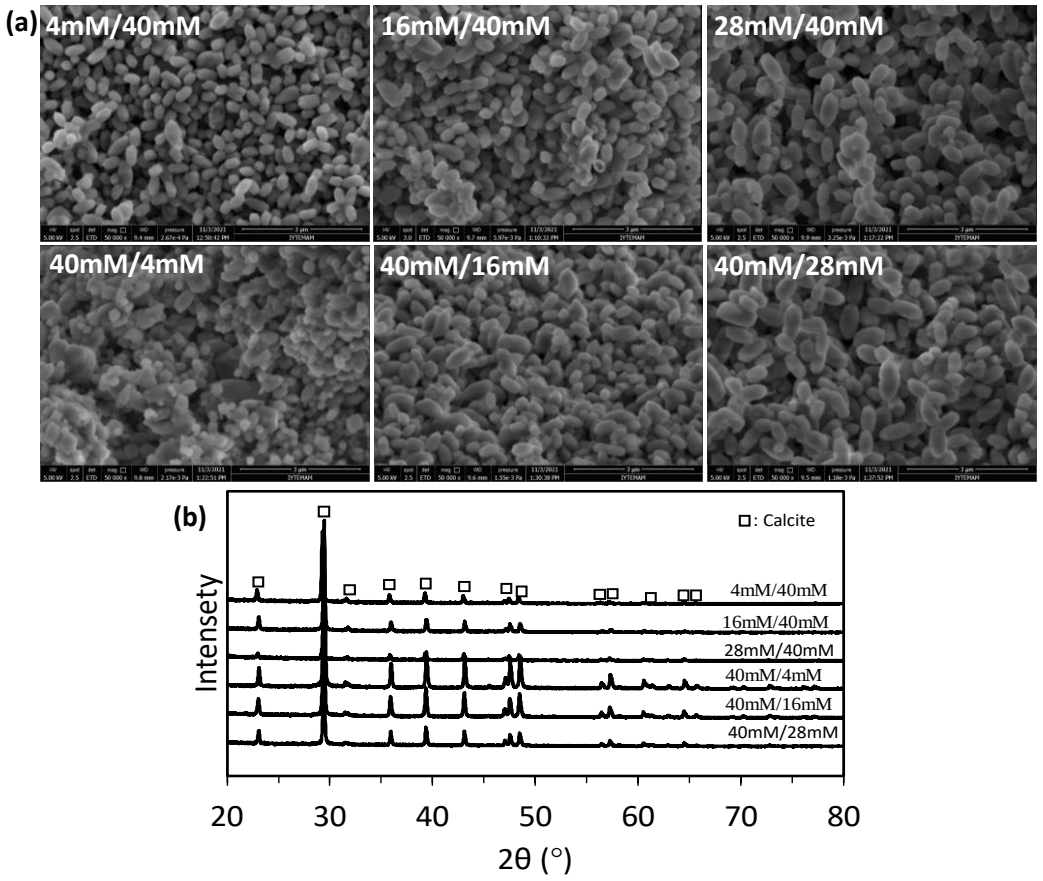

Figure 4.44. (a) SEM images of particles synthesized in $Ca(OH)_2$ stabilizer solution by the chemical method when different $Ca^{++}/CO_3^{=}$ mole ratios used, and (b) their XRD diffraction peaks.

4.8. Continuous Production of $CaCO_3$ Particles in Nano Sizes

It is generally known that micron-sized $CaCO_3$ particles are produced by the chemical method, larger than 3 μm. Also, production of nano-sized $CaCO_3$ is very rare or none by the chemical method. An example was shown in Figure 4.45(a). As shown in the figure, $CaCO_3$ particles larger than 13 μm were produced by mixing 160 mM of $CaCl_2$

and Na_2CO_3 each in a PFR plug flow reactor with a retention time of 9 seconds. The XRD patterns shown in Figure 4.45(b) indicated that these particles were vaterite and calcite, and no ACC or Aragonite, which are the other forms of $CaCO_3$, were discerned. Figure 4.45(c) shows the compositions of $CaCO_3$ particles obtained at different reactants concentrations. As shown in the figure, the crystal forms of $CaCO_3$ synthesized were about 20% of vaterite and 80%of calcite at low reactant concentrations of 20 mM. The vaterite and calcite composition changed when the reactant concentrations were changed. The calcite composition decreased, and the vaterite compassions increased as the reactants concentrations increased to 160 mM. Terefore, the vaterite and calcite compositions obtained in the chemical method are depended on the reactant's concentrations.

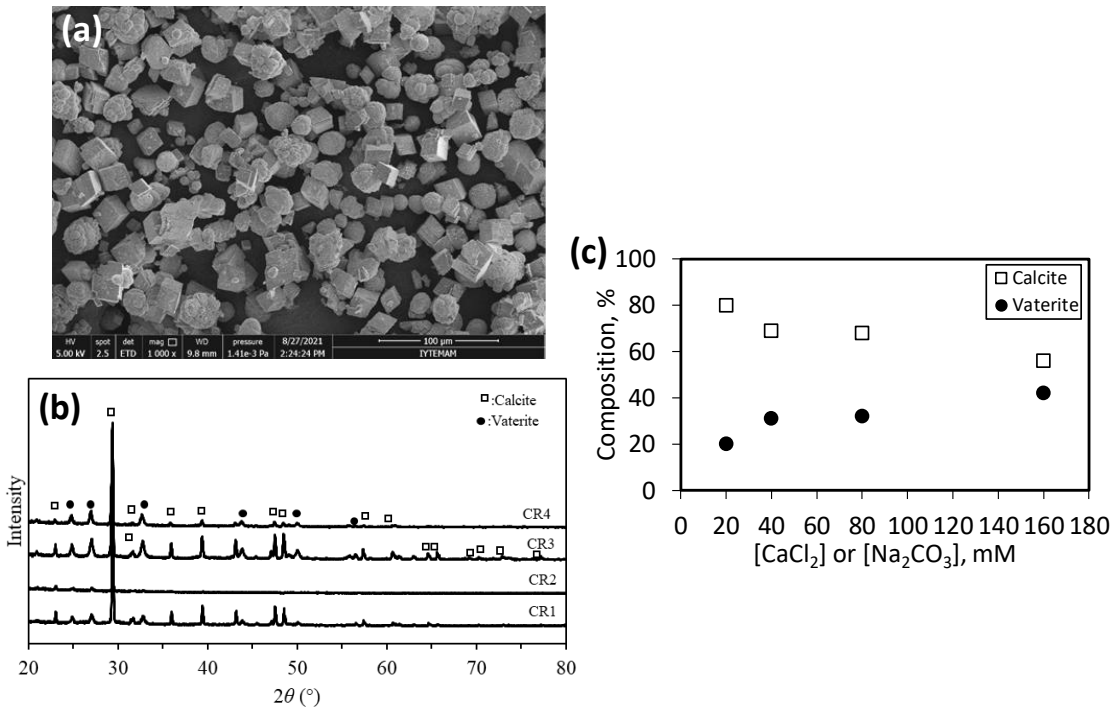

Figure 4.45. (a) SEM image of $CaCO_3$ particles synthesized by chemical method, (b) XRD patterns of the particles produced by chemical method using different concentrations of reactants of $CaCl_2$ and Na_2CO_3, where CR1=20 mM,

CR2=40 mM, CR3=80 mM, and CR4=160 mM, and (c) the vaterite and calcite compassions obtained at different reactants concentrations.

Figure 4.46 shows the SEM images on the progress of synthesis of calcite and vaterite particles in the chemical method. Figure 4.46(a) shows calcite and vaterite particles. Figure 4.46(b) shows a vaterite particle and nucleation of calcite crystal on the surface of a vaterite particle. Figure 4.46(c) shows the surface of a vaterite particles composed of crystallites. Figure 4.46(d) shows the aggregation of crystalline particles on the vaterite particle. Interestingly, it is clearly shown in Figure 4.46(e) that the crystalline particles are loosely aggregated within the vaterite particles and they were vulnerable to dissolve in the solution. Figure 4.46(e) shows the dissolution and reprecipitation of crystalline participles on the surfaces of other particles. We anticipate that the newly synthesized $CaCO_3$ particles can be dissolved in $Ca(OH)_2$ solution and reprecipitate to a much smaller size, therefore, nano-$CaCO_3$ particles could be produced by the chemical method.

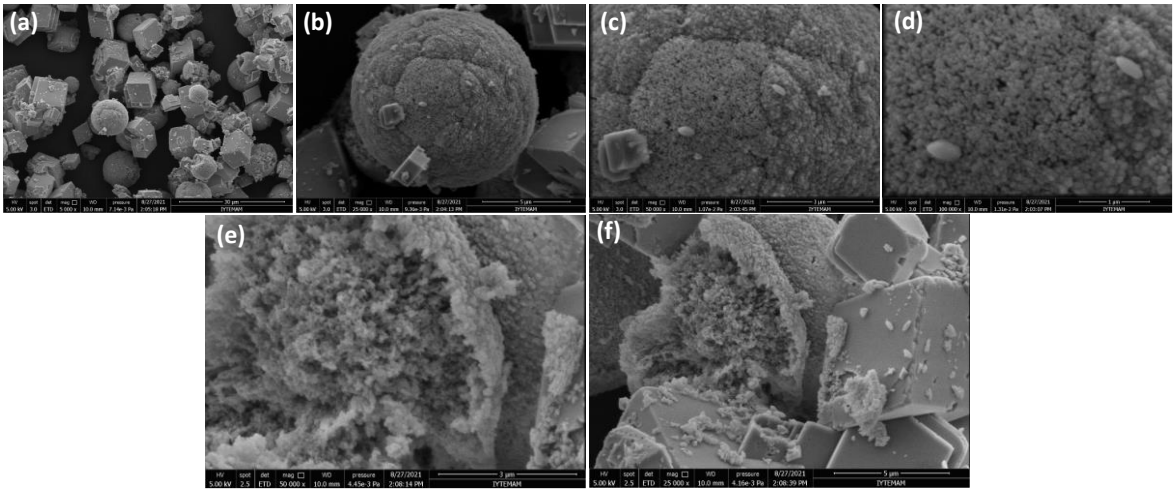

Figure 4.46. SEM image of $CaCO_3$ particles synthesized by chemical method, (b) a vaterite particle, (c) nucleation of calcite on the vaterite surface, (d) aggregation of crystalline particles on the vaterite particle, (e) dissolution of loosely aggregated crystalline particles from a vaterite particle, and (f) dissolution and precipitation of crystalline participles on the surfaces of other particles.

It was understood from studies and findings in our lab that $CaCO_3$ particles were dissolved and recrystallize in $Ca(OH)_2$ solutions. Therefore, our goal was to develop a process to continuously produce nano-calcite particles by the chemical method. A design was developed and shown in Figure 3.2 to continuously produce nano-$CaCO_3$ particles by the chemical method.

In the developed design, 10 mM of $Ca(OH)_2$ solution was prepared as the stabilizer solution. The reactant concentrations of 80 mM were also prepared. A 250 ml of $Ca(OH)_2$ solution was added into the CSTR reactor. Then, the rest of the solution was fed to the CSTR reactor with a flow rate of 20 ml/min. The flow rate of $CaCl_2$ and Na_2CO_3 solutions were 10 ml/min each to the PFR tubular reactor which has a diameter of 0.3 cm and a length of 40 cm so that the retention time was calculated to be 8.5 seconds for crystallization. Then, the $CaCO_3$ medium was fed to the CSTR by a total volumetric flow rate of 20 ml/min. The product output flow rate was set to 40 ml/min for a continuous operation. The retention time was calculated in the CSTR as 6.25 minutes, when the two streams were fed, with a volumetric flow rate of 40 ml/min, into the CSTR containing 250 ml of stabilization solution. The CSTR was run about 2 minutes before taking samples for analysis. As shown in Figure 4.48(a), pH decreased and conductivity increased during the first 6 minutes indicating that the CSTR did not reach steady-state, instead, the progress in particle stabilization were analyzed. Figure 4.48(b) shows the average size and zeta potential for the particles. As can be seen in the figure, the average particle sizes were about 300 nm and slightly increased to about 400 nm at 5^{th} minutes. At 6^{th} minute, the average particle size suddenly increased from 400 nm to 600 nm, and further data were not taken to find out if there is a continuation of increasing particle sizes or not. We think that the sudden increase could be due to the aggregation of particles in the stabilization medium during the measurement since the zeta potential values are all positive and were greater than +25 mV.

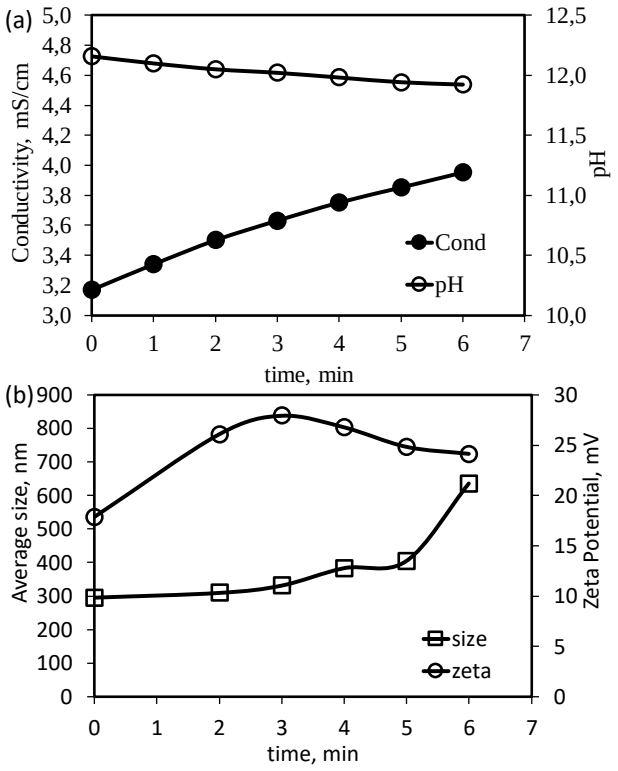

Figure 4.47. (a) pH and conductivity values measured in the CSTR containing $Ca(OH)_2$ stabilization solution, (b) average size and zeta potential for the particles

Figure 4.48(a) shows the SEM images of $CaCO_3$ particles synthesized by the chemical method and stabilized in $Ca(OH)_2$ solution with a continuous process. The XRD diffraction peaks for the particles were also shown in Figure 4.48(b). Because the retention time in the CSTR was 6.25 minutes, these SEM images also shows the progress in the particle formation. The first image shows the vaterite and calcite particles synthesized in the PFR plug flow reactor as indicate din the XRD patterns. As can be seen in the image, the calcite and vaterite $CaCO_3$ particles had sizes larger than 13 μm. When these globular particles were added into the $Ca(OH)_2$ stabilization solution, they dissolved and reprecipitated into much smaller $CaCO_3$ particles. These particles were seen to be rice-like and elliptic calcite particles. Much smaller particles with sizes less than 200 nm were seen in the image up to 2 minutes. The particle size and the number of particles increased as the addition progressed. Also, amorphous-like solid debris were also discerned among the nano particles in the images indicating that the dissolution and recrystallization are still in progress in the developed method since the steady state has

yet not been reached. Almost homogenously distributed nano-$CaCO_3$ particles were produced by the presently developed technique by the chemical method.

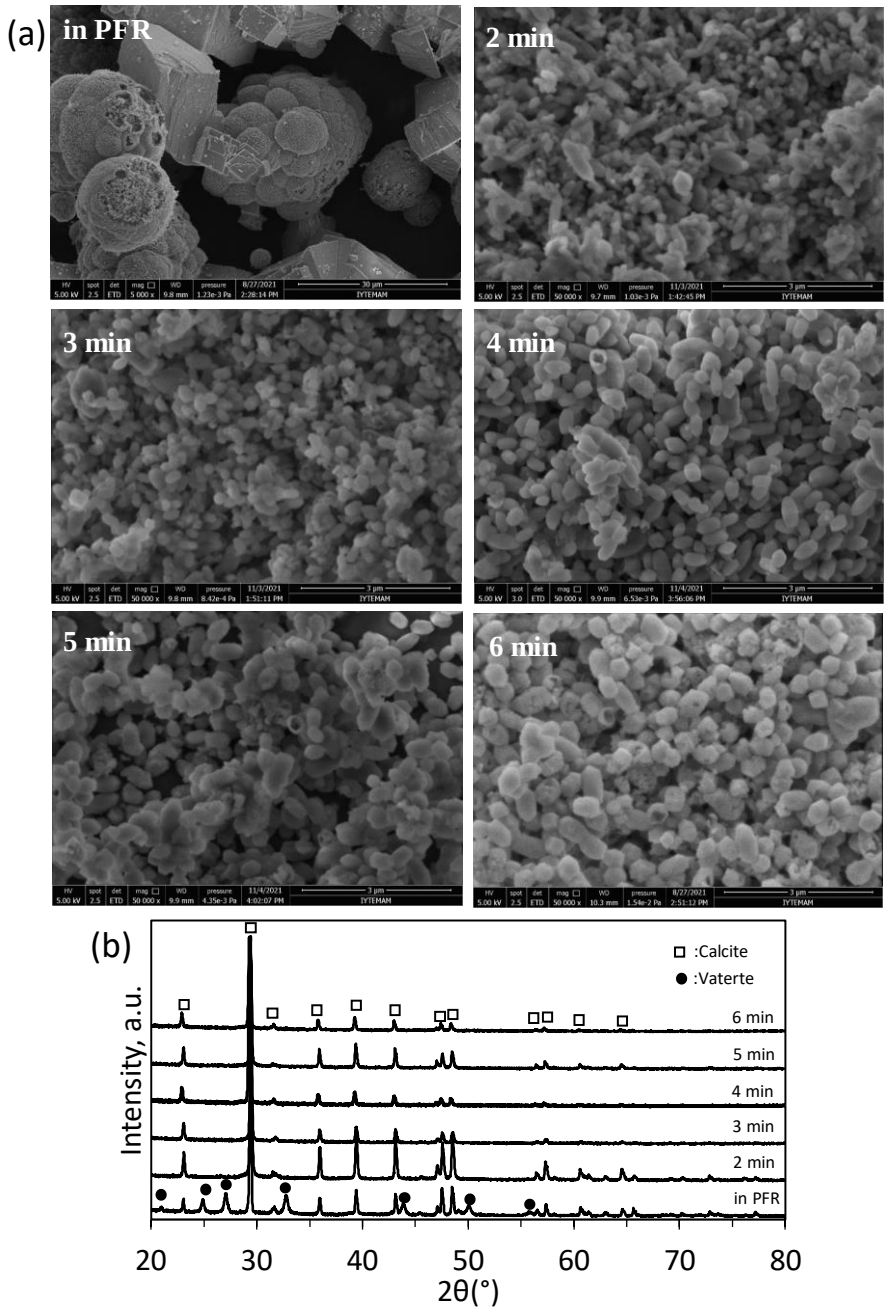

Figure 4.48. (a) SEM images of $CaCO_3$ particles synthesized by chemical method and stabilized in $Ca(OH)_2$ solution with a continuous process, (b) XRD diffraction peaks for the particles

In a separate study, different reactant concentrations from 20 mM to 160 mM were studied with the developed continuous CSTR reactor. The volumetric flow rates were 10 ml/min each to the PFR reactor. Crystallization took inside the tubular reactor with a retention time of 8.5 minutes and directly added into the stabilization solution. The CSTR reactor contained 10 mM and 250ml of $Ca(OH)_2$ solution as the stabilization solution. The continuous operation was achieved by sending 10 mM of $Ca(OH)_2$ solution and $CaCO_3$ media to the CSTR with volumetric flow rates of 20 ml/min and an outlet volumetric flow rate of 40 ml/min. Samples were withdrawn from the CSTR reactor at 7^{th} minute, centrifuged, washed with acetone, dried in vacuum oven at 85 ^oC under vacuum, and their SEM images were obtained. This procedure was repeated to other concentrations of the reactant solutions of 40 mM, 80 mM, and 160 mM.

Ina follow up study, the concentration of the stabilizer solution of $Ca(OH)_2$ was increased to 15 mM and used in the CSTR reactor and in the stream of stabilizer soluton. Figure 4.48 shows the SEM images of nano-$CaCO_3$ particles obtained in a CSTR reactor by using different $CaCl_2$ and Na_2CO_3 concentrations and stabilized in either 10 mM or 15 mM of $Ca(OH)_2$ stabilizer solution. As shown in the figure, much smaller and homogenous size distribution of nano-calcite particles were obtained at low concentrations of reactant solutions and in 10 mM of Ca(OH)2 solution. As the reactant concentrations increased, smaller particles were obtained in the 10 mM of Ca(OH)2 solution, however, some of these particles were seen to dissolved in crystallite particles, or most probably, those crystallites were about resynthesized in the Ca(OH)2 stabilization solution. The particles synthesized with 20 mM of reactant solutions and stabilized in 15 mM of $Ca(OH)_2$ were much smaller in size about 200 nm. These particles had almost homogenous size distribution, and their morphology was mostly rice-like. As the reactant concentrations increased, much aggregated crystallite particles were seen.

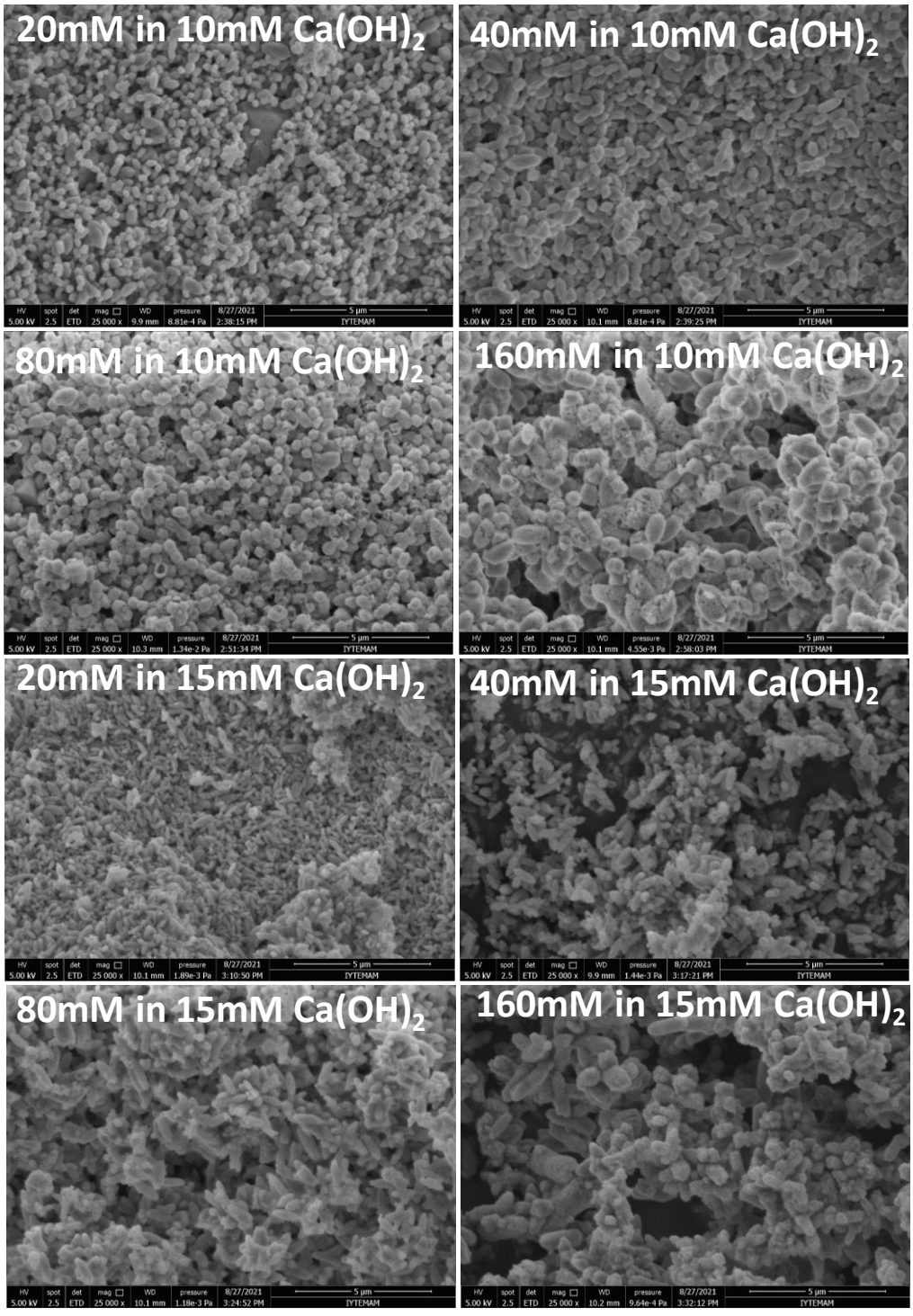

Figure 4.49. SEM images of nano-$CaCO_3$ particles obtained in a CSTR reactor by using different $CaCl_2$ and Na_2CO_3 concentrations and stabilized in either 10 mM or 15 mM of $Ca(OH)_2$ stabilizer solution.

4.9.A Mechanism for $CaCO_3$ Crystallization by Chemical Method

A mechanism was suggested for $CaCO_3$ crystallization by the chemical method. The first step in $CaCO_3$ crystallization by the chemical method is to dissolve the reactant solutions. When Na_2CO_3 was dissolved in water, Na^+ and $CO_3^=$ ions generated according to Eq.(4.8). When $CaCl_2$ was dissolved in water, Ca^{++} and Cl^- ions formed according to Eq.(4.9). Water dissociation also generates H^+ and OH^- ions according to Eq.(4.10).

Solution making:

$$Na_2CO_3 \rightarrow 2Na^+ + CO_3^= \quad (4.8)$$

$$CaCl2 \rightarrow 2Cl^- + Ca^{2+} \quad (4.9)$$

$$H_2O \leftrightarrow H^+ + OH^- \quad (4.10)$$

When pH was lower than 10, some of the $CO_3^=$ ions converted into HCO_3^- ions according to Eq.(4.11). Ca^{++} ions couple with the HCO_3^- ions and form $CaHCO_3^+$ ions according to Eq.(4.12). In the presence of OH^- ions, Ca^{++} ions couple with OH^- ions to give $CaOH^+$ ions in the solution according to Eq.(4.13). Also, Ca^{++} and $CO_3^=$ ions couple in the solution to give $CaCO_3^o$ uncharged couples according to Eq.(4.14).

Pairing of ions:

$$CO_3^= + H^+ \leftrightarrow HCO_3^- \quad (4.11)$$

$$Ca^{++} + HCO_3^- \leftrightarrow CaHCO_3^+ \quad (4.12)$$

$$Ca^{++} + OH^- \leftrightarrow CaOH^+ \quad (4.13)$$

$$CO_3^= + Ca^{2+} \leftrightarrow CaCO_3^o \quad (4.14)$$

With the classical view, the polymerization of Ca^{++} and $CO_3^=$ ions will yield solid crystal $CaCO_3$ particles according to Eq.(4.15).

Crystal growth:

$$CO_3^= + Ca^{2+} \rightarrow CaCO_{3(s)} \quad (4.15)$$

The equations from Eq.(4.8) to Eq.(4.15) play a critical role in $CaCO_3$ crystallization and particle formation by the chemical method as suggested by a mechanism as shown in Figure 4.50. In this mechanism, ions and couples' ions will form

in the solution. When $CaHCO_3^+$, Ca^{++}, $CaOH^+$, $CaCO_3^o$, and $CO_3^=$ combined all together until a critical size was reached, clusters will form. These clusters contained water in it and form ACC particulates. The ACC particulates contain charged species and easily aggregated to form aggregated ACC. When the water expelled from the ACC structure, crystalline particulates will form. Those particulates have opposite charges on their surfaces and easily aggregate to form vaterite particle. Those vaterite particles usually larger in size and can dissociate into smaller particulates which then dissolve in the solution and recrystallize into more stable calcite form. Depending on the high temperatures than 40°C[75–80] or the presence of additives, ACC can be transformed into rod-like aragonite particles. In the presence of other ions such as Ca^{++}, OH^-, $CaOH^+$, Ba^{++}, and/or $BaOH^+$ ions, the aggregated crystalline particulates within the giant vaterite particle can easily dissolve and recrystallize into calcite particles in nano-sizes and stabilized as nano-calcite particles as occurred in this thesis.

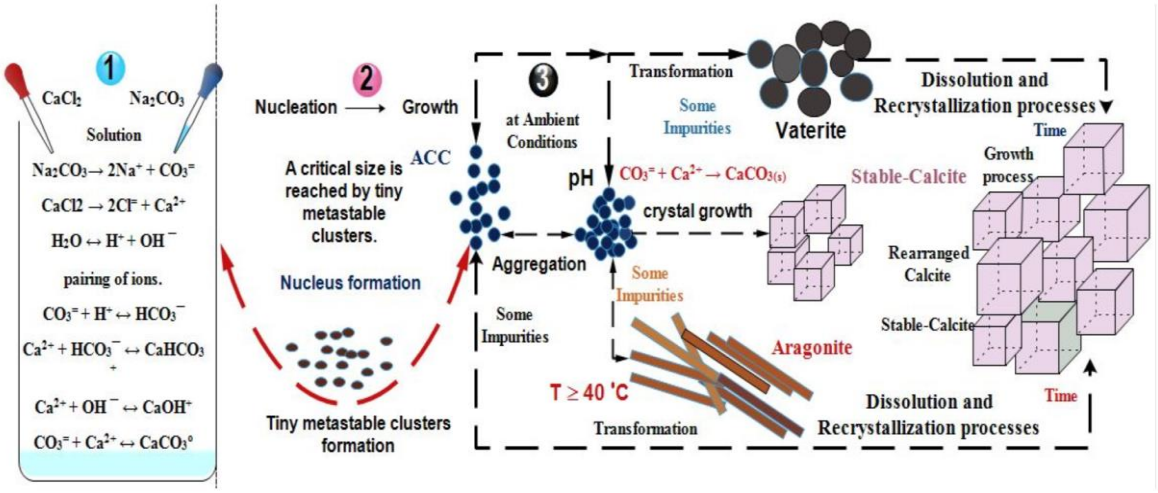

Figure 4.50. A mechanism suggested for $CaCO_3$ crystallization by the chemical method

CHAPTER 5

CONCLUSION

The results show that anions such as $SO_4^{=}$, NO_3^{-}, and $CO_3^{=}$ do not influence the size of newly precipitated $CaCO_3$. $CO_3^{=}$ ions favors vaterite formation by inhibiting or delaying the transformation of metastable-vaterite to stable-calcite. The $SO_4^{=}$ and NO_3^{-} ions seem to have no discernible effect on the size and morphology of $CaCO_3$ as they demonstrated a poor or insignificant affinity for adsorption on the surface of $CaCO_3$. Monovalent Na^{+} and K^{+} cations affected the morphology of $CaCO^3$ particles by resulting in calcite with an asymmetrical morphology. When $HPO_4^{=}$ is employed, the $CaCO_3$ is fully dissolved and resulted in formation of monetite and hydroxyapatite by a chemical displacement reaction. Ba^{++} ions exhibited an extraordinary ability to inhibit overgrowth by adsorbing onto the $CaCO_3$ crystal surfaces and incorporation within the $CaCO_3$ particles. Synthesis of Barytocalcite was a significant indicator that aggregated consistently throughout a wide particle size range as a consequence of a chemical interaction between Ba^{++} and $CaCO_3$. These transformations indicated that the synthesized vaterite and calcite particles in the plug flow reactor dissolved and recrystallized either into calcite form or in other crystals such as hydroxyapatite or Barytocalcite in the stabilization solution in the semi-batch stirred tank reactor.

When $CaCO_3$ at concentrations less than 50 mM reactant solution were added into 10mM of $Ba(OH)_2$ solution, The CaCO3 nearly completely transformed to Barytocalcite. Decreasing the $Ba((OH)_2$ concentrations or increasing the reactant concentrations resulted in a decrease in Barytocalcite crystals and at higher concentrations, Barytocalcite totally diminished from the stabilizing solution, during which the crystals totally converted to calcite with smaller sizes.

It was found that the $Ca(OH)_2$ solution greatly influenced the crystal structure, size, and the crystallization processes. The particles produced in the PFR tubular reactor using $CaCl_2$ and Na_2CO_3 as the reactants were found to be vaterite and calcite with particle sizes larger than 13 μm. Once the particles were added into DI water as the stabilizing solution, the particles were a mixture of micron-sized calcite and vaterite. Upon addition of these particles into $Ca(OH)_2$ stabilization solution, nano-sized calcite

particles were produced with sizes less than 350 nm. Therefore, nano-calcite particles could be synthesized by the chemical method with the developed synthesis method which would otherwise be larger than 3 μm. It was proved and demonstrated the synthesis of nano-$CaCO_3$ particles by dissolution and recrystallization of freshly precipitated $CaCO_3$ produced by the chemical method not previously described in the literature.

REFERENCES

(1) Tai, C. Y.; Chen, F. B. Polymorphism of CaCO3 Precipitated in a Constant-Composition Environment. *AIChE Journal* **1998**, *44* (8), 1790–1798..

(2) Muryanto, S.; Bayuseno, A. P.; Ma'mun, H.; Usamah, M.; Jotho. Calcium Carbonate Scale Formation in Pipes: Effect of Flow Rates, Temperature, and Malic Acid as Additives on the Mass and Morphology of the Scale. *Procedia Chemistry* **2014**, *9* (December), 69–76.

(3) Osman, A. F.; Mariatti, M. Properties of Aluminum Filled Polypropylene Composites. *Polymers and Polymer Composites* **2006**, *14* (6), 623–634..

(4) Ulkeryildiz, E.; Kilic, S.; Ozdemir, E. Nano-CaCO3 Synthesis by Jet Flow. *Colloids and Surfaces A: Physicochemical and Engineering Aspects* **2017**, *512*, 34–40.

(5) Ulkeryildiz, E.; Kilic, S.; Ozdemir, E. Rice-like Hollow Nano-CaCO3 Synthesis. *Journal of Crystal Growth* **2016**, *450*, 174–180.

(6) Trushina, D. B.; Bukreeva, T. v.; Antipina, M. N. Size-Controlled Synthesis of Vaterite Calcium Carbonate by the Mixing Method: Aiming for Nanosized Particles. *Crystal Growth and Design* **2016**, *16* (3), 1311–1319.

(7) Submitted, T. INFLUENCE OF Ca 2 + IONS ON FRESHLY PRECIPITATED CaCO 3 PARTICLES. **2019**, No. July.

(8) Koivula, H.; Toivakka, M.; Gane, P. Short Time Spreading and Wetting of Offset Printing Liquids on Model Calcium Carbonate Coating Structures. *Journal of Colloid and Interface Science* **2012**, *369* (1), 426–434.

(9) Liang, J. Z.; Zhou, L.; Tang, C. Y.; Tsui, C. P. Crystalline Properties of Poly(L-Lactic Acid) Composites Filled with Nanometer Calcium Carbonate. *Composites Part B: Engineering* **2013**, *45* (1), 1646–1650.

(10) Chen, C. H. O.; Teng, C. C.; Su, S. F.; Wu, W. C.; Yang, C. H. Effects of Microscale Calcium Carbonate and Nanoscale Calcium Carbonate on the Fusion,

Thermal, and Mechanical Characterizations of Rigid Poly(Vinyl Chloride)/Calcium Carbonate Composites. *Journal of Polymer Science, Part B: Polymer Physics* **2006**, *44* (2),

(11) Kemal, I.; Whittle, A.; Burford, R.; Vodenitcharova, T.; Hoffman, M. Toughening of Unmodified Polyvinylchloride through the Addition of Nanoparticulate Calcium Carbonate. *Polymer* **2009**, *50* (16), 4066–4079.

(12) Afshar, A.; Massoumi, I.; Khosh, R. L.; Bagheri, R. Fracture Behavior Dependence on Load-Bearing Capacity of Filler in Nano- and Microcomposites of Polypropylene Containing Calcium Carbonate. *Materials and Design* **2010**, *31* (2), 802–807.

(13) Richards, S. N.; Leon-Saval, S.; Goodwin, M.; Zheng, J.; Lawrence, J. S.; Bryant, J. J.; Bland-Hawthorn, J.; Norris, B.; Cvetojevic, N.; Argyros, A. Performance of a Novel PMMA Polymer Imaging Bundle for Field Acquisition and Wavefront Sensing. *Publications of the Astronomical Society of Australia* **2017**, *34* (2017).

(14) Aghajanian, S.; Koiranen, T. Dynamic Modeling and Semibatch Reactive Crystallization of Calcium Carbonate through CO2 Capture in Highly Alkaline Water. *Journal of CO2 Utilization* **2020**, *38* (February), 366–374.

(15) Sahebian, S.; Zebarjad, S. M.; Khaki, J. V.; Sajjadi, S. A. The Effect of Nano-Sized Calcium Carbonate on Thermodynamic Parameters of HDPE. *Journal of Materials Processing Technology* **2009**, *209* (3), 1310–1317.

(16) Lucas-Girot, A.; Verdier, M. C.; Tribut, O.; Sangleboeuf, J. C.; Allain, H.; Oudadesse, H. Gentamicin-Loaded Calcium Carbonate Materials: Comparison of Two Drug-Loading Modes. *Journal of Biomedical Materials Research - Part B Applied Biomaterials* **2005**, *73* (1), 164–170.

(17) Pickles, M. J.; Evans, M.; Philpotts, C. J.; Joiner, A.; Lynch, R. J. M.; Noel, N.; Laucello, M. In Vitro Efficacy of a Whitening Toothpaste Containing Calcium Carbonate and Perlite. *International Dental Journal* **2005**, *55* (3 SUPPL. 1), 197–202.

(18) Sintov, A. C.; Wormser, U. Topical Iodine Facilitates Transdermal Delivery of Insulin. *Journal of Controlled Release* **2007**, *118* (2), 185–188.

(19) García-Carmona, J.; Morales, J. G.; Clemente, R. R. Morphological Control of Precipitated Calcite Obtained by Adjusting the Electrical Conductivity in the Ca(OH)2-H2O-CO2 System. *Journal of Crystal Growth* **2003**, *249* (3–4), 561–571.

(20) Wang, X.; Wang, X.; Xu, X. The Construction of Sandbag Microstructure in Polyamide 6/Ethylene-Propylene-Diene Terpolymer/Nanometer Calcium Carbonate Ternary Composite. *Journal of Macromolecular Science, Part B: Physics* **2010**, *49* (1), 33–42.

(21) Bots, P.; Benning, L. G.; Roncal-herrero, T.; Shaw, S. Mechanistic Insights into the Crystallization of Amorphous Calcium Carbonate (ACC). **2012**.

(22) Rodriguez-Blanco, J. D.; Shaw, S.; Benning, L. G. How to Make 'Stable' ACC: Protocol and Preliminary Structural Characterization. *Mineralogical Magazine* **2008**, *72* (1), 283–286.

(23) López-Arce, P.; Gómez-Villalba, L. S.; Martínez-Ramírez, S.; Álvarez de Buergo, M.; Fort, R. Influence of Relative Humidity on the Carbonation of Calcium Hydroxide Nanoparticles and the Formation of Calcium Carbonate Polymorphs. *Powder Technology* **2011**, *205* (1–3), 263–269.

(24) Rodriguez-Blanco, J. D.; Shaw, S.; Benning, L. G. The Kinetics and Mechanisms of Amorphous Calcium Carbonate (ACC) Crystallization to Calcite, via Vaterite. *Nanoscale* **2011**, *3* (1), 265–271.

(25) Mergelsberg, S. T.; de Yoreo, J. J.; Miller, Q. R. S.; Marc Michel, F.; Ulrich, R. N.; Dove, P. M. Metastable Solubility and Local Structure of Amorphous Calcium Carbonate (ACC). *Geochimica et Cosmochimica Acta* **2020**, *289*, 196–206.

(26) Liendo, F.; Arduino, M.; Deorsola, F. A.; Bensaid, S. Nucleation and Growth Kinetics of CaCO3 Crystals in the Presence of Foreign Monovalent Ions. *Journal of Crystal Growth* **2021**, 126406.

(27) Paper, F.; Schlomach, J.; Quarch, K.; Kind, M. Investigation of Precipitation of Calcium Carbonate at High Supersaturations. **2006**, No. 2, 215–220.

(28) Kontrec, J.; Ukrainczyk, M.; Džakula, B. N.; Kralj, D. Precipitation and Characterization of Hollow Calcite Nanoparticles. *Crystal Research and Technology* **2013**, *48* (9), 622–626.

(29) Ogino, T.; Suzuki, T.; Sawada, K. The Formation and Transformation Mechanism of Calcium Carbonate in Water. *Geochimica et Cosmochimica Acta* **1987**, *51* (10), 2757–2767.

(30) Bolze, J.; Peng, B.; Dingenouts, N.; Panine, P.; Narayanan, T.; Ballauff, M. Formation and Growth of Amorphous Colloidal CaCO3 Precursor Particles as Detected by Time-Resolved SAXS. *Langmuir* **2002**, *18* (22), 8364–8369.

(31) Rodriguez-Blanco, J. D.; Shaw, S.; Benning, L. G. The Kinetics and Mechanisms of Amorphous Calcium Carbonate (ACC) Crystallization to Calcite, via Vaterite. *Nanoscale* **2011**, *3* (1), 265–271.

(32) Rodriguez-Blanco, J. D.; Shaw, S.; Benning, L. G. How to Make 'Stable' ACC: Protocol and Preliminary Structural Characterization. *Mineralogical Magazine* **2008**, *72* (1), 283–286.

(33) Ogino, T.; Suzuki, T.; Sawada, K. The Rate and Mechanism of Polymorphic Transformation of Calcium Carbonate in Water. *Journal of Crystal Growth* **1990**, *100* (1–2), 159–167.

(34) Wada, N.; Yamashita, K.; Umegaki, T. Effects of Divalent Cations upon Nucleation, Growth and Transformation of Calcium Carbonate Polymorphs under Conditions of Double Diffusion. *Journal of Crystal Growth* **1995**, *148* (3), 297–304.

(35) Benslimane, S.; Perrot, H.; Bennezar, R.; Bouhidel, K. E. Thermodynamic Study of Zn2 + Inhibition Properties and Mechanism on Calcium Carbonate Precipitation by Chemical and Electrochemical Methods. *Desalination* **2016**, *398*, 114–120.

(36) Benslimane, S.; Bouhidel, K. E.; Ferfache, A.; Farhi, S. Mechanistic Study of the Synergetic Inhibiting Effects of Zn2+, Cu2+ and Mg2+ Ions on Calcium Carbonate Precipitation. *Water Research* **2020**, *186*.

(37) Brečević, L.; Nöthig-Laslo, V.; Kralj, D.; Popović, S. Effect of Divalent Cations on the Formation and Structure of Calcium Carbonate Polymorphs. *Journal of the Chemical Society - Faraday Transactions* **1996**, *92* (6), 1017–1022.

(38) Abeywardena, M. R.; Elkaduwe, R. K. W. H. M. K.; Karunarathne, D. G. G. P.; Pitawala, H. M. T. G. A.; Rajapakse, R. M. G.; Manipura, A.; Mantilaka, M. M. M. G. P. G. Surfactant Assisted Synthesis of Precipitated Calcium Carbonate Nanoparticles Using Dolomite: Effect of PH on Morphology and Particle Size. *Advanced Powder Technology* **2020**, *31* (1), 269–278.

(39) Cizer, Ö.; Rodriguez-Navarro, C.; Ruiz-Agudo, E.; Elsen, J.; van Gemert, D.; van Balen, K. Phase and Morphology Evolution of Calcium Carbonate Precipitated by Carbonation of Hydrated Lime. *Journal of Materials Science* **2012**, *47* (16), 6151–6165.

(40) Kobeleva, A. R.; Poilov, V. Z. Technology for Production of Calcium Carbonate with Prescribed Properties. *Russian Journal of Applied Chemistry* **2007**, *80* (9), 1447–1452.

(41) Kontrec, J.; Kralj, D.; Brečević, L.; Falini, G. Influence of Some Polysaccharides on the Production of Calcium Carbonate Filler Particles. *Journal of Crystal Growth* **2008**, *310* (21), 4554–4560.

(42) Instruments, M. Manual: Zetasizer Nano User Manual. *(Man0317-5.0) inc addendum - (26-05-10)* **2009**, 1–308.

(43) Thompson, P. A.; Troian, S. M. A General Boundary Condition for Liquid Flow at Solid Surfaces. *Nature* **1997**, *389* (6649), 360–362.

(44) Kilic, S.; Toprak, G.; Ozdemir, E. Stability of CaCO3 in Ca(OH)2 Solution. *International Journal of Mineral Processing* **2016**, *147*, 1–9.

(45) Moulin, P.; Roques, H. Zeta Potential Measurement of Calcium Carbonate. *Journal of Colloid and Interface Science* **2003**, *261* (1), 115–126.

(46) Gaumet, M.; Vargas, A.; Gurny, R.; Delie, F. Nanoparticles for Drug Delivery: The Need for Precision in Reporting Particle Size Parameters. *European Journal of Pharmaceutics and Biopharmaceutics* **2008**, *69* (1), 1–9.

(47) Fu, S. Y.; Feng, X. Q.; Lauke, B.; Mai, Y. W. Effects of Particle Size, Particle/Matrix Interface Adhesion and Particle Loading on Mechanical Properties of Particulate-Polymer Composites. *Composites Part B: Engineering* **2008**, *39* (6), 933–961.

(48) Meng, T.; Yu, Y.; Wang, Z. Effect of Nano-CaCO3 Slurry on the Mechanical Properties and Micro-Structure of Concrete with and without Fly Ash. *Composites Part B: Engineering* **2017**, *117*, 124–129.

(49) Lin, J.; Huang, L.; Xiang, R.; Ou, H.; Li, X.; Chen, A.; Liu, Z. Blood Compatibility Evaluations of CaCO3 Particles. *Biomedical Materials (Bristol)* **2021**, *16* (5).

(50) Chen, Y.; Lian, X.; Li, Z.; Zheng, S.; Wang, Z. Effects of Rotation Speed and Media Density on Particle Size Distribution and Structure of Ground Calcium Carbonate in a Planetary Ball Mill. *Advanced Powder Technology* **2015**, *26* (2), 505–510.

(51) Trushina, D. B.; Bukreeva, T. v.; Kovalchuk, M. v.; Antipina, M. N. CaCO3 Vaterite Microparticles for Biomedical and Personal Care Applications. *Materials Science and Engineering C* **2014**, *45*, 644–658.

(52) Parakhonskiy, B. v.; Yashchenok, A. M.; Donatan, S.; Volodkin, D. v.; Tessarolo, F.; Antolini, R.; Möhwald, H.; Skirtach, A. G. Macromolecule Loading into Spherical, Elliptical, Star-Like and Cubic Calcium Carbonate Carriers. *ChemPhysChem* **2014**, *15* (13), 2817–2822.

(53) Naka, K.; Chujo, Y. Control of Crystal Nucleation and Growth of Calcium Carbonate by Synthetic Substrates. *Chemistry of Materials* **2001**, *13* (10), 3245–3259.

(54) Meyer, H. J. The Influence of Impurities on the Growth Rate of Calcite. *Journal of Crystal Growth* **1984**, *66* (3), 639–646.

(55) Njegić-Džakula, B.; Brečević, L.; Falini, G.; Kralj, D. Calcite Crystal Growth Kinetics in the Presence of Charged Synthetic Polypeptides. *Crystal Growth and Design* **2009**, *9* (5), 2425–2434.

(56) Chibowski, E.; Hotysz, L.; Szcześ, A. Time Dependent Changes in Zeta Potential of Freshly Precipitated Calcium Carbonate. *Colloids and Surfaces A: Physicochemical and Engineering Aspects* **2003**, *222* (1–3), 41–54.

(57) Liu, J.; Zhou, F.; Dai, Q.; Gao, H. Effect of Ca2+, Mg2+, Ba2+ and Sr2+ Cations on Calcium Carbonate Scaling Formation in Oil-Gas Well: Based on Density Functional Theory Study and Molecular Dynamics Simulation. *Journal of Crystal Growth* **2021**, *563* (February), 126089.

(58) al Mahrouqi, D.; Vinogradov, J.; Jackson, M. D. Zeta Potential of Artificial and Natural Calcite in Aqueous Solution. *Advances in Colloid and Interface Science* **2017**, *240*, 60–76.

(59) Cartlidge, D. Preface to Fourth Edition. *New Aspects of Quantity Surveying Practice* **2017**, xvii.

(60) Sheng Han, Y.; Hadiko, G.; Fuji, M.; Takahashi, M. Crystallization and Transformation of Vaterite at Controlled PH. *Journal of Crystal Growth* **2006**, *289* (1), 269–274.

(61) Jung, T.; Kim, W. S.; Choi, C. K. Effect of Monovalent Salts on Morphology of Calcium Carbonate Crystallized in Couette-Taylor Reactor. *Crystal Research and Technology* **2005**, *40* (6), 586–592.

(62) Chen, P. C.; Tai, C. Y.; Lee, K. C. Morphology and Growth Rate of Calcium Carbonate Crystals in a Gas-Liquid-Solid Reactive Crystallizer. *Chemical Engineering Science* **1997**, *52* (21–22), 4171–4177.

(63) Parkhurst, D. L.; Appelo, C. a. J. Description of Input and Examples for PHREEQC Version 3 — A Computer Program for Speciation , Batch-Reaction , One-Dimensional Transport , and Inverse Geochemical Calculations. U.S. Geological Survey Techniques and Methods, Book 6, Chapter A43, 497 p. *U.S. Geological Survey Techniques and Methods, book 6, chapter A43* **2013**, 6-43A.

(64) Kralj, D.; Brečević, L.; Nielsen, A. E. Vaterite Growth and Dissolution in Aqueous Solution I. Kinetics of Crystal Growth. *Journal of Crystal Growth* **1990**, *104* (4), 793–800.

(65) Han, Y. S.; Hadiko, G.; Fuji, M.; Takahashi, M. Effect of Flow Rate and CO2 Content on the Phase and Morphology of CaCO3 Prepared by Bubbling Method. *Journal of Crystal Growth* **2005**, *276* (3–4), 541–548.

(66) Kaye, G. W. C.; Laby, T. H. Tables of Physical and Chemical Constants, and Some Mathematical Functions. *Journal of the Röntgen Society* **1912**, *8* (30), 28–28.

(67) Jenkins, S. H. Aquatic Chemistry. *Water Research* **1971**, *5* (9), 786.

(68) Oral, Ç. M.; Ercan, B. Influence of PH on Morphology, Size and Polymorph of Room Temperature Synthesized Calcium Carbonate Particles. *Powder Technology* **2018**, *339*, 781–788.

(69) Tetteh, J. T.; Alimoradi, S.; Brady, P. v.; Barati Ghahfarokhi, R. Electrokinetics at Calcite-Rich Limestone Surface: Understanding the Role of Ions in Modified Salinity Waterflooding. *Journal of Molecular Liquids* **2020**, *297* (xxxx), 111868.

(70) Akinwekomi, V.; Maree, J. P.; Wolkersdorfer, C. Die Nutzung von Calciumkarbonat/-Hydroxid Und Bariumcarbonat Zu Fällung von Sulfaten in Bergbauabwasser. *Mine Water and the Environment* **2017**, *36* (2), 264–272.

(71) I. Puigdomenech, "HYDRA (Hydrochemical Equilibrium- Constant Database) and MEDUSA (Make Equilibrium Diagrams Using Sophisticated Algorithms) Programs," Royal Institute of Technology, Sweden. - References - Scientific Research Publishing.

(72) BOISTELLE, R.; ASTIER, J. P. Journal of Crystal Growth 90 (1988) 14—30 Crystallization Mechanisms Solution.Pdf. *Journal of Crystal Growth* **1988**, *90*, 14–30.

(73) Jensen, W.R. The Lewis Acid-Base Definitions: A Status Report, *Chemical Reviews* **1978**, 78 (1), 1-22.

(74) Kobelava, A.R and Pollow, V.Z. Technology for Production of Calcium Carbonate with Prescribed Properties, *Russian Journal of Applied Chemistry*, **2007**, 80(9), 1447-1452.

(75) Kontrec, J.; Tomašić, N.; Mlinarić, N. M.; Kralj, D.; Džakula, B. N. Effect of Ph and Type of Stirring on the Spontaneous Precipitation of CaCo3 at Identical Initial

Supersaturation, Ionic Strength and a(Ca2+)/a(Co32−) Ratio. *Crystals* **2021**, *11* (9).

(76) Larsen, K.; Bechgaard, K.; Stipp, S. L. S. The Effect of the Ca2+ to CO32 - Activity Ratio on Spiral Growth at the Calcite {1 0 over(1,¯) 4} Surface. *Geochimica et Cosmochimica Acta* **2010**, *74* (7), 2099–2109.

(77) Dou, J.; Zhao, F.; Fan, W.; Chen, Z.; Guo, X. Preparation of Non-Spherical Vaterite CaCO3 Particles by Flash Nano Precipitation Technique for Targeted and Extended Drug Delivery. *Journal of Drug Delivery Science and Technology* **2020**, *57* (April), 101768.

(78) Muhammad, T.; Xiao, Y.; Puig-Bargués, J.; Liu, W.; Liu, Z.; Chen, X.; Li, Y. Effects of Coupling Multiple Factors on CaCO3 Fouling in Agricultural Saline Water Distribution Systems. *Agricultural Water Management* **2021**, *248* (December 2020).

(79) Chang, R.; Kim, S.; Lee, S.; Choi, S.; Kim, M.; Park, Y. Calcium Carbonate Precipitation for CO 2 Storage and Utilization: A Review of the Carbonate Crystallization and Polymorphism. *Frontiers in Energy Research* **2017**, *5* (JUL), 1–12.

(80) Chen, J.; Xiang, L. Controllable Synthesis of Calcium Carbonate Polymorphs at Different Temperatures. *Powder Technology* **2009**, *189* (1), 64–69.